NASA TECHNICAL MEMORANDUM

NASA TM X-62,432

NASA TM X-62,432

WIND TUNNEL PRESSURE SIGNATURES FOR A 0.0041-SCALE MODEL OF THE SPACE SHUTTLE ORBITER

Joel P. Mendoza

Ames Research Center
Moffett Field, Calif. 94035

May 1975

1. Report No.	2. Government Accession No.	3. Recipient's Catalog No.
NASA TM X-62,432		

4. Title and Subtitle	5. Report Date
WIND TUNNEL PRESSURE SIGNATURES FOR A 0.0041-SCALE MODEL OF THE SPACE SHUTTLE ORBITER	6. Performing Organization Code

7. Author(s)	8. Performing Organization Report No.
Joel P. Mendoza	A-6067
	10. Work Unit No. 506-26-31
9. Performing Organization Name and Address	11. Contract or Grant No.
Ames Research Center, NASA Moffett Field, California 94035	
	13. Type of Report and Period Covered
12. Sponsoring Agency Name and Address	Technical Memorandum
National Aeronautics and Space Administration Washington, D. C. 20546	14. Sponsoring Agency Code

15. Supplementary Notes

16. Abstract

Pressure signatures for a 0.0041-scale model of a space shuttle orbiter were measured in a wind tunnel at Mach numbers from 1.30 to 3.02. The model was tested at 10° and 25° angle of attack and roll angles were varied from 0° to 180° in 30° increments. Comparisons of sonic boom levels were made for a delta wing configuration and for the latest space shuttle orbiter which were assumed to have identical lengths and entry trajectories. The sonic boom levels for the latest orbiter were slightly higher than those for the delta wing orbiter. An example is presented showing that the existing data base for the delta wing orbiter can be used to predict the ground level sonic booms for the latest orbiter.

17. Key Words (Suggested by Author(s))	18. Distribution Statement
Space shuttle orbiter Sonic booms Delta wing orbiter Pressure signatures Straight wing orbiter	Unclassified - Unlimited STAR Category - 02

19. Security Classif. (of this report)	20. Security Classif. (of this page)	21. No. of Pages	22. Price*
Unclassified	Unclassified	69	$4.25

*For sale by the National Technical Information Service, Springfield, Virginia 22151

SYMBOLS

h	model altitude, distance between model reference and axis of static pressure probe (fig. 4)
K_R	reflection factor
l	reference length, body length
M	Mach number
p	reference pressure, free stream static pressure
Δp	incremental pressure due to flow field of model
Δx	distance along abscissa of pressure signature
α	angle of attack
ϕ	roll angle

WIND TUNNEL PRESSURE SIGNATURES FOR A 0.0041-SCALE MODEL OF THE SPACE SHUTTLE ORBITER

Joel P. Mendoza
Ames Research Center

SUMMARY

Pressure signatures for a 0.0041-scale model of a space shuttle orbiter were measured in a wind tunnel at Mach numbers from 1.30 to 3.02. The model was tested at 10° and 25° angle of attack and roll angles were varied from 0° to 180° in 30° increments. Comparisons of sonic boom levels were made for a delta wing configuration and for the latest space shuttle orbiter which were assumed to have identical lengths and entry trajectories. The comparisons of the sonic boom footprints (Δp vs. distance from the ground track) at the nominal Mach numbers from 1.2 to 2.2 showed that the sonic booms for the latest orbiter were slightly higher than those for the delta wing orbiter. An example is presented showing that the existing data base for the delta wing orbiter can be used to predict the ground level sonic booms for the latest orbiter. Sonic boom footprints for the latest orbiter following a given trajectory were derived using data for the two different orbiters (latest orbiter and delta wing orbiters) following a different entry trajectory.

INTRODUCTION

A large data base (refs. 1 and 2) of sonic boom pressure signatures measured in a wind tunnel over a wide range of Mach numbers and model attitudes has been assembled for the delta wing version of the space shuttle orbiter. These data have been used to predict the ground level intensities of the sonic booms produced by the delta wing orbiter under various reentry conditions. Since the publication of reference 2, the space shuttle orbiter has undergone major configuration modifications. As a result, a wind tunnel investigation was conducted using a 0.0041-scale model of the latest space shuttle orbiter to determine the effects on the ground overpressure characteristics due to changes in the geometry and the aerodynamic characteristics of the orbiter. The results of the investigation are presented in this report.

MODEL AND TEST PROCEDURES

A wind tunnel sonic boom investigation using a 0.0041-scale model of the space shuttle orbiter (fig. 1) was conducted in the 20-inch supersonic wind tunnel at the Jet Propulsion Laboratory. Recognizing that the various elements of the space shuttle (the orbiter, external tank, and solid propellant rocket

boosters) are continuously undergoing design modifications, some of the components of the orbiter model may not exactly represent those on the full scale orbiter. For sonic boom tests, however, the overall shape of the orbiter model is considered to be close enough to the final configuration of the full scale orbiter. The model, which is constructed of steel, is complete except for the rocket engines.

Sketches of the delta wing (refs. 1 and 2) and the straight wing (ref. 2) orbiter models are shown in figures 2 and 3, respectively. Results from previous tests conducted on these models will be discussed later together with the results of the present investigation.

Shown in figure 4 is the arrangement of the model and the conical (2° included angle) static pressure probe. To define the distribution of the model flow field static pressures, the space shuttle orbiter model was mounted on a linear actuator which permitted longitudinal travel parallel to the centerline of the test section. The static pressure probe was mounted on spacers fixed to the floor of the test section. By adjusting the height of the static pressure probe above the floor of the test section the shockwaves reflected from the floor could be prevented from interfering with the measured pressure signature. A capacitance type pressure transducer was used to measure the pressures. Schlieren photographs were also taken at each test condition.

Shown in figure 5 are two different methods for setting model angle of attack. Method A was used exclusively for the 10° angle of attack setting at Mach numbers from 1.30 to 2.21. At M = 2.61, this method proved to be unsatisfactory because the sector (fig. 5) generated a shockwave which interfered with the rear shock wave system of the model. Method B (fig. 5) eliminated this problem.

The table presented below shows the Mach number and angle of attack conditions for the present wind tunnel investigation which was conducted at the stagnation pressure of 132598.9 N/m^2.

M	1.30	1.64	2.21	2.61	3.02
α	10°	10°	10°	10° 25°	25°

At each angle of attack, flow field static pressure distributions were measured at 30° increments in roll angle from 0° to 180°. This was accomplished by rolling the model and the angle of attack apparatus together on the linear actuator (fig. 5).

Shown in figure 6 are installation photographs of the space shuttle model in the 20-inch supersonic wind tunnel at the Jet Propulsion Laboratory.

PRESENTATION OF THE DATA

Schlieren photographs of the model of the latest space shuttle orbiter are shown in figures 7 through 12. The flow field pressure distributions are shown in figures 13 through 18.

Since the objective of the present investigation was to determine the differences in the sonic boom levels for the delta wing and the latest space shuttle orbiters, comparisons of the intensities of the ground level sonic booms were made with orbiters of the same body length and the same entry trajectories. In order to expedite the sonic boom comparisons, modifications were made to currently planned entry trajectories so that the previously reported wind tunnel data and data from the present investigation could be used directly without further data processing. Shown in figures 19(a) and 19(b) are two different space shuttle entry trajectories with modified angle of attack and roll angle schedules. These modified trajectories were used to compute the sonic booms for the delta wing and latest space shuttle orbiters.

Shown in figures 20(a) and 20(b) are comparisons of the sonic boom footprints (Δp vs. distance from the ground track) for the two space shuttle orbiters. During the configuration development phase of the delta wing space shuttle orbiter, overall lengths in excess of 50 m were considered. For this reason ground track sonic boom levels for an orbiter length of 51.5 m are included in figure 20(a) for comparison with those of the latest 32.77 m orbiter length.

In order to show configuration effects, comparisons of the ground track overpressures for three different orbiter configurations are shown in figure 21. Sonic boom levels for the delta wing and latest orbiter configurations are compared for two different entry trajectories (A and B). Also shown in the figure is a comparison of the sonic boom levels, reproduced herein from reference 3, for the straight- and delta-wing orbiters at 60° angle of attack. The trajectory followed by these two orbiters is presented in reference 3 and is not shown in this report.

The difference in sonic boom levels for the straight- and delta-wing orbiters at 60° angle of attack is observed to be smaller than the difference in sonic boom levels for the latest orbiter and the delta wing orbiter at 10° angle of attack (trajectories A and B). This suggests that overpressure levels become less sensitive to differences in orbiter geometry as angle of attack is increased. The experimental and theoretical results presented in reference 4 verify this. The results showed that at low values of lift, differences in model geometry produced significant differences in the sonic boom levels, while at high values of lift the differences in the sonic boom levels were noticeably reduced.

A brief study was conducted to determine the feasibility of calculating the sonic booms for the current orbiter for a wide range of conditions using the existing large data base for the delta wing orbiter and data from the present investigation. It was assumed that

$$\left[\frac{\Delta p \text{ (latest)}}{\Delta p \text{ (delta)}}\right]_{\text{trajectory A}} = \left[\frac{\Delta p \text{ (latest)}}{\Delta p \text{ (delta)}}\right]_{\text{trajectory B}} \quad (1)$$

would hold at all distances from the ground track. Expression (1) can, then, be rearranged in the following manner:

$$\Delta p \text{ (latest)}_{\text{trajectory B}} = \left[\frac{\Delta p \text{ (latest)}}{\Delta p \text{ (delta)}}\right]_{\text{trajectory A}} \times \Delta p \text{ (delta)}_{\text{trajectory B}} \quad (2)$$

Shown in figure 22 for comparison are the sonic boom levels for the latest space shuttle orbiter. The points represented by the circles were obtained by using expression (2) while the solid line represents the data for the latest space shuttle orbiter from figure 20(b). Good agreement is shown between the two sets of data, indicating that the existing large data base for the delta wing configuration can be used to estimate sonic booms for the latest orbiter.

Ames Research Center
National Aeronautics and Space Administration
Moffett Field, California 94035

REFERENCES

1. Hicks, Raymond M.; and Mendoza, Joel P.: Wind Tunnel Pressure Signatures for a Delta Wing Space Shuttle Vehicle. NASA TM X-62,040, Aug. 4, 1971.

2. Hicks, Raymond M.; and Mendoza, Joel P.: Wind Tunnel Pressure Signatures for a Delta Wing Space Shuttle Vehicle and a Space Shuttle Fuel Tank. NASA TM X-62,119, April 11, 1972.

3. Hicks, Raymond M.; Mendoza, Joel P.; and Levy, Lionel L., Jr.: An Investigation of Sonic Boom for Straight- and Delta-Wing Space Shuttle Orbiters. NASA TM X-62,030, April 9, 1971.

4. Hunton, Lynn W.; Hicks, Raymond M.; and Mendoza, Joel P.: Some Effects of Wing Planform on Sonic Boom. NASA TN D-7160, Jan. 1973.

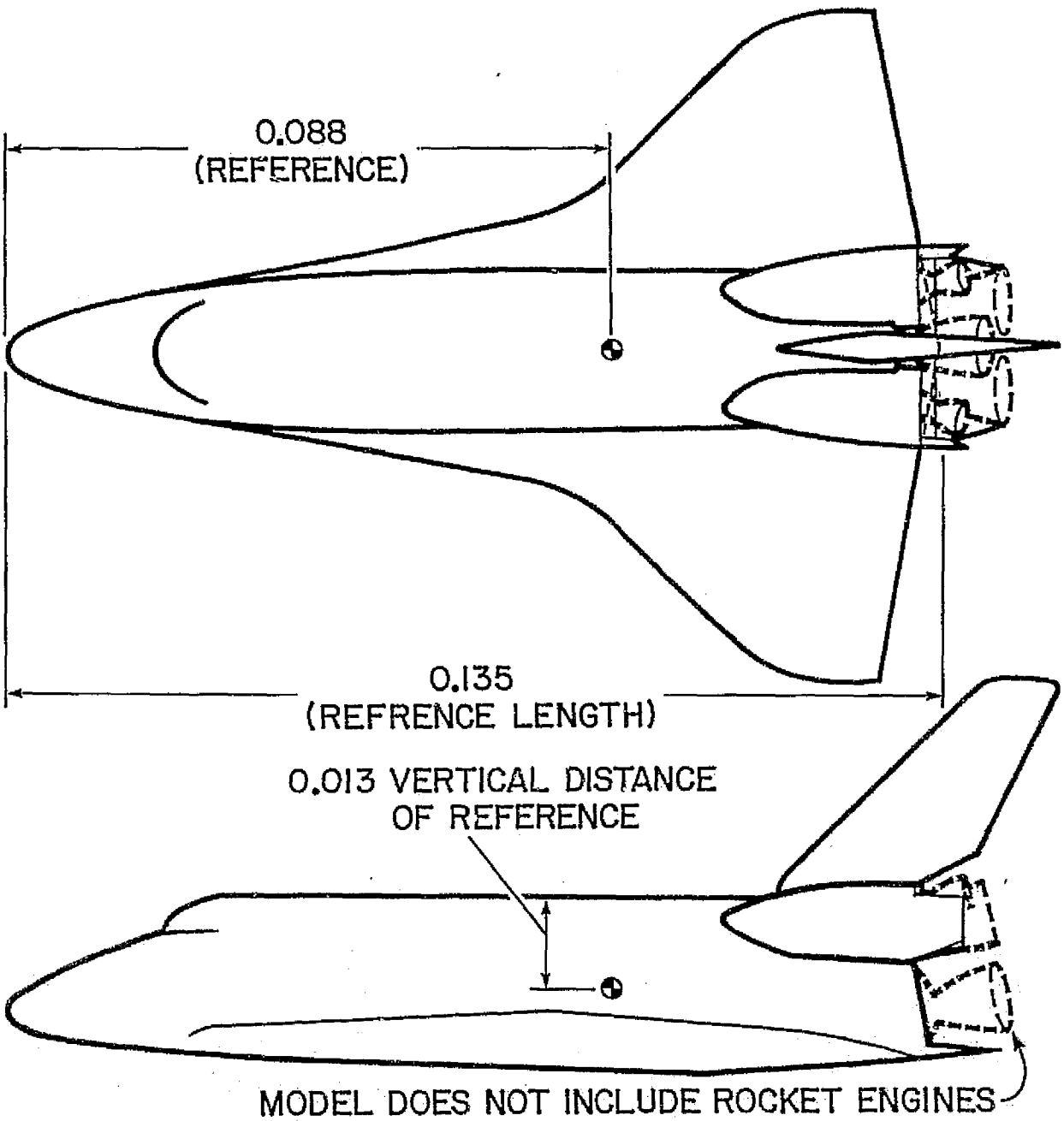

Figure 1.- The 0.0041-scale model of the latest space shuttle orbiter.

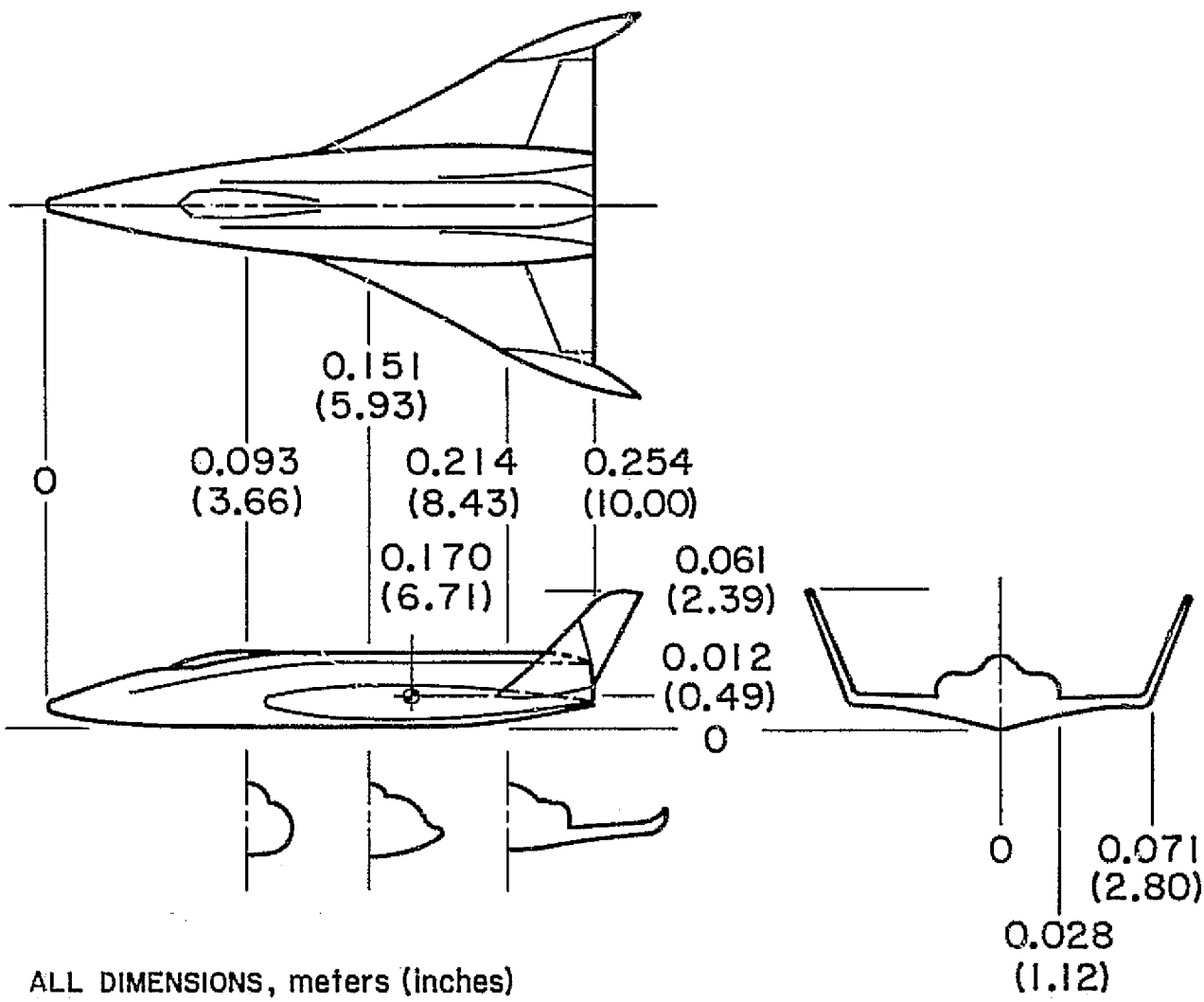

Figure 2.- Model of the delta wing orbiter tested in previous investigations.

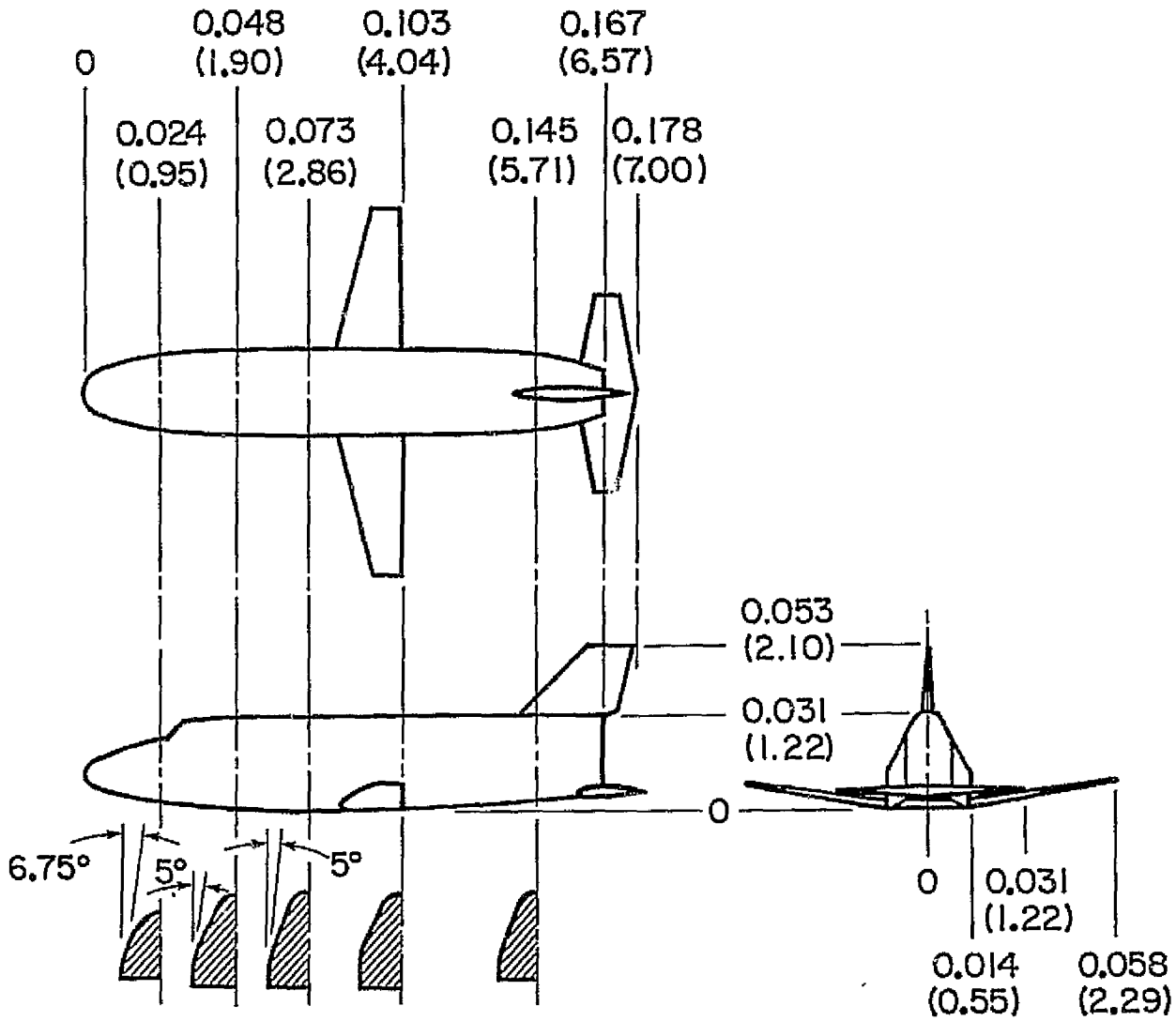

Figure 3.- Model of the straight wing orbiter tested in a previous investigation.

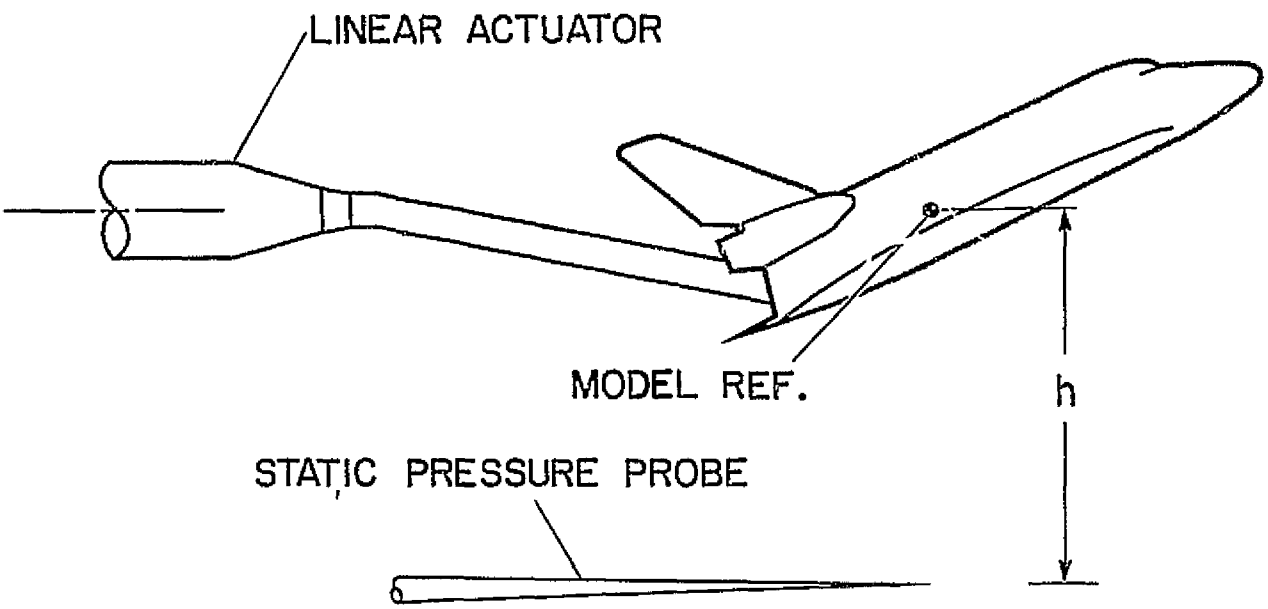

Figure 4.- General arrangement of the 0.0041-scale model and static pressure probe.

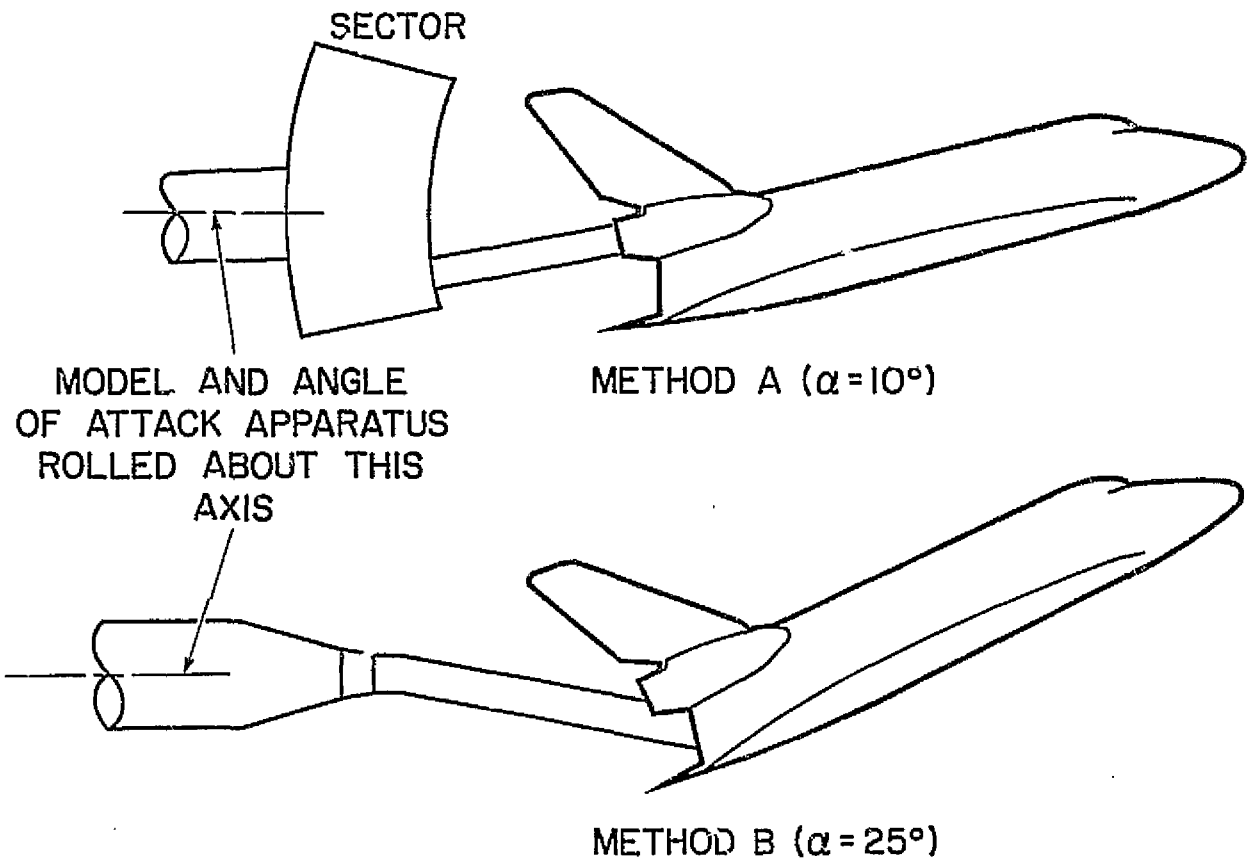

Figure 5.- Two methods for setting model angle of attack.

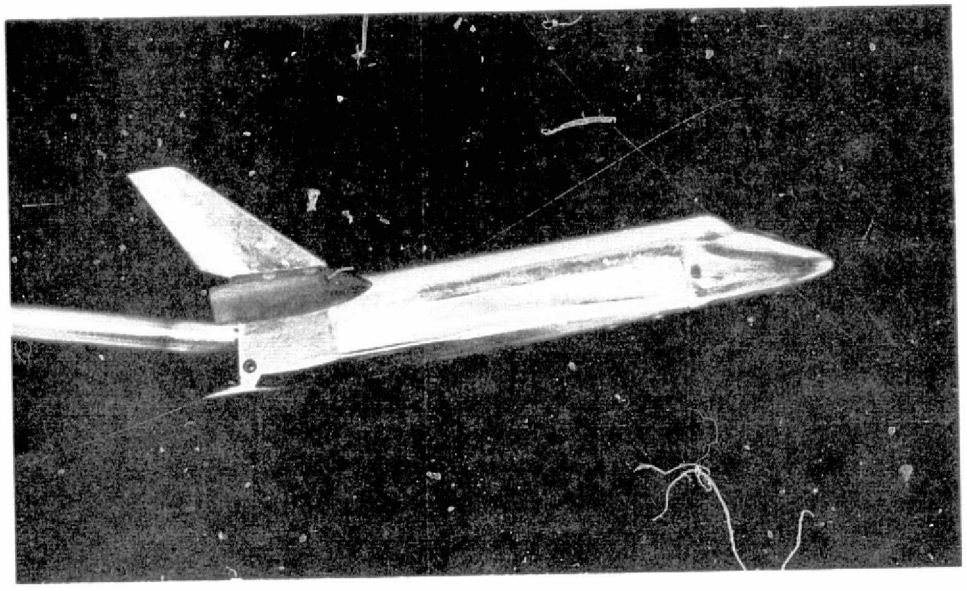

(a) $\alpha = 10°$.

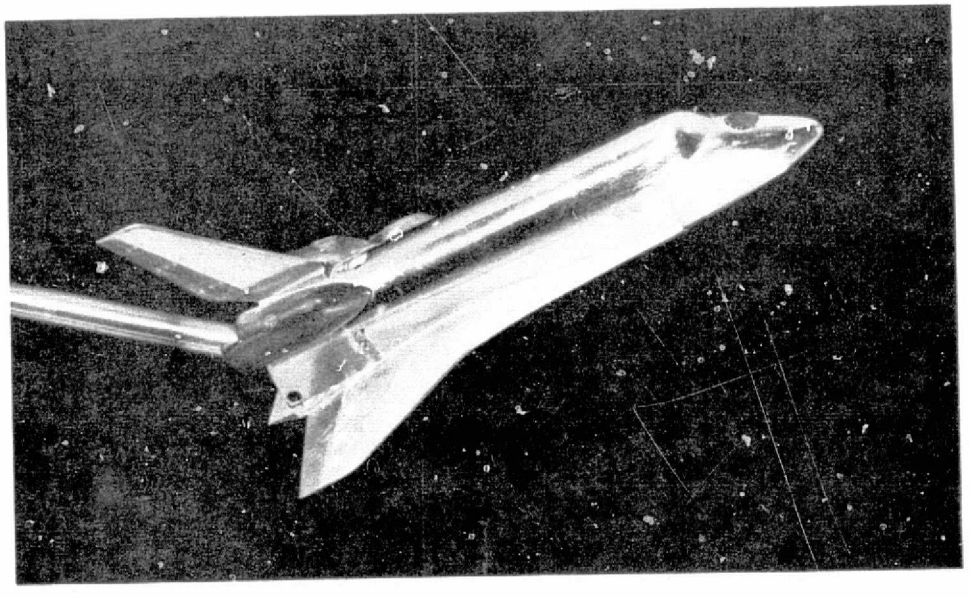

(b) $\alpha = 25°$.

Figure 6.- Installation photograph of the 0.0041-scale space shuttle model.

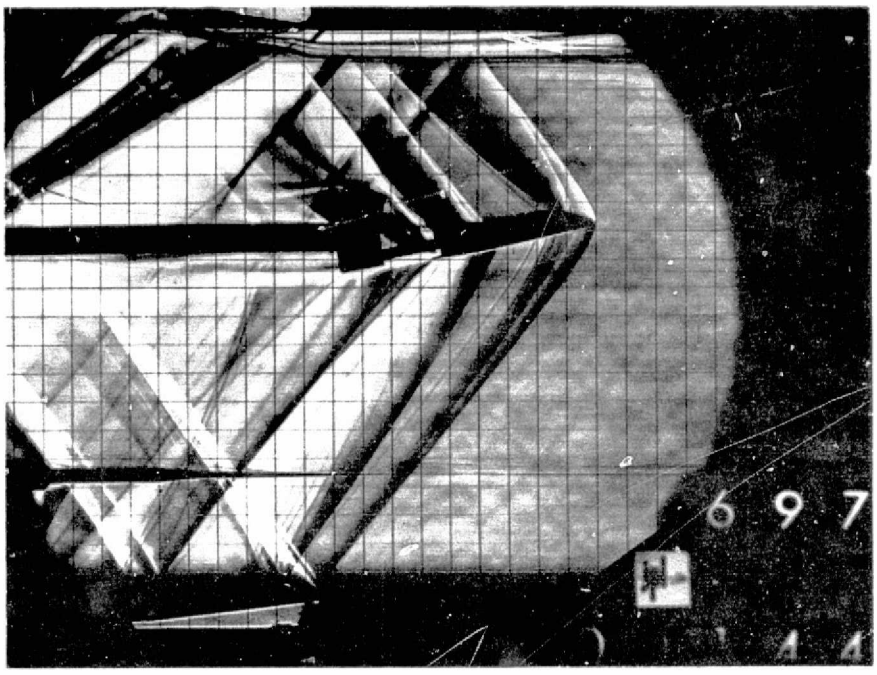

(a) $\phi = 0°$.

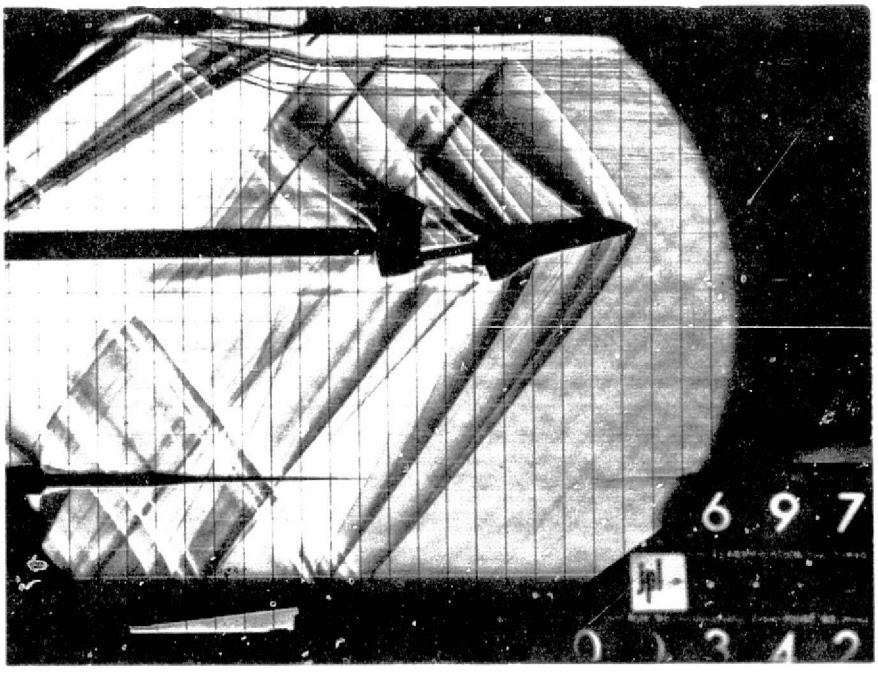

(b) $\phi = 30°$.

Figure 7.- Schlieren photographs, M = 1.30, $\alpha = 10°$.

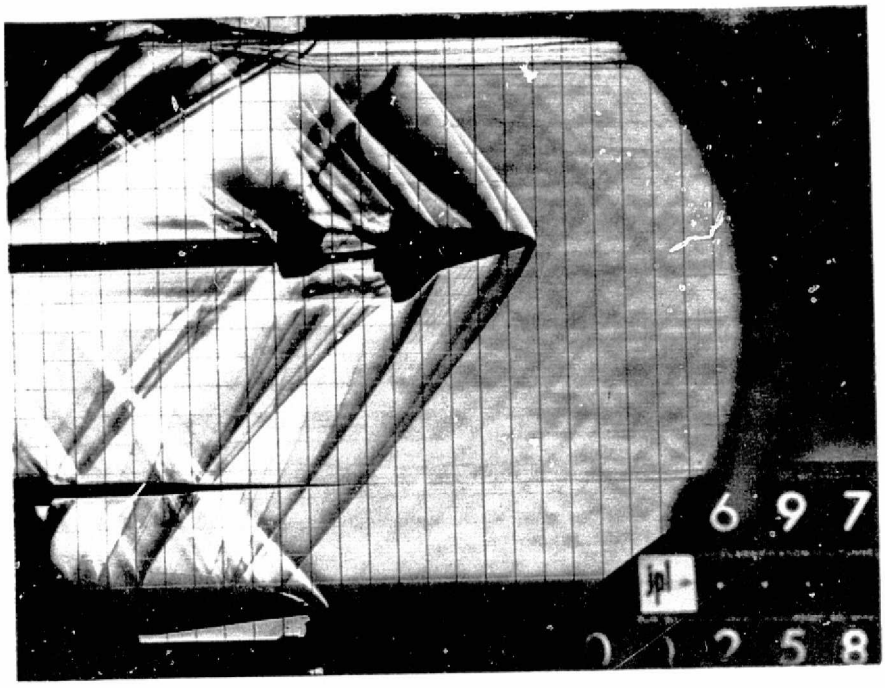

(c) $\phi = 60°$.

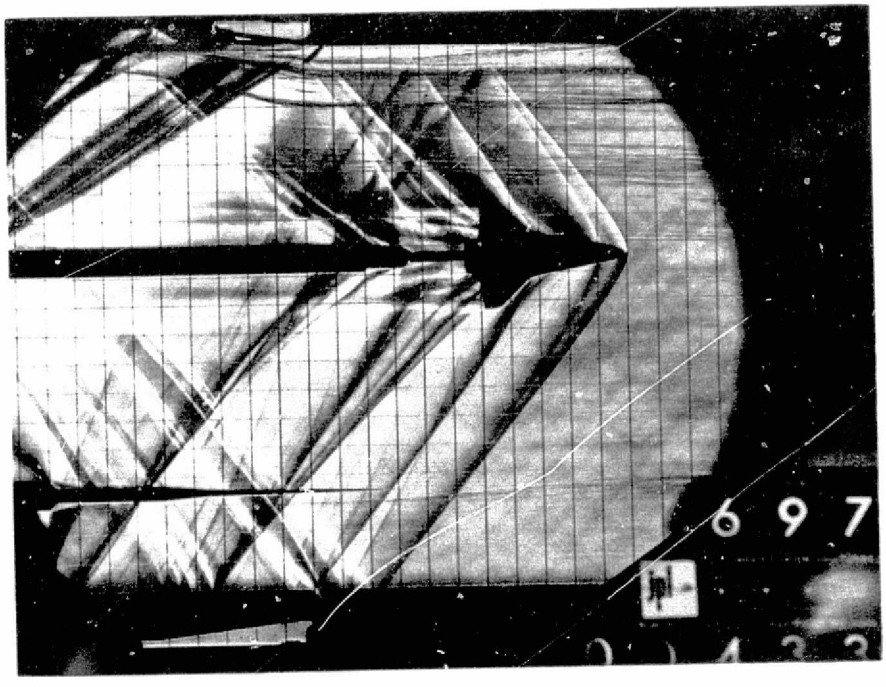

(d) $\phi = 90°$.

Figure 7.- Continued.

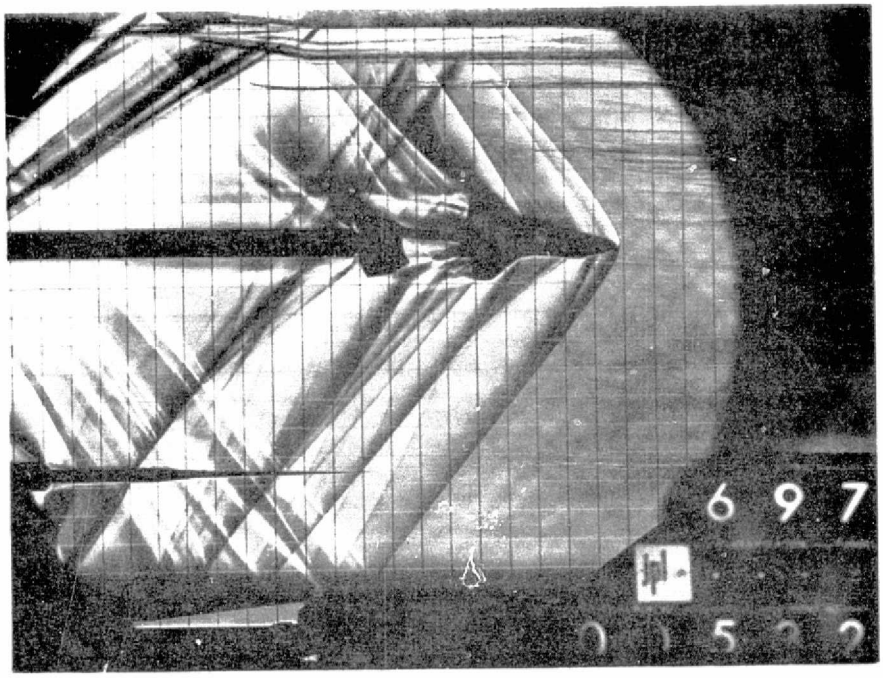

(e) $\phi = 120°$.

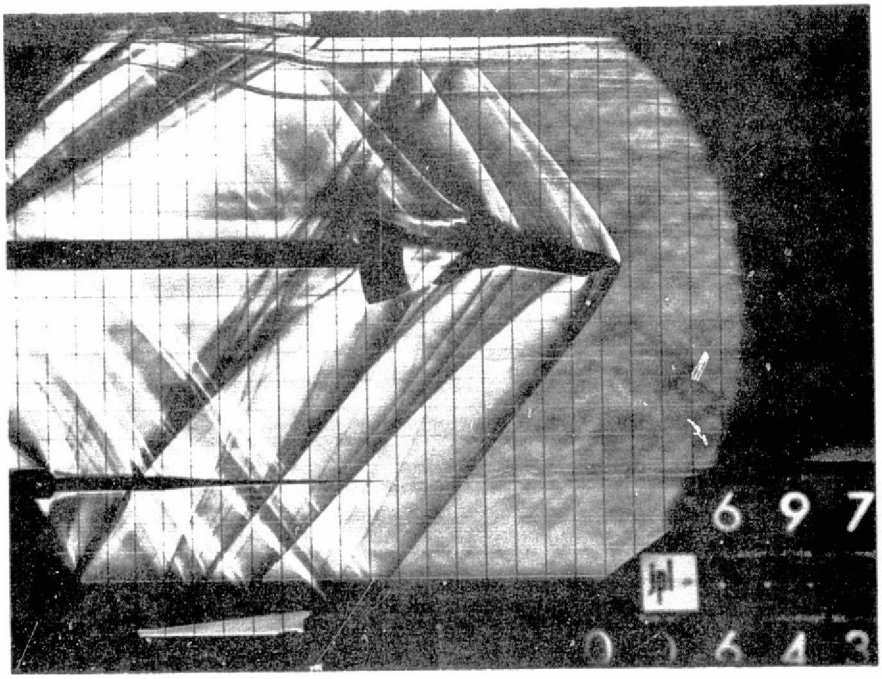

(f) $\phi = 150°$.

Figure 7.- Continued.

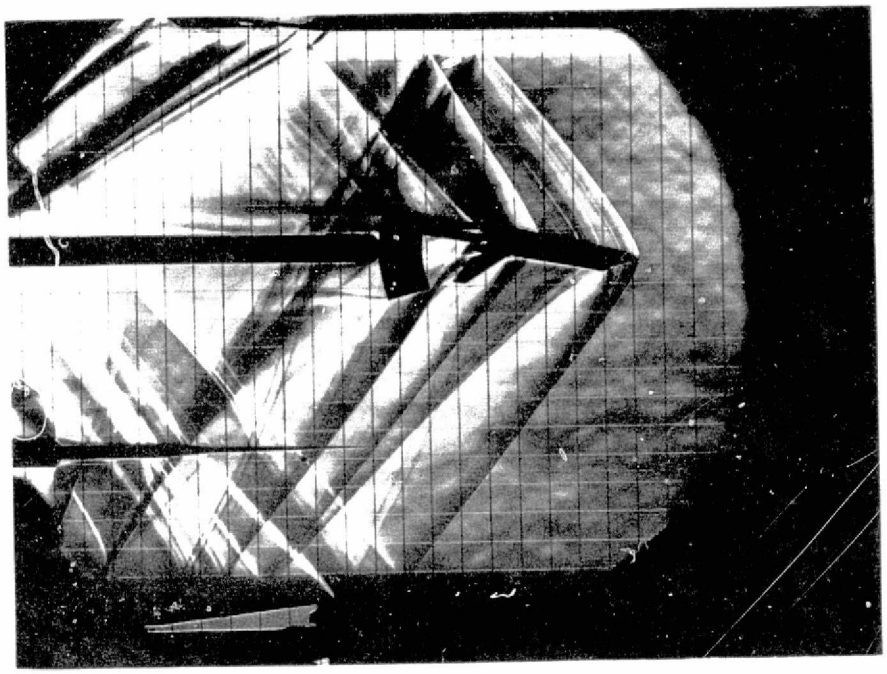

(g) $\phi = 180°$.

Figure 7.- Concluded.

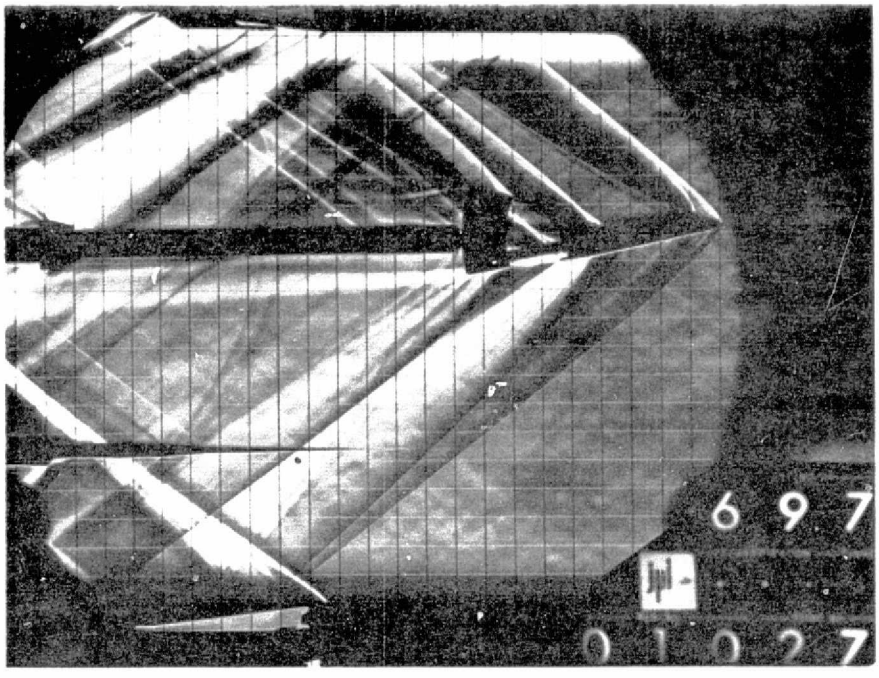

(a) $\phi = 0°$.

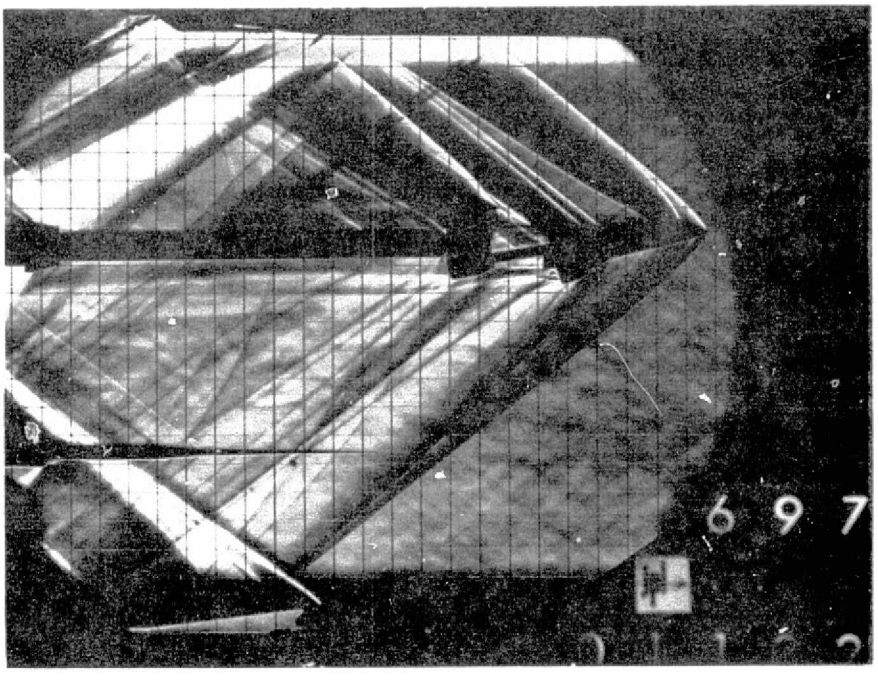

(b) $\phi = 30°$.

Figure 8.- Schlieren photographs, $M = 1.64$, $\alpha = 10°$.

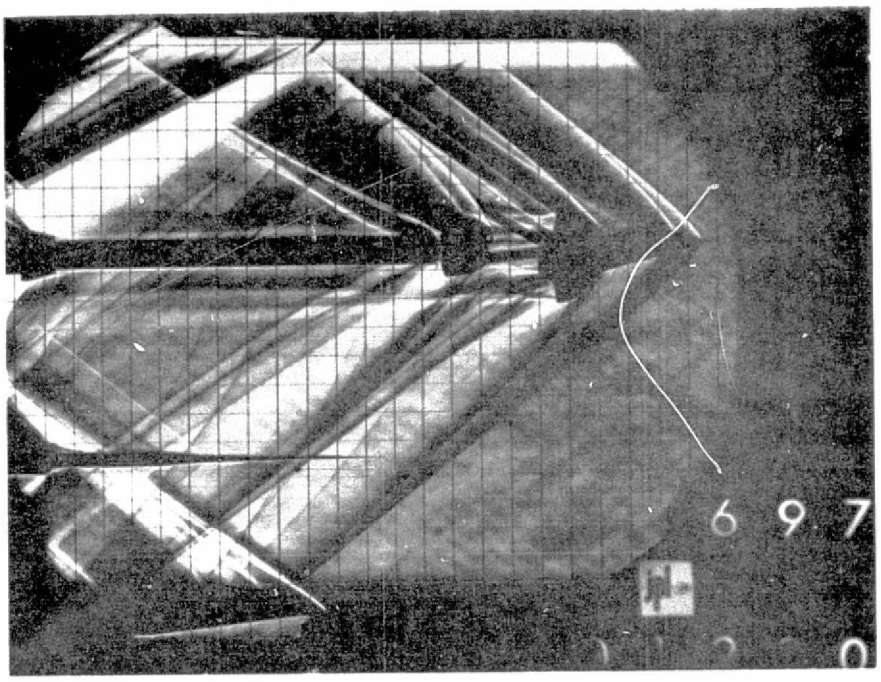

(c) $\phi = 60°$.

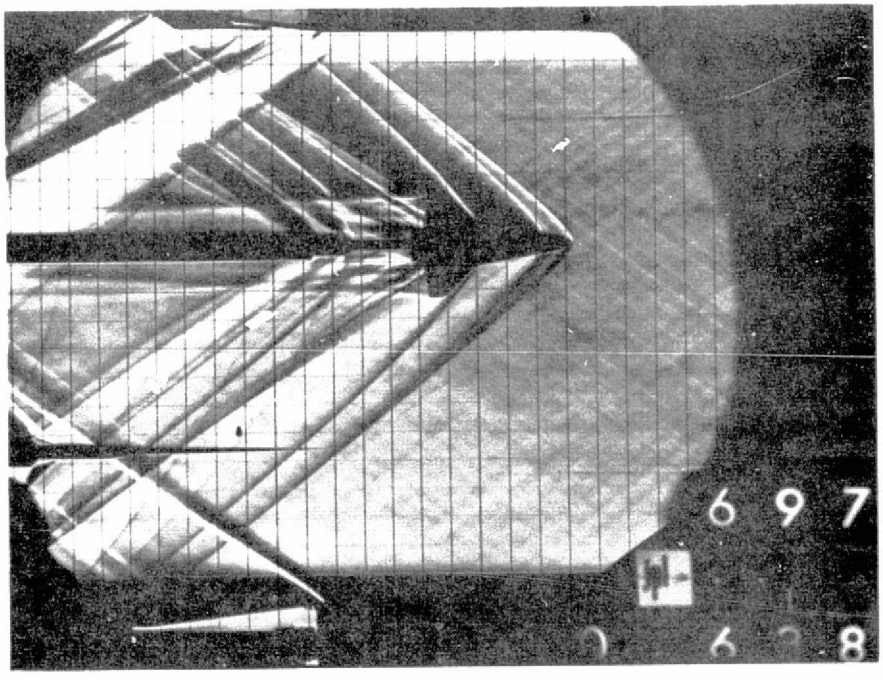

(d) $\phi = 90°$.

Figure 8.- Continued.

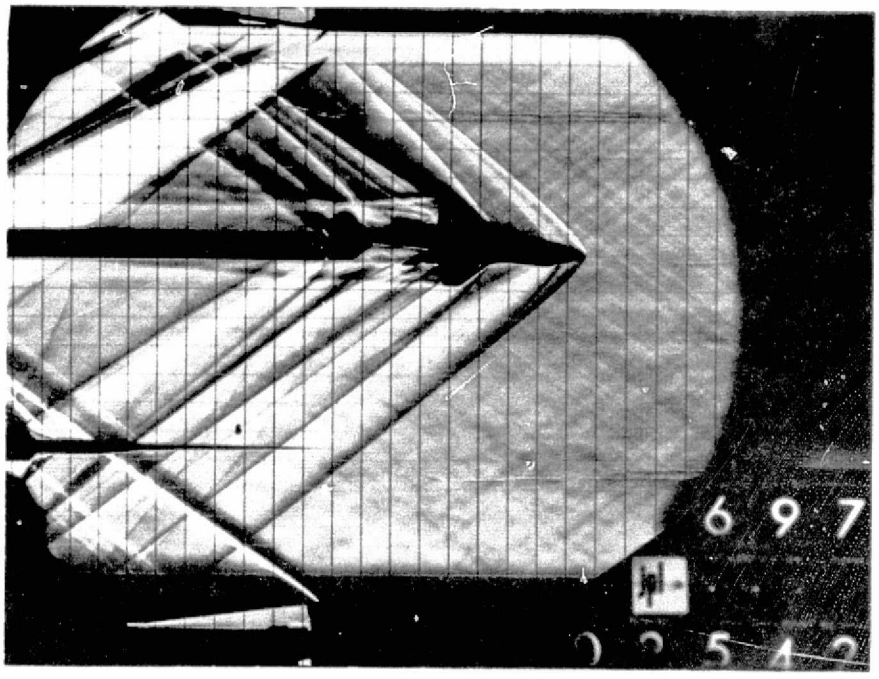

(e) ϕ = 120°.

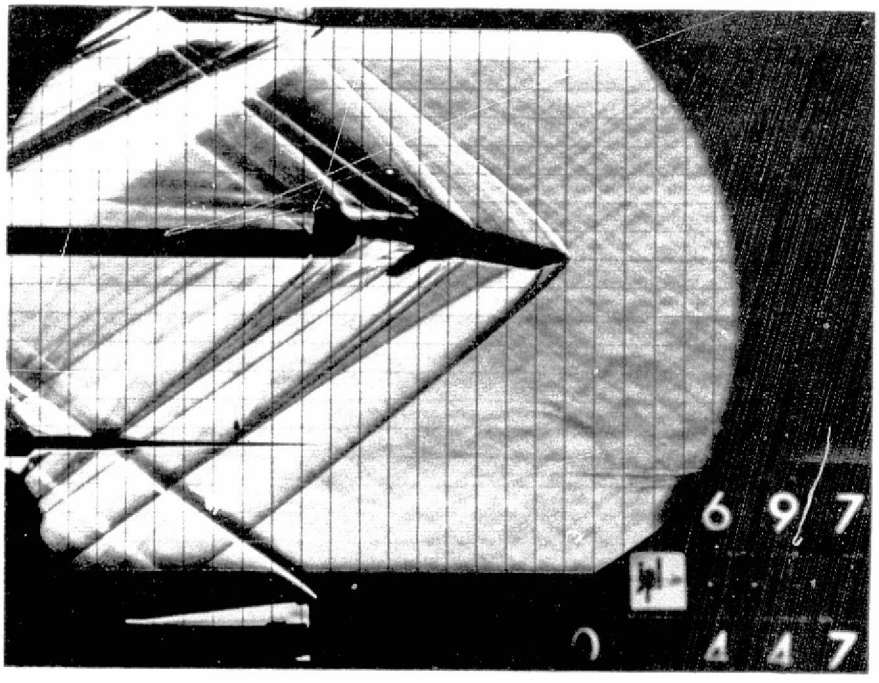

(f) ϕ = 150°.

Figure 8.- Continued.

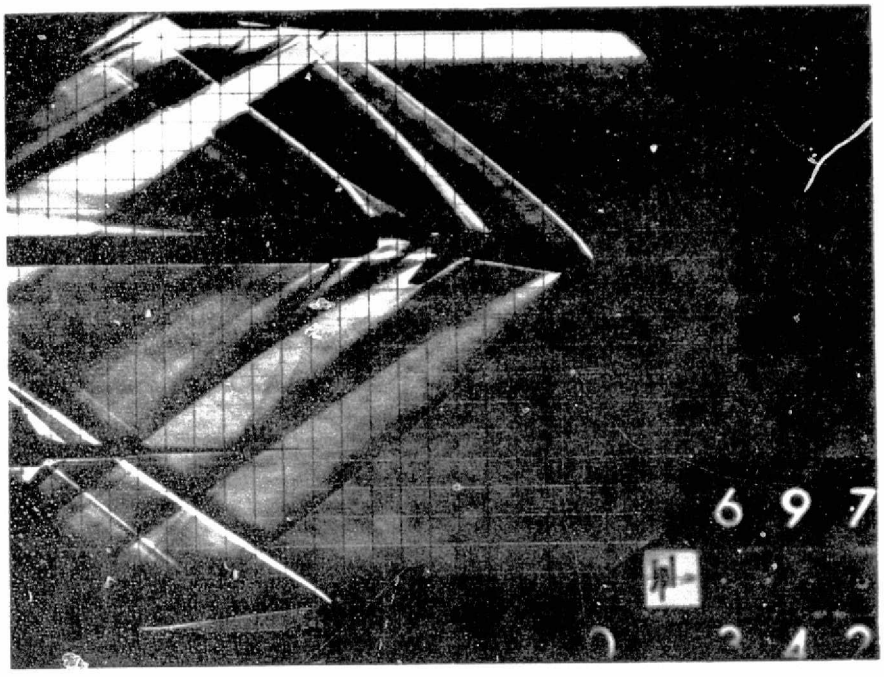

(g) $\phi = 180°$.

Figure 8.- Concluded.

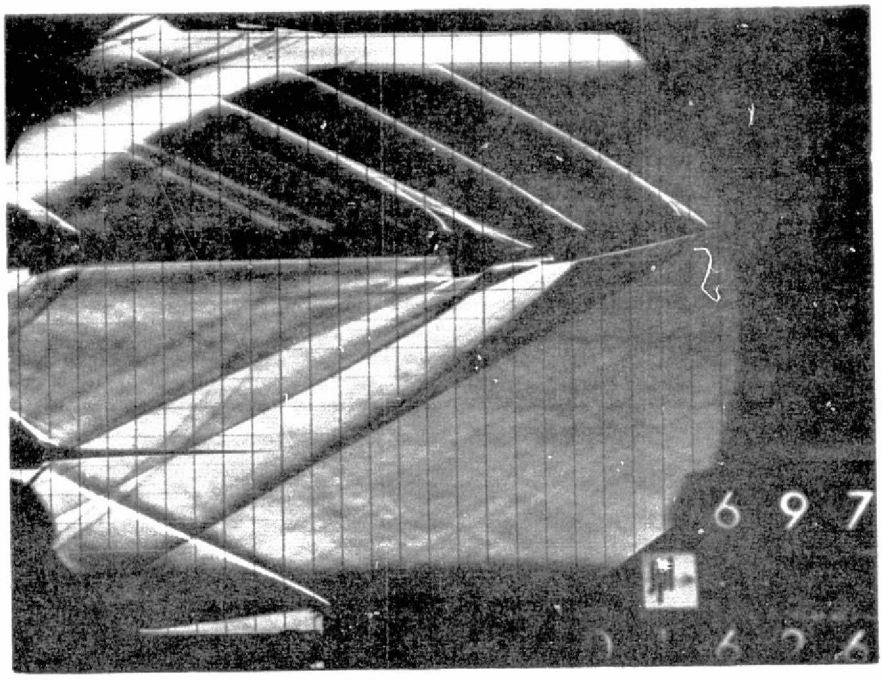

(a) $\phi = 0°$.

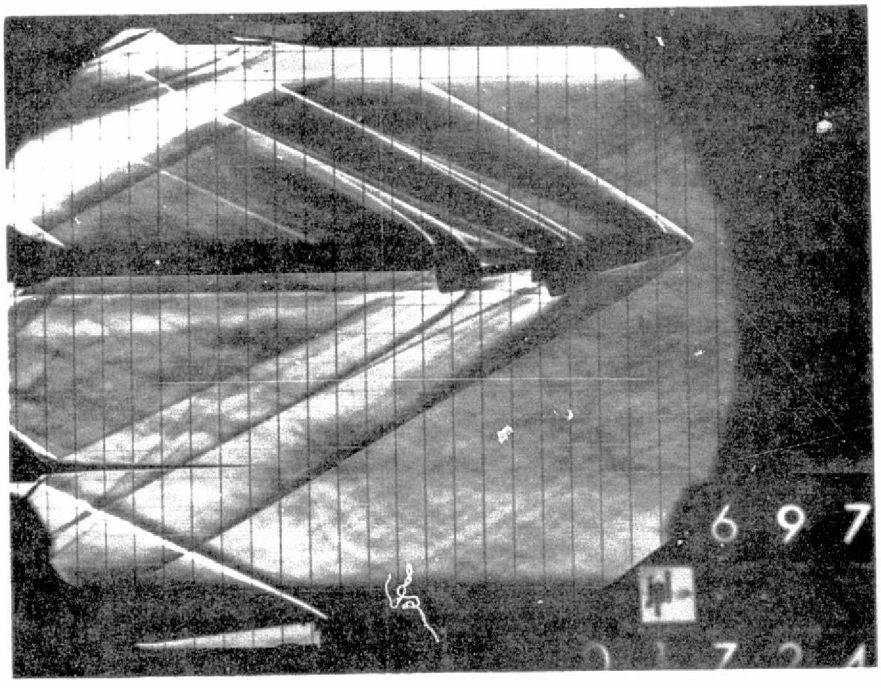

(b) $\phi = 30°$.

Figure 9.- Schlieren photographs, $M = 2.21$, $\alpha = 10°$.

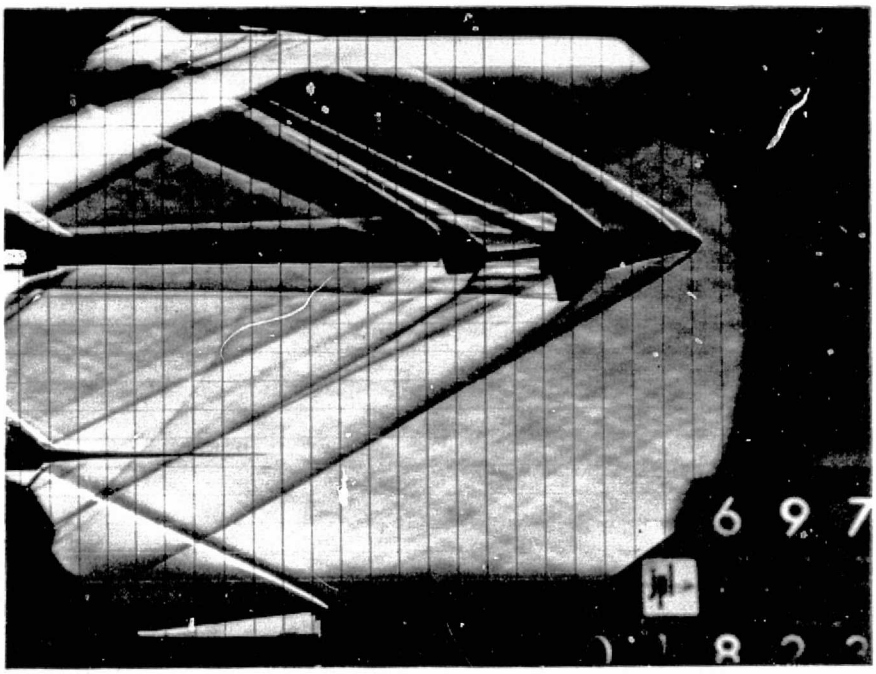

(c) $\phi = 60°$.

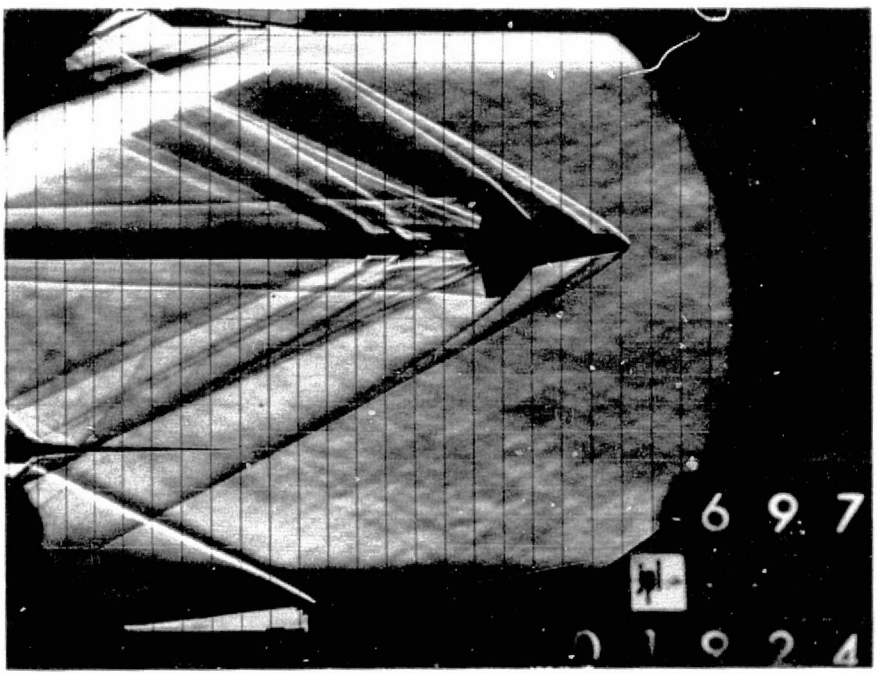

(d) $\phi = 90°$.

Figure 9.- Continued.

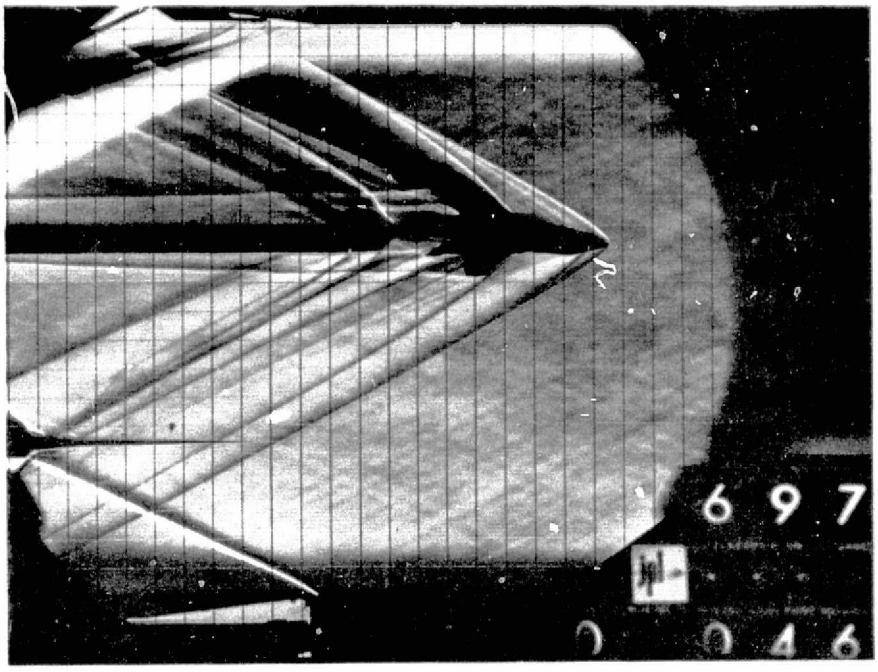

(e) $\phi = 120°$.

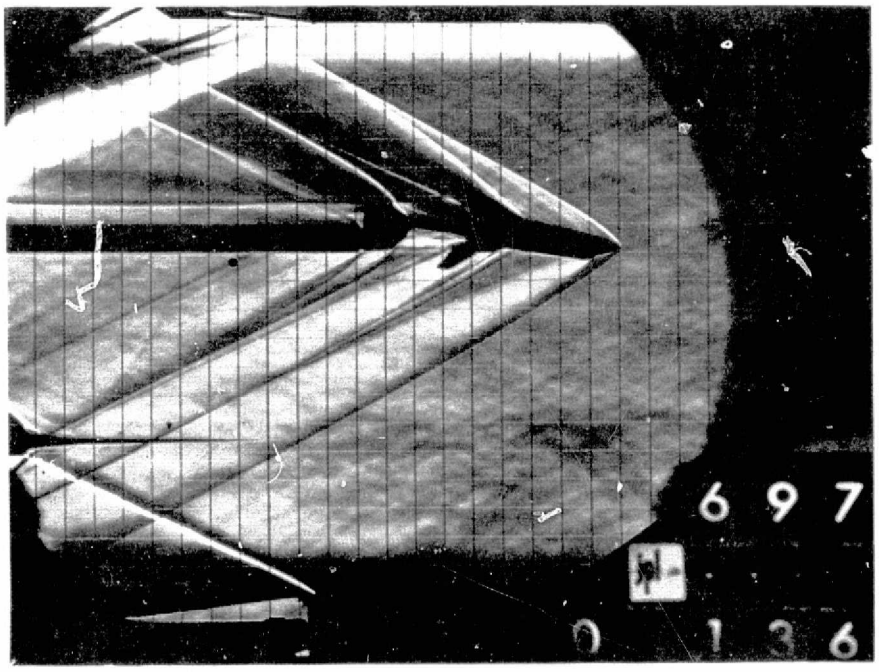

(f) $\phi = 150°$.

Figure 9.- Continued.

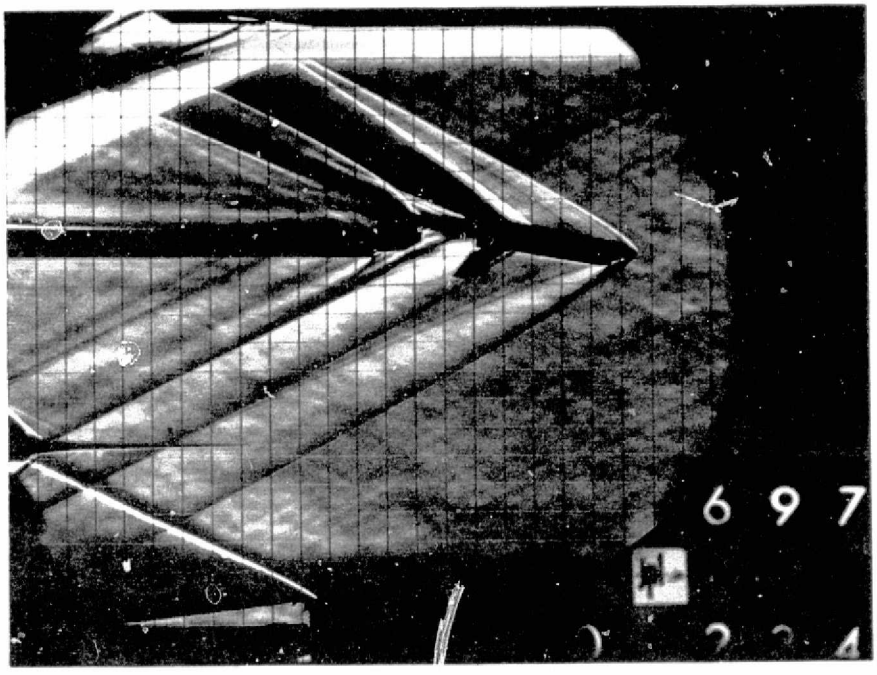

(g) $\phi = 180°$.

Figure 9.- Concluded.

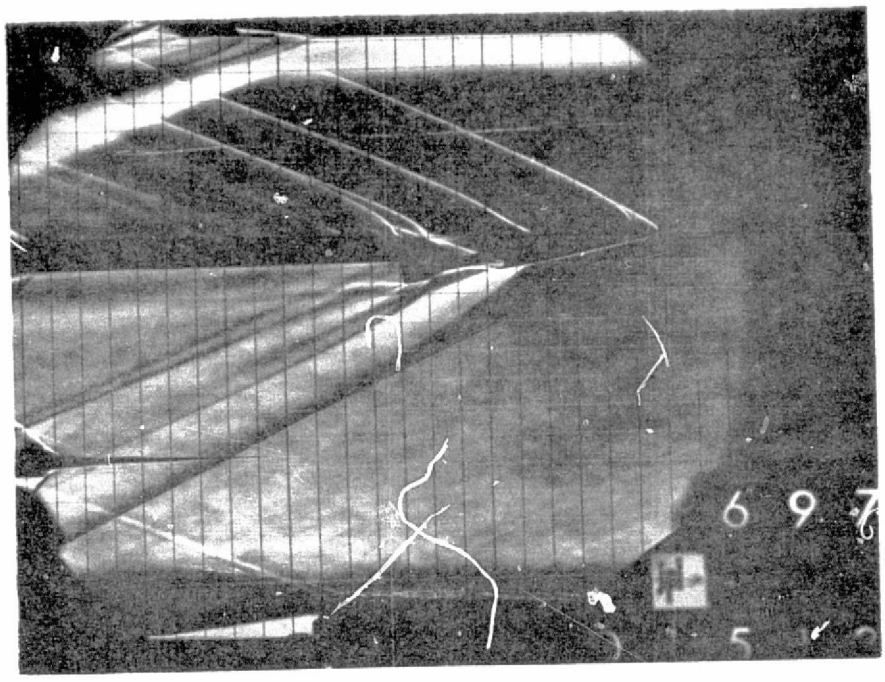

(a) $\phi = 0°$.

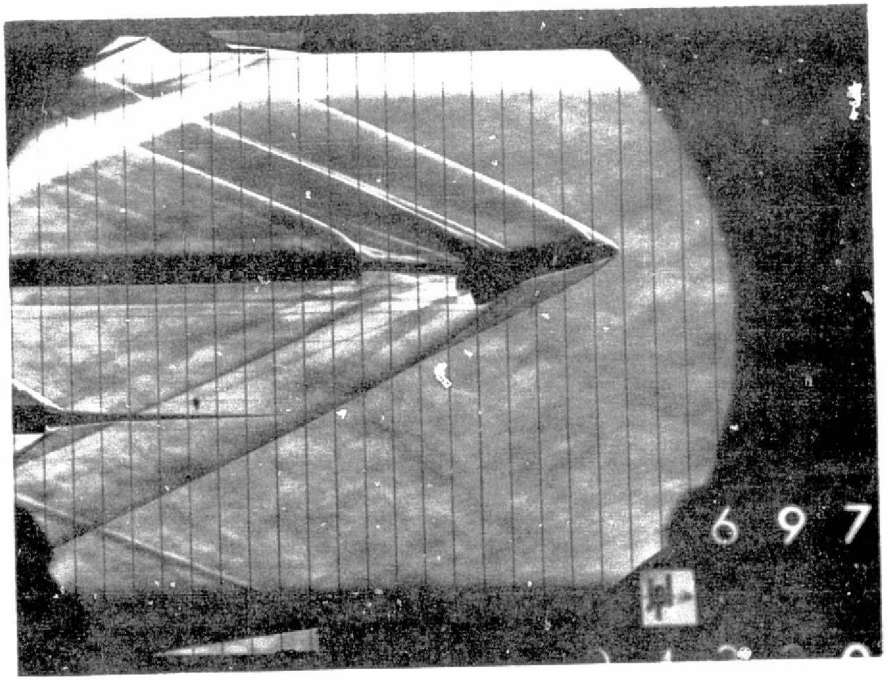

(b) $\phi = 30°$.

Figure 10.- Schlieren photographs, $M = 2.61$, $\alpha = 10°$.

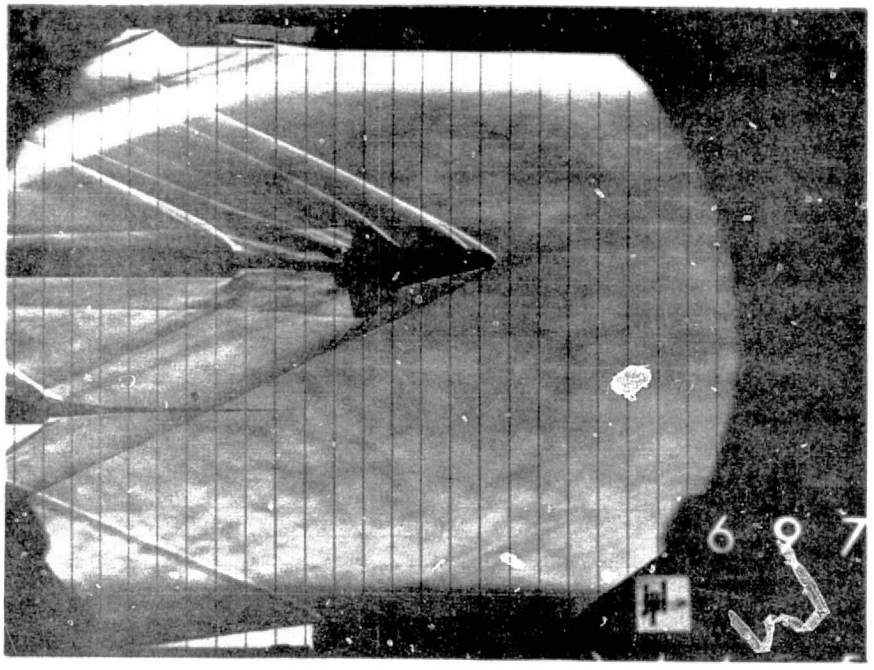

(c) $\phi = 60°$.

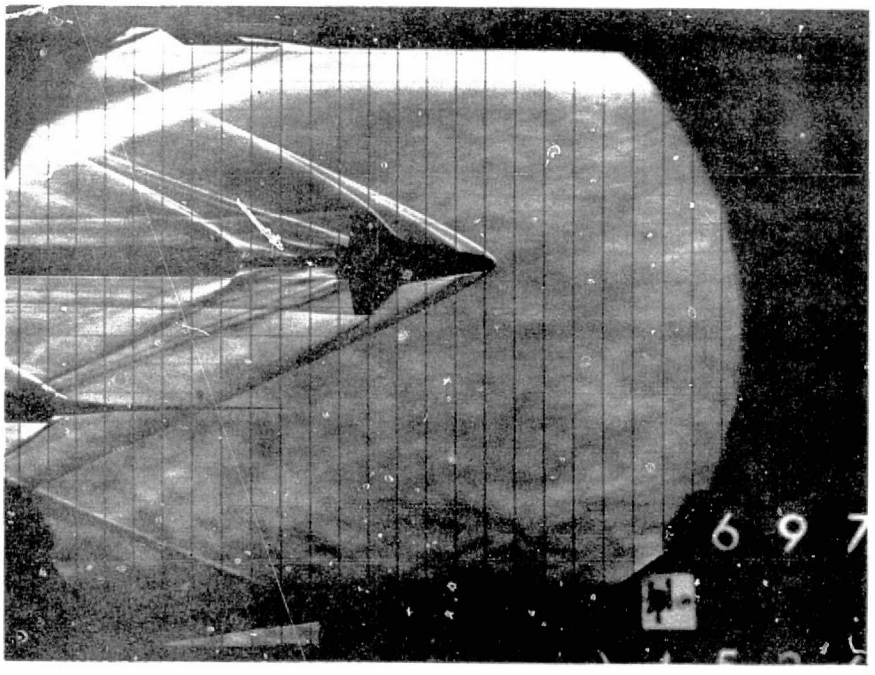

(d) $\phi = 90°$.

Figure 10.- Continued.

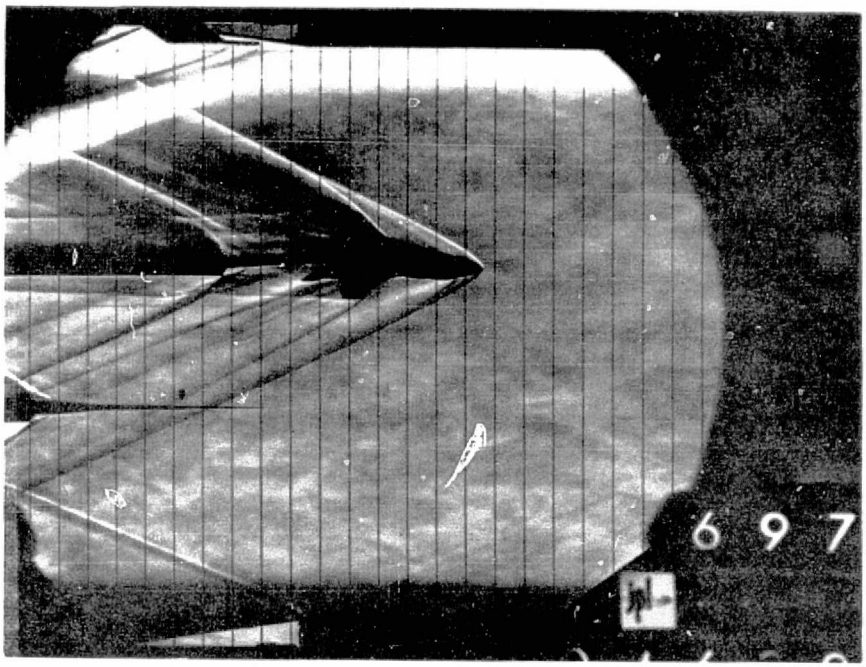

(e) $\phi = 120°$.

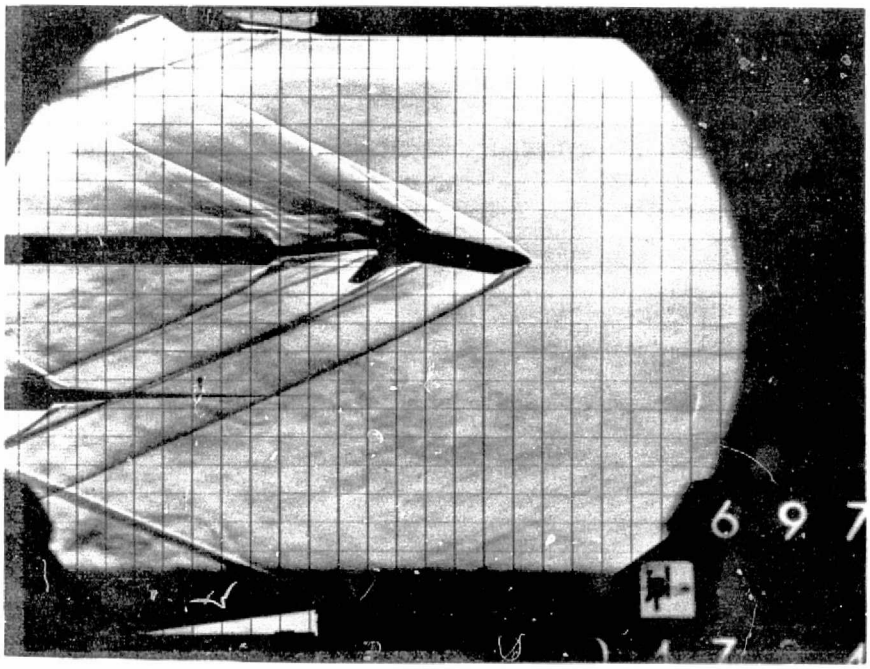

(f) $\phi = 150°$.

Figure 10.- Continued.

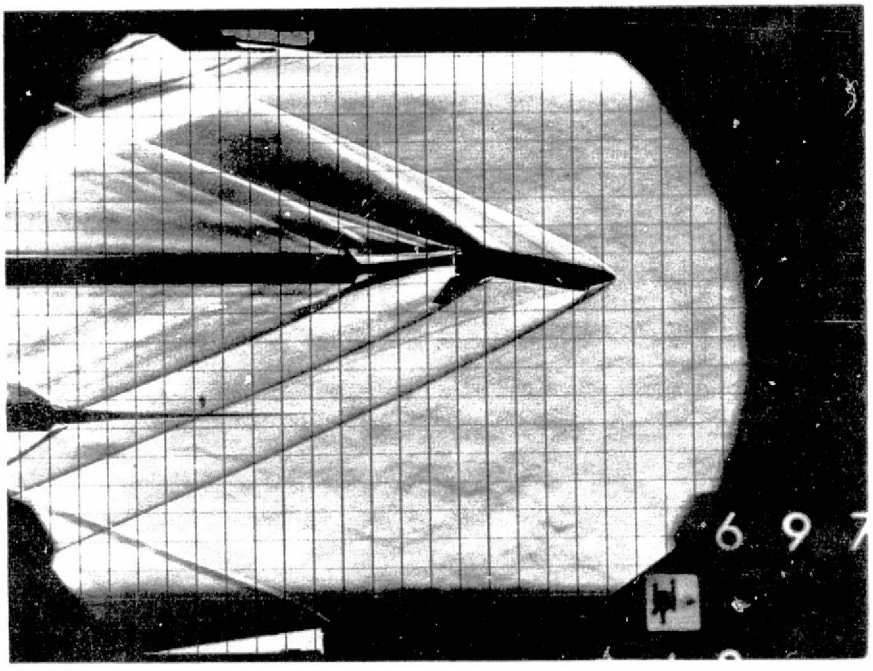

(g) $\phi = 180°$.

Figure 10.- Concluded.

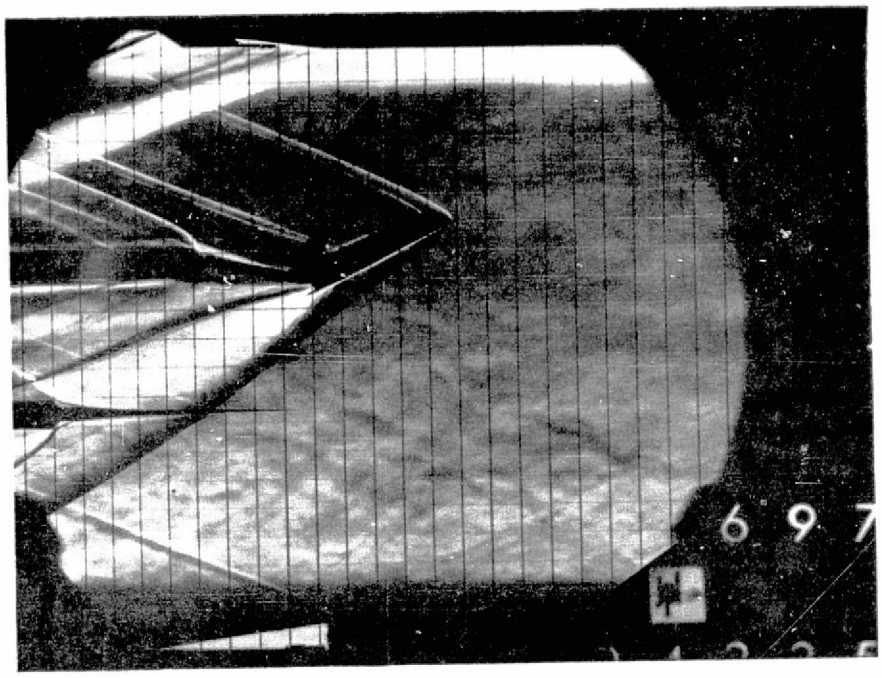

(a) $\phi = 0°$.

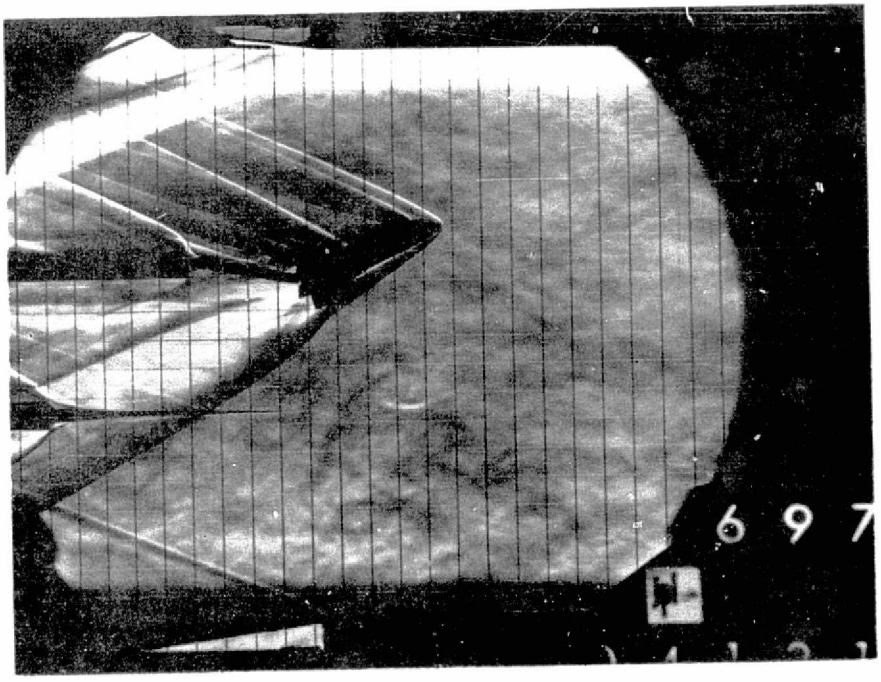

(b) $\phi = 30°$.

Figure 11.- Schlieren photographs, M = 2.61, $\alpha = 25°$.

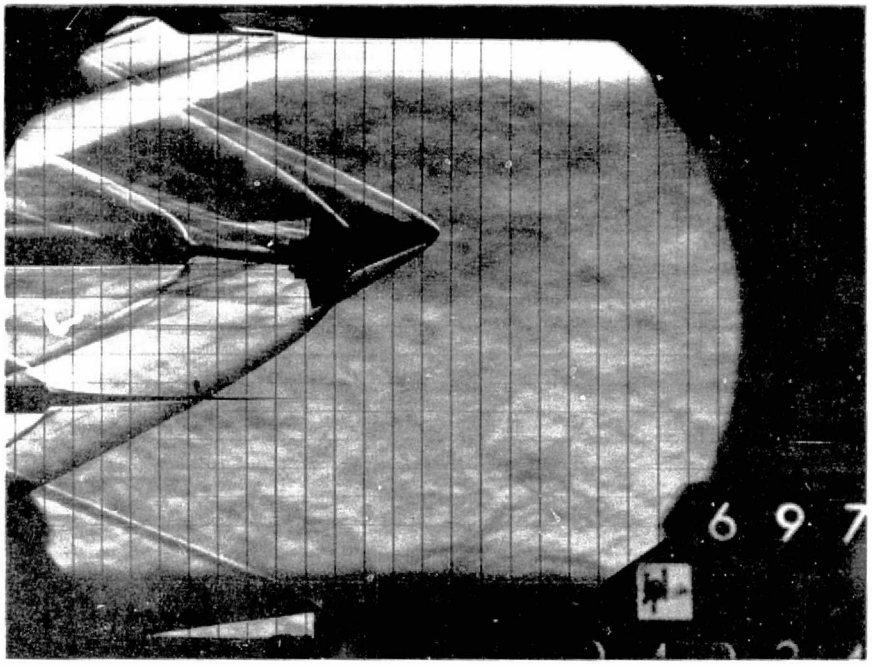

(c) $\phi = 60°$.

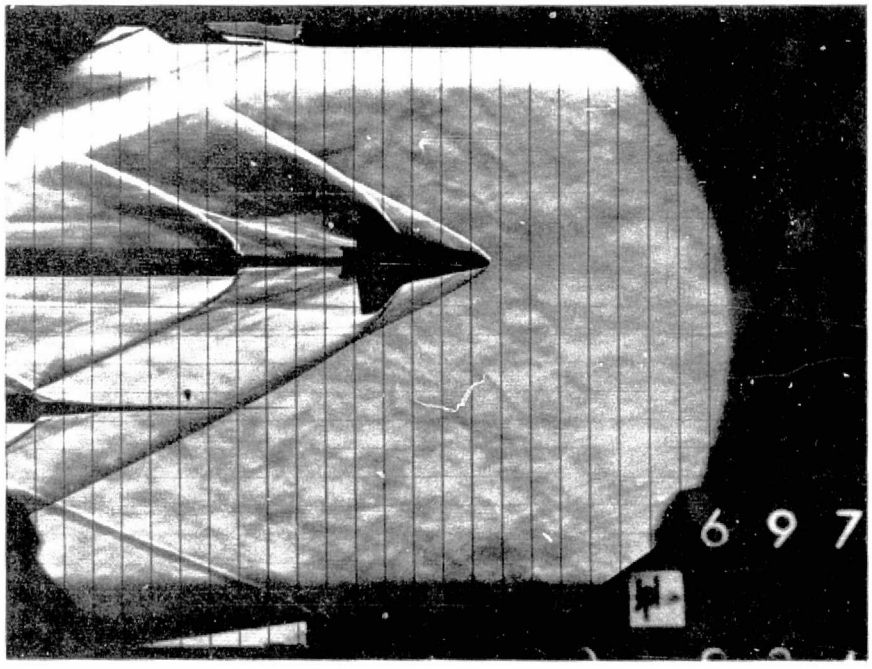

(d) $\phi = 90°$.

Figure 11.- Continued.

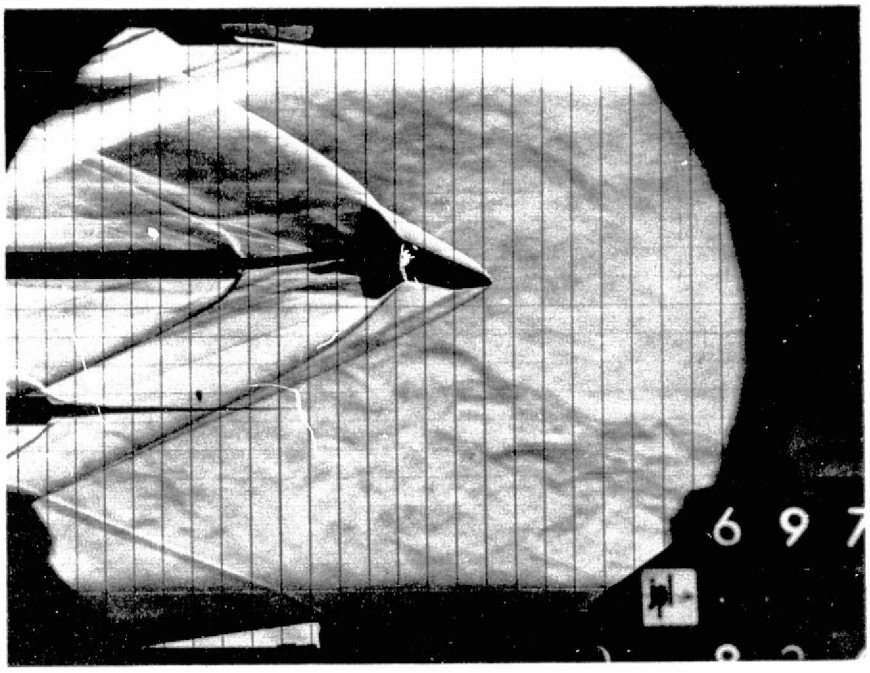

(e) ϕ = 120°.

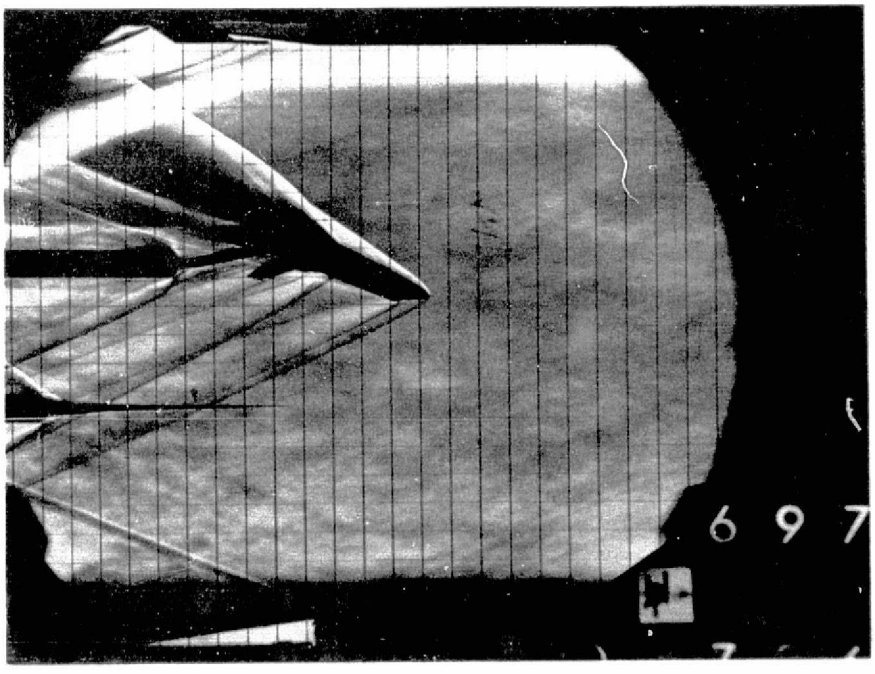

(f) ϕ = 150°.

Figure 11.- Continued.

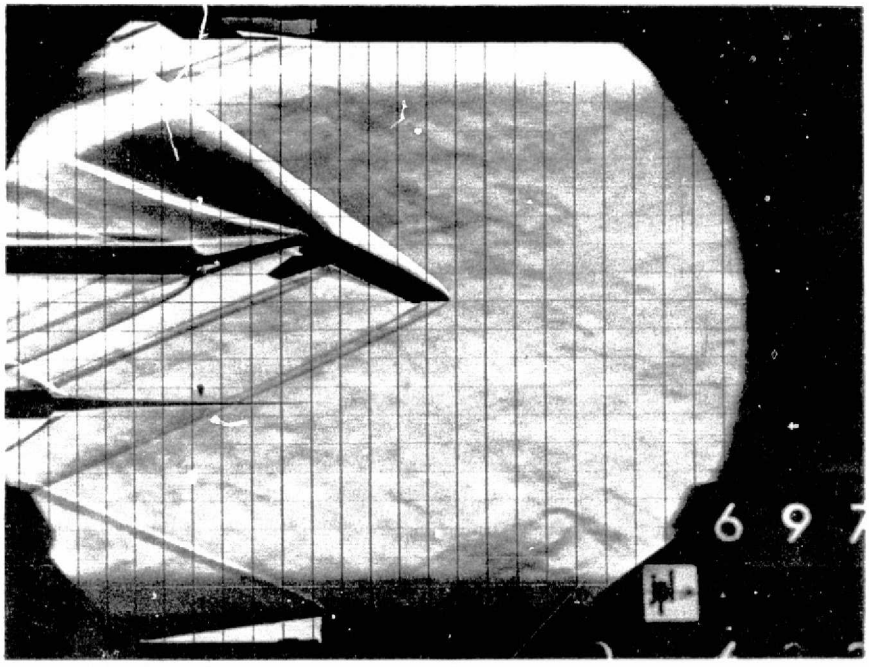

(g) $\phi = 180°$.

Figure 11.- Concluded.

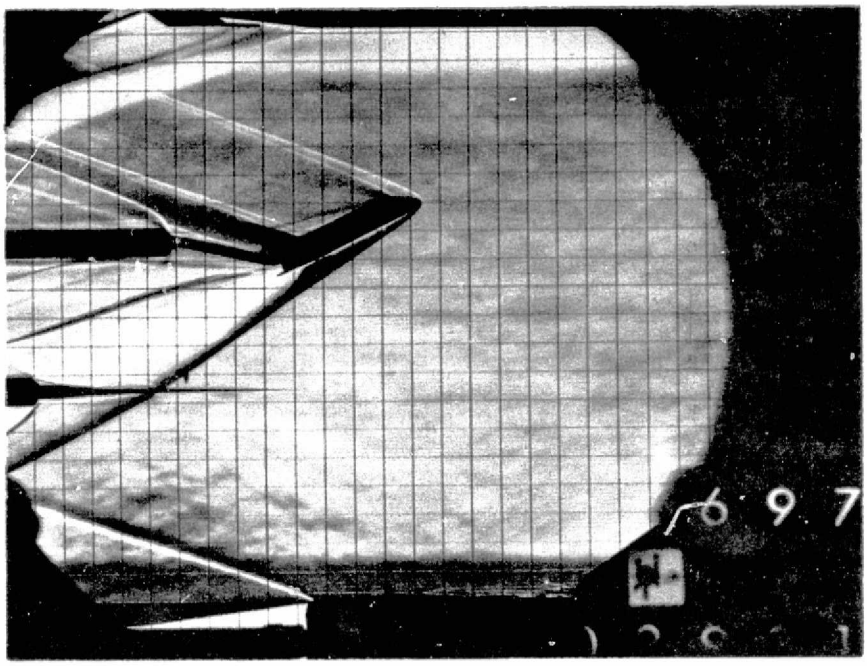

(a) $\phi = 0°$.

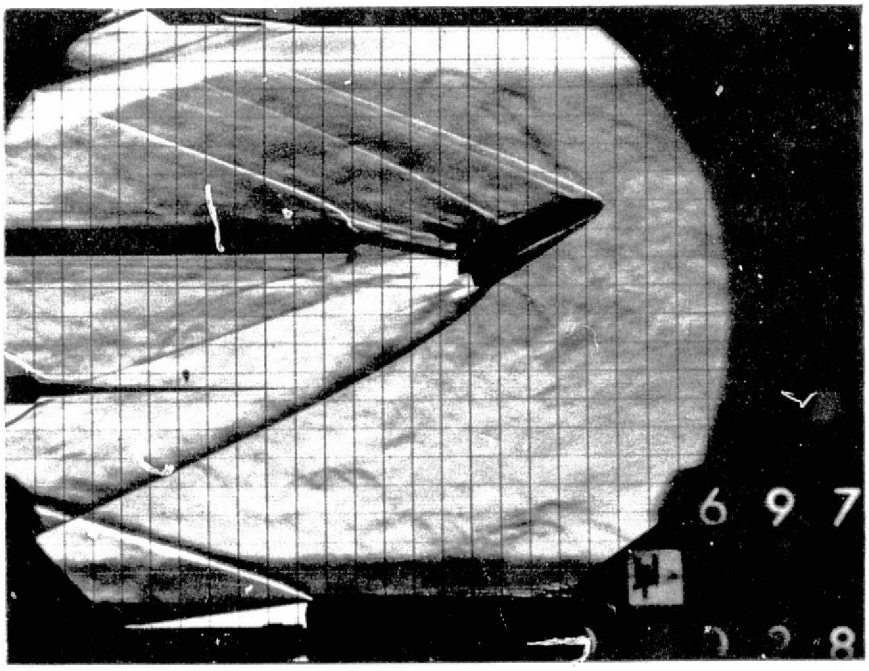

(b) $\phi = 30°$.

Figure 12.- Schlieren photographs, M = 3.02, $\alpha = 25°$.

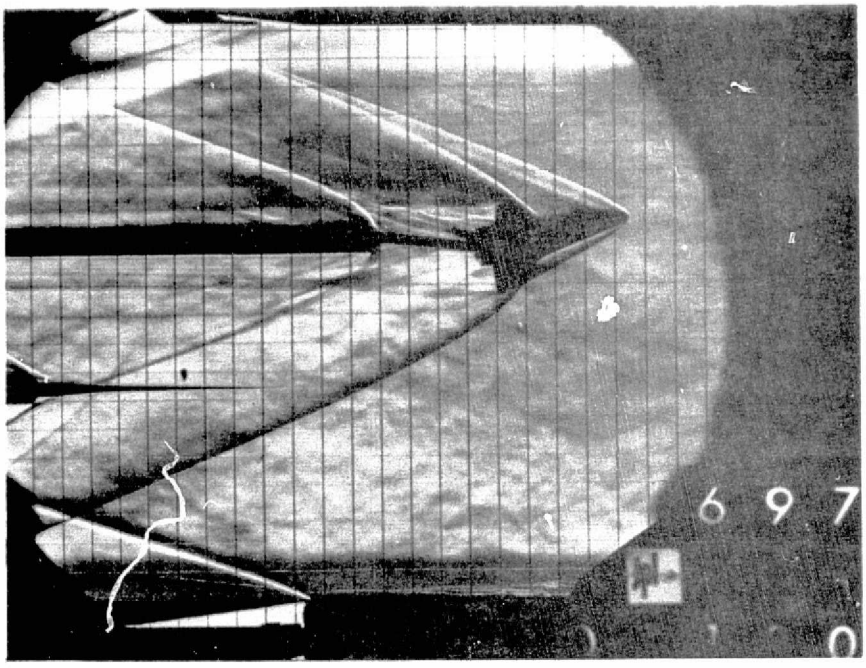

(c) $\phi = 60°$.

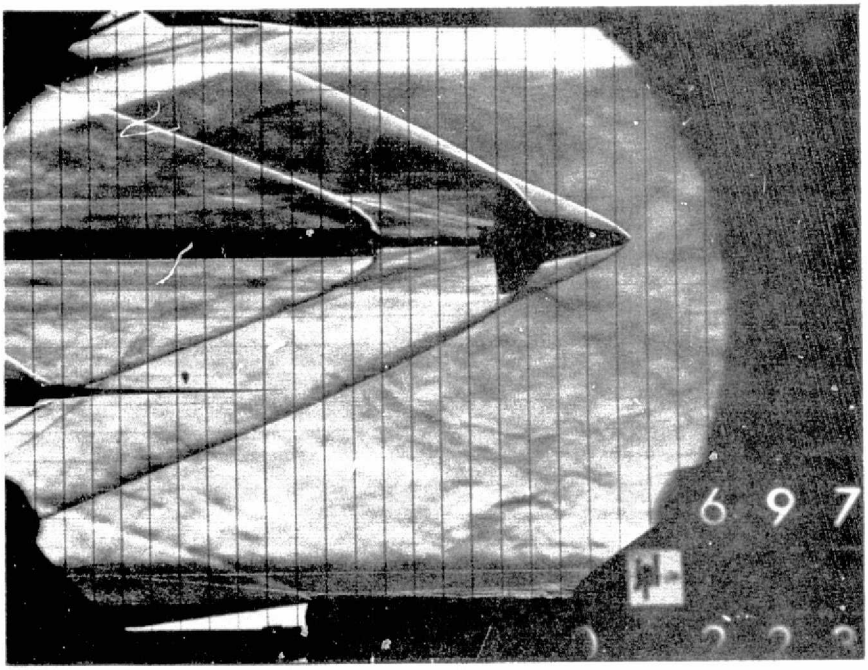

(d) $\phi = 90°$.

Figure 12.- Continued.

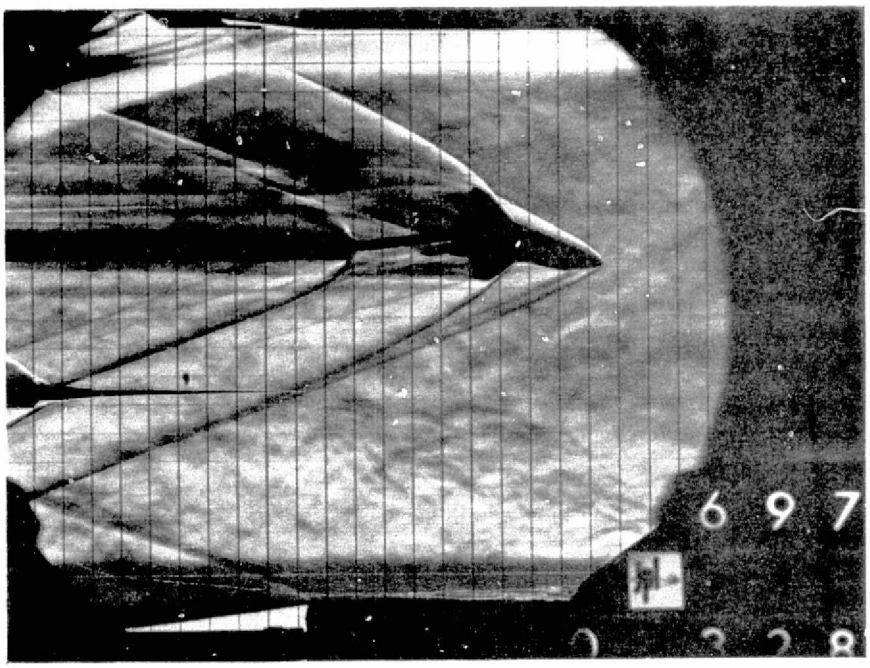

(e) $\phi = 120°$.

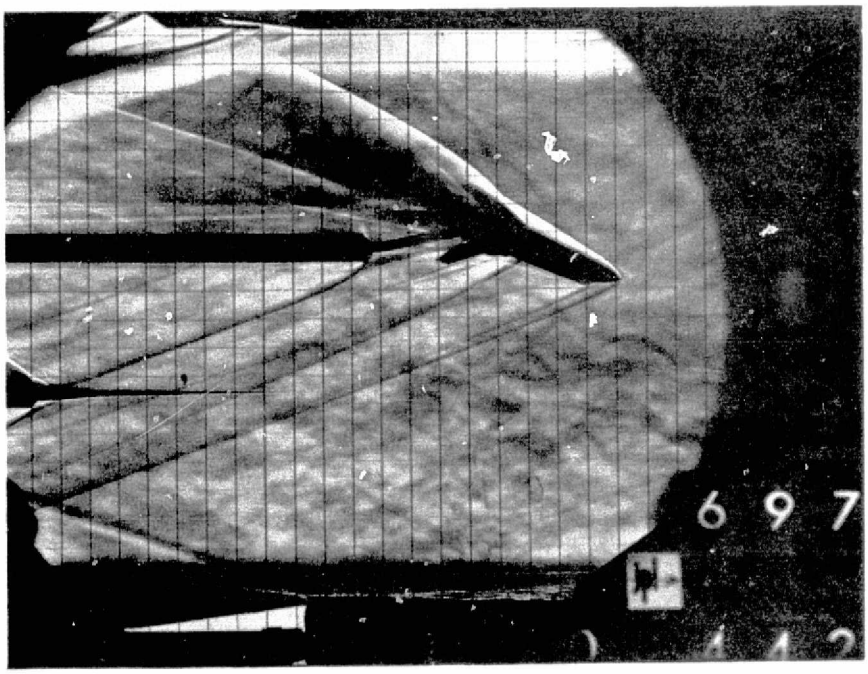

(f) $\phi = 150°$.

Figure 12.- Continued.

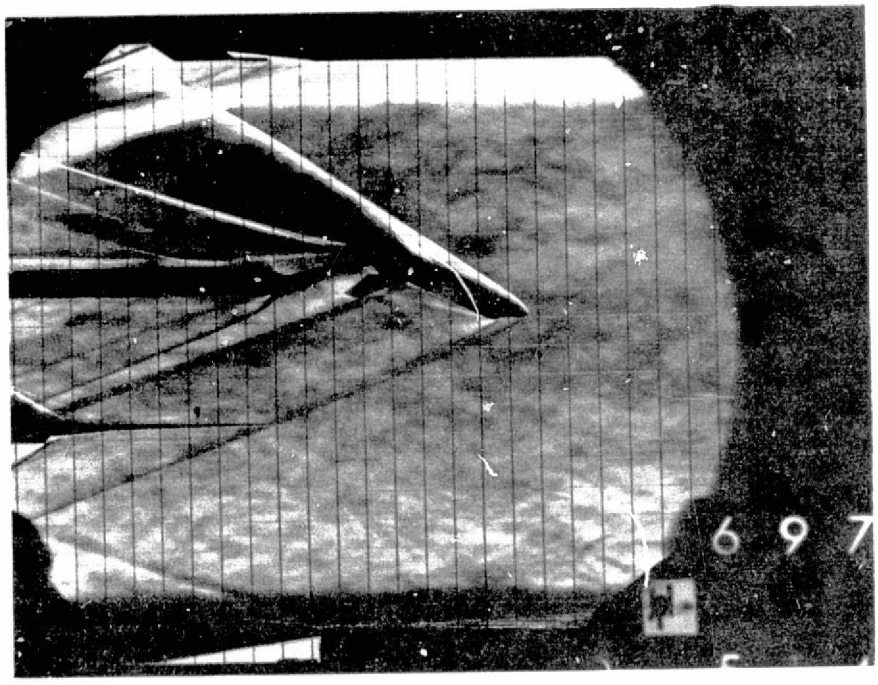

(g) $\phi = 180°$.

Figure 12.- Concluded.

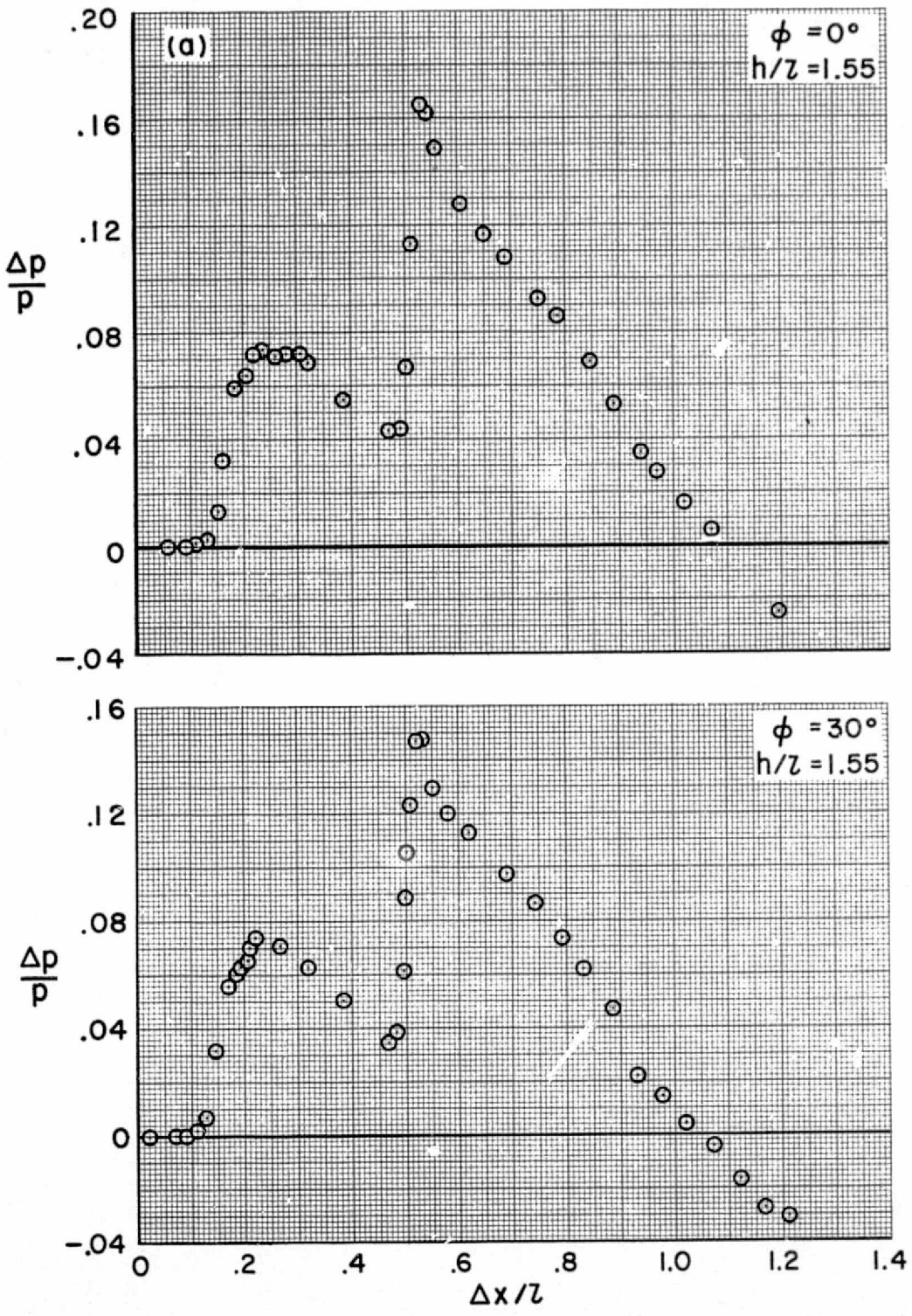

(a) $\phi = 0°, 30°$.

Figure 13.- Pressure signatures for the 0.0041-scale orbiter model, M = 1.3, $\alpha = 10°$.

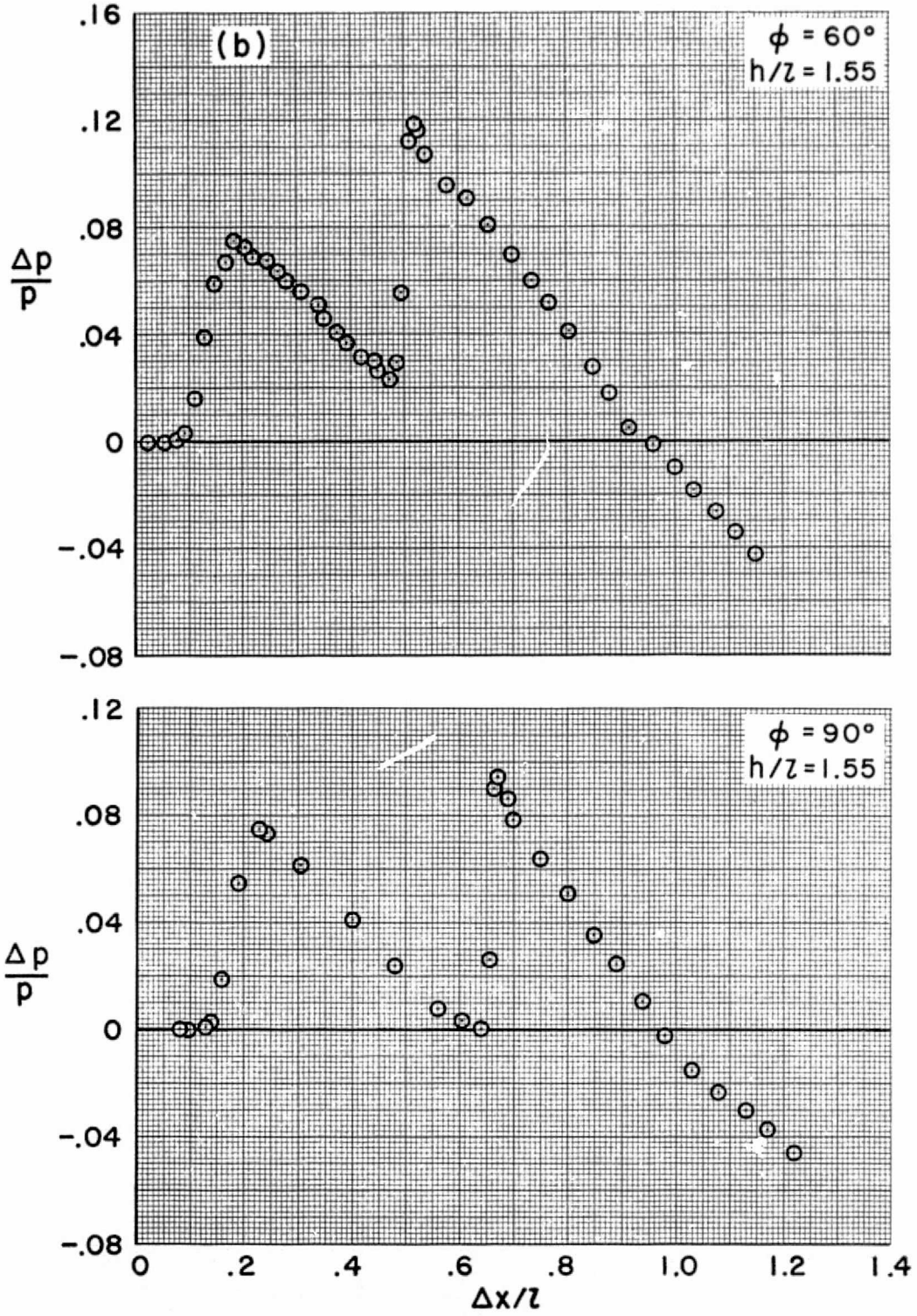

(b) $\phi = 60°, 90°$.

Figure 13.- Continued.

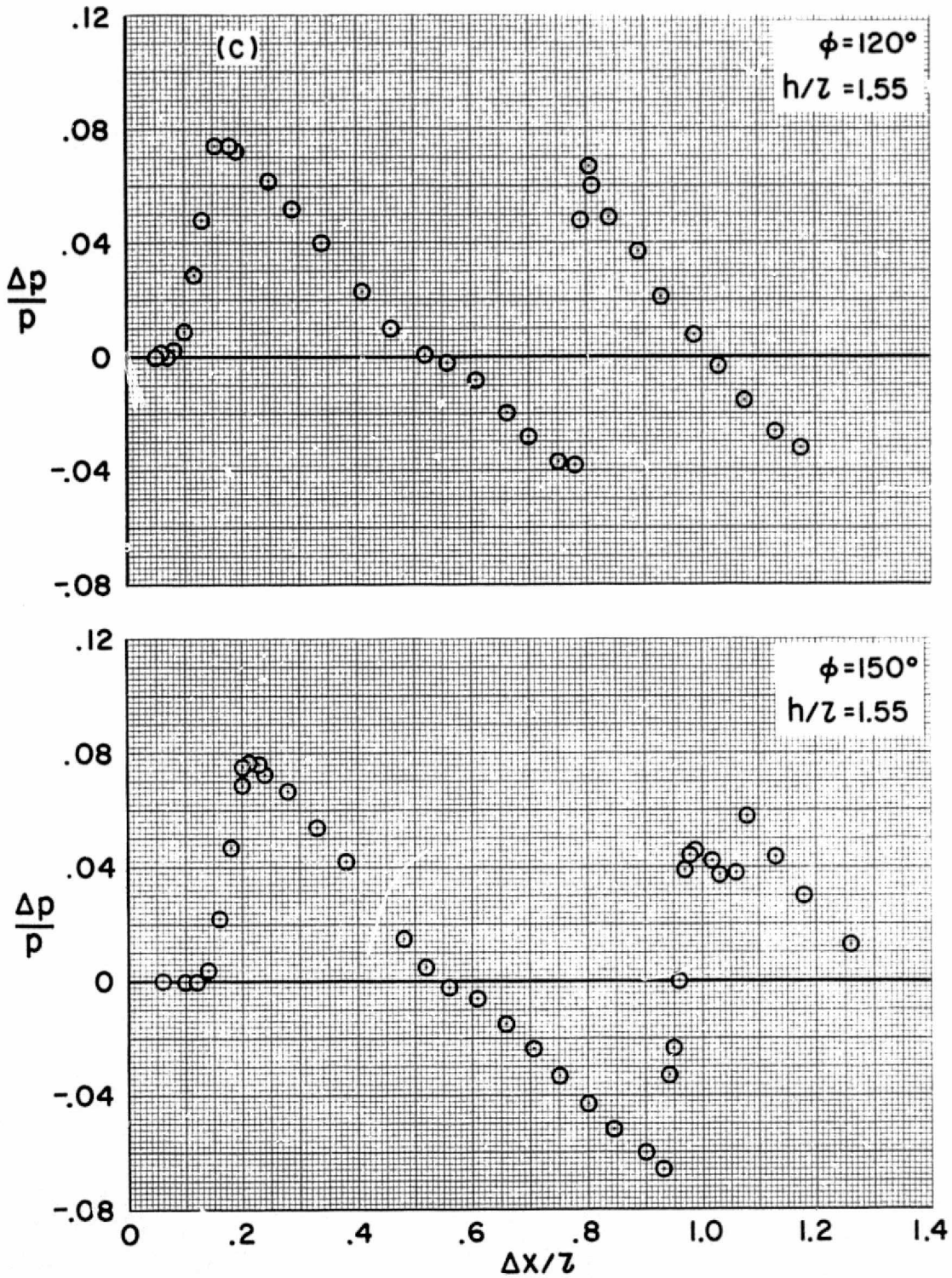

(c) ϕ = 120°, 150°.

Figure 13.- Continued.

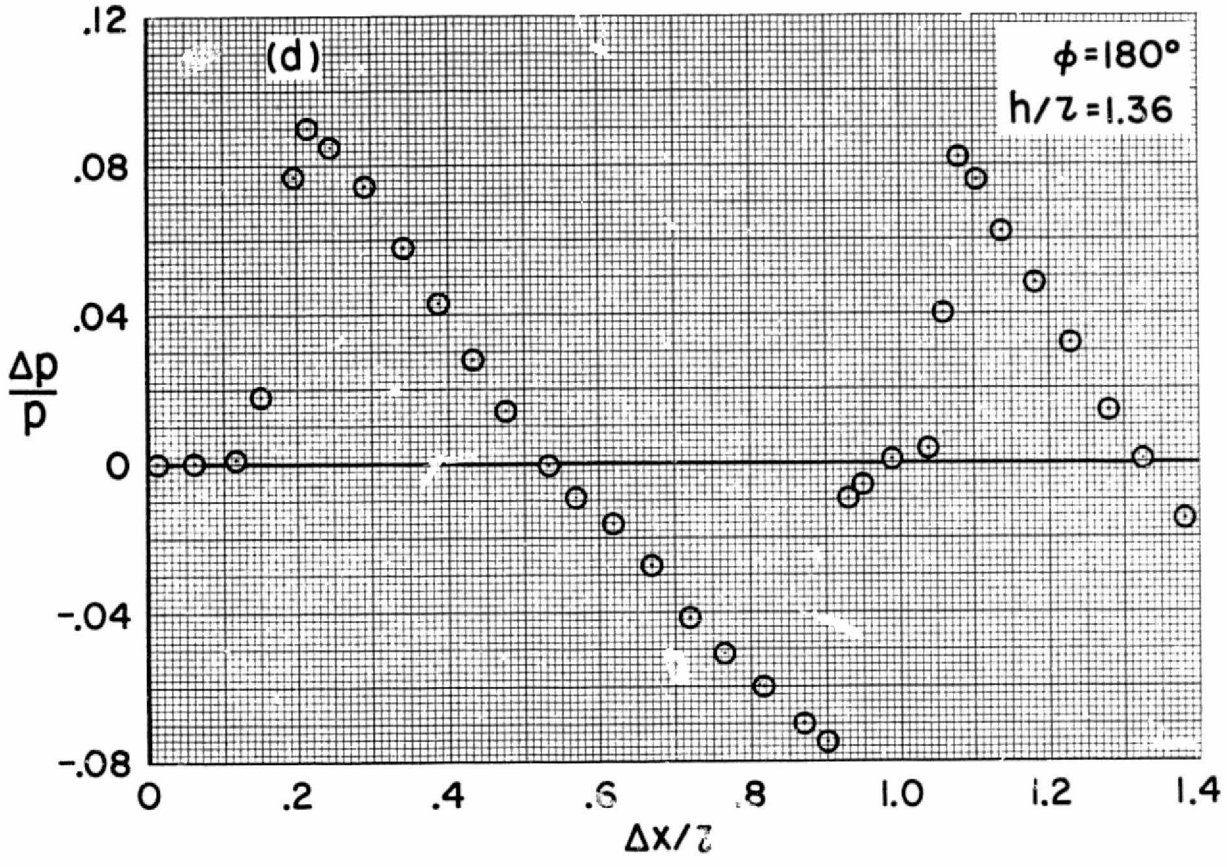

(d) $\phi = 180°$.

Figure 13.- Concluded.

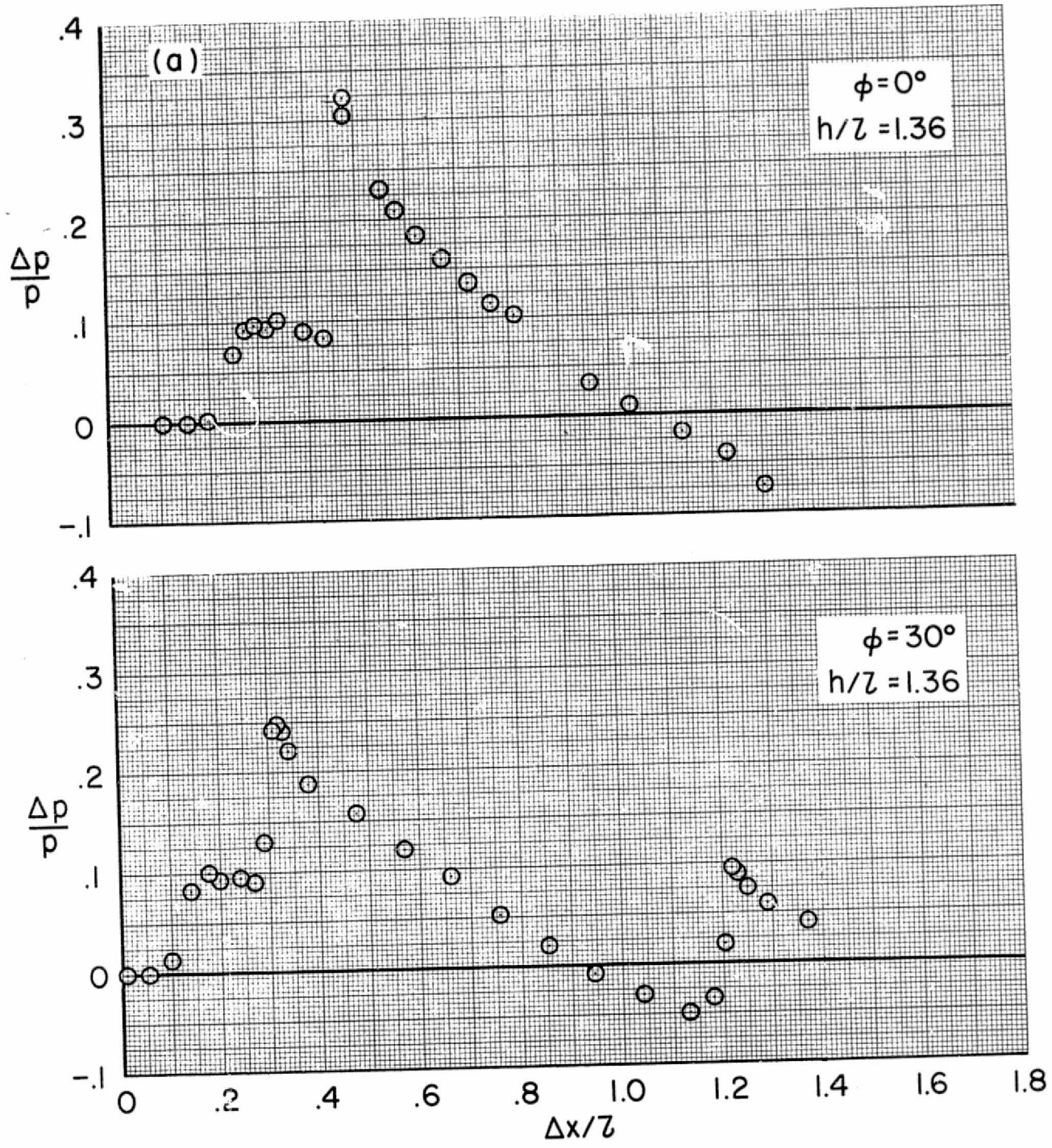

(a) ϕ = 0°, 30°.

Figure 14.- Pressure signatures for the 0.0041-scale orbiter model, M = 1.64, α = 10°.

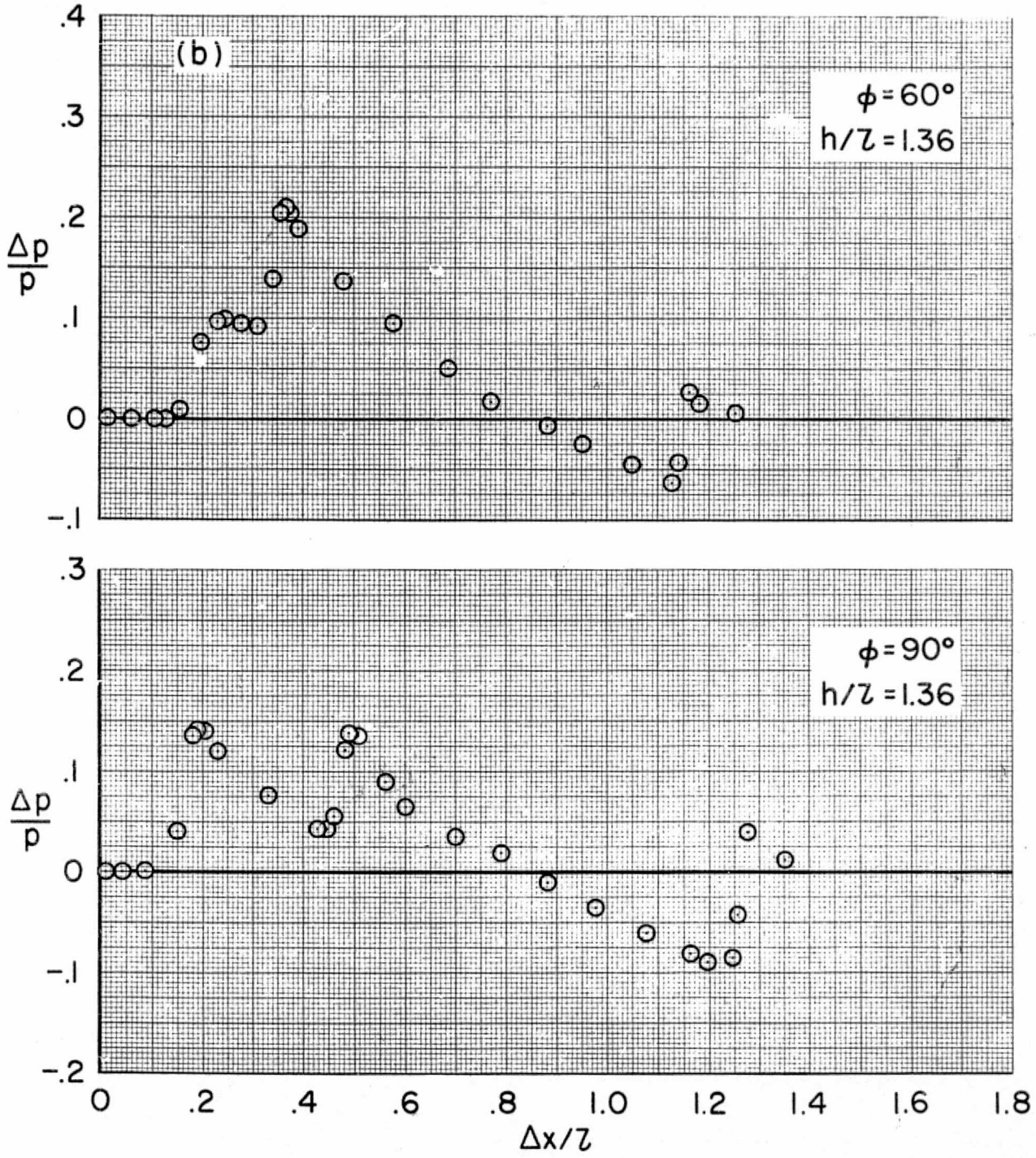

(b) ϕ = 60°, 90°.

Figure 14.- Continued.

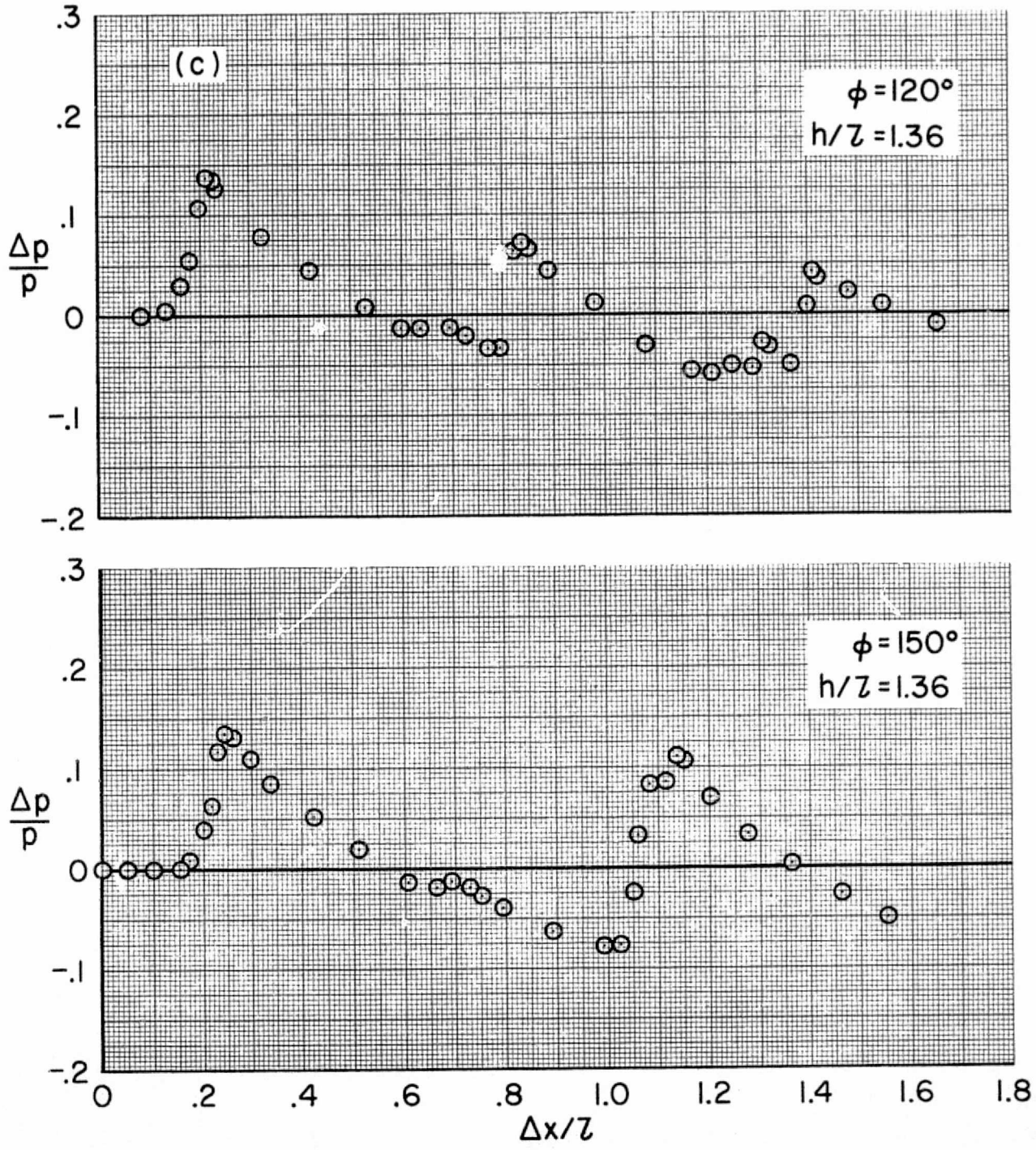

(c) ϕ = 120°, 150°.

Figure 14.- Continued.

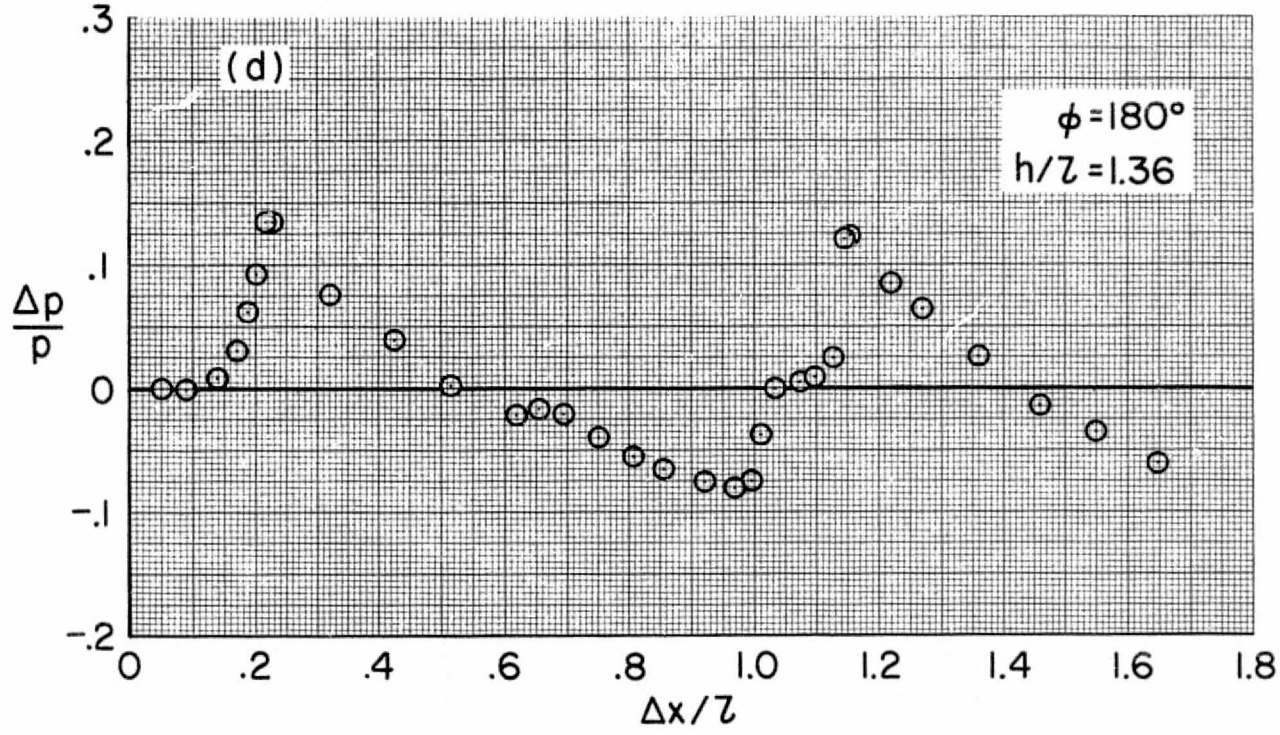

(d) ϕ = 180°.

Figure 14.- Concluded.

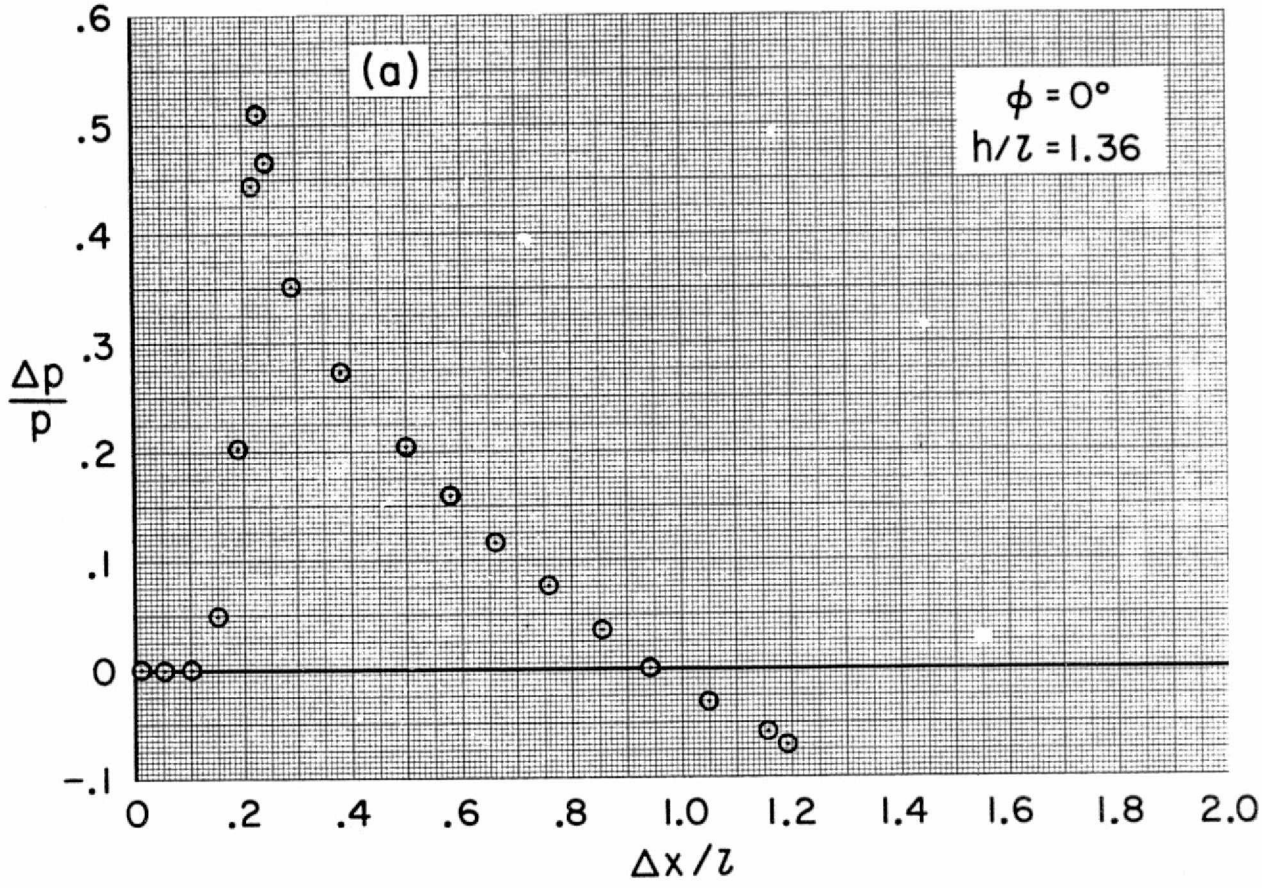

(a) $\phi = 0°$.

Figure 15.- Pressure signatures for the 0.0041-scale orbiter model, M = 2.21, $\alpha = 10°$.

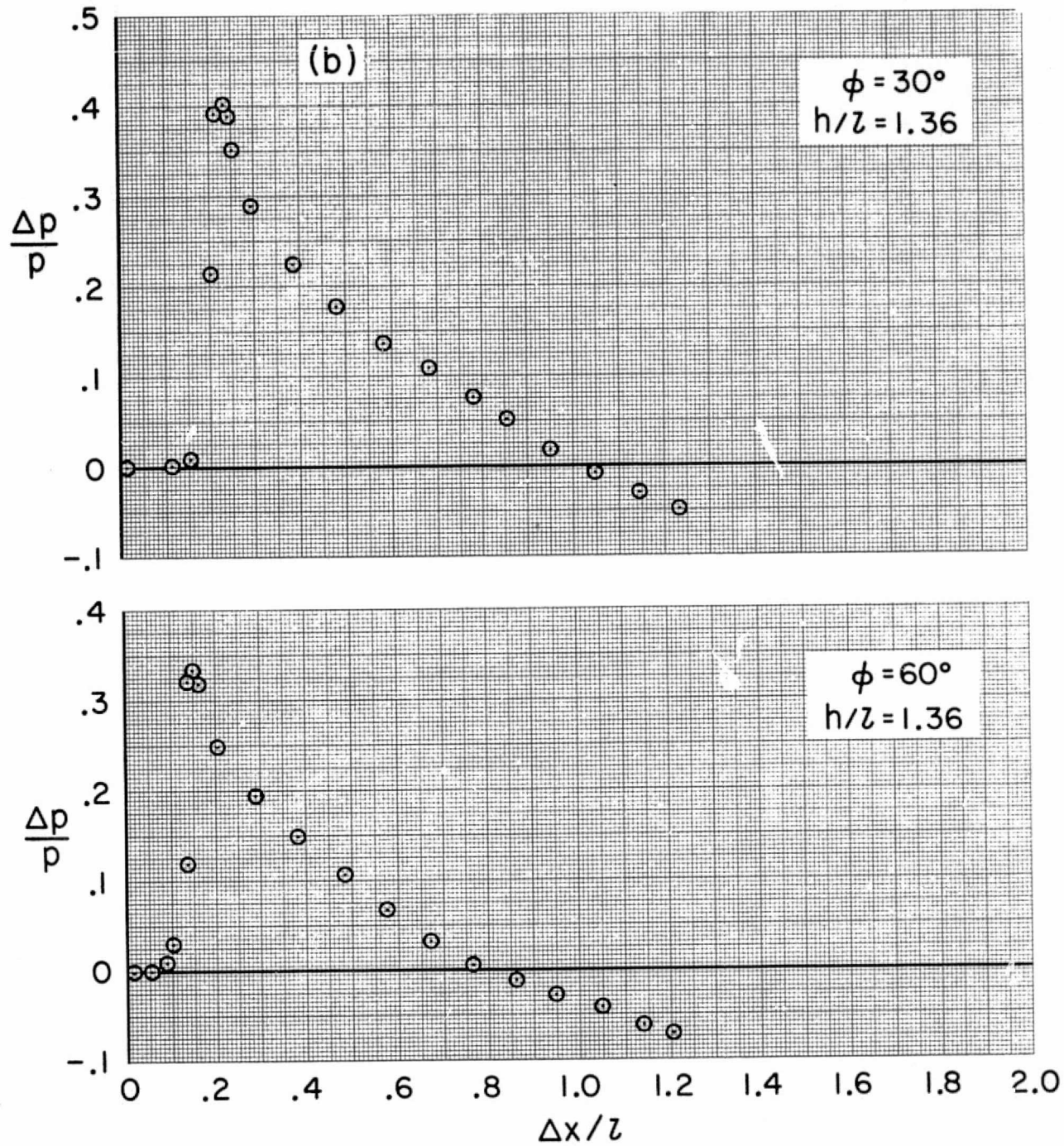

(b) ϕ = 30°, 60°.

Figure 15.- Continued.

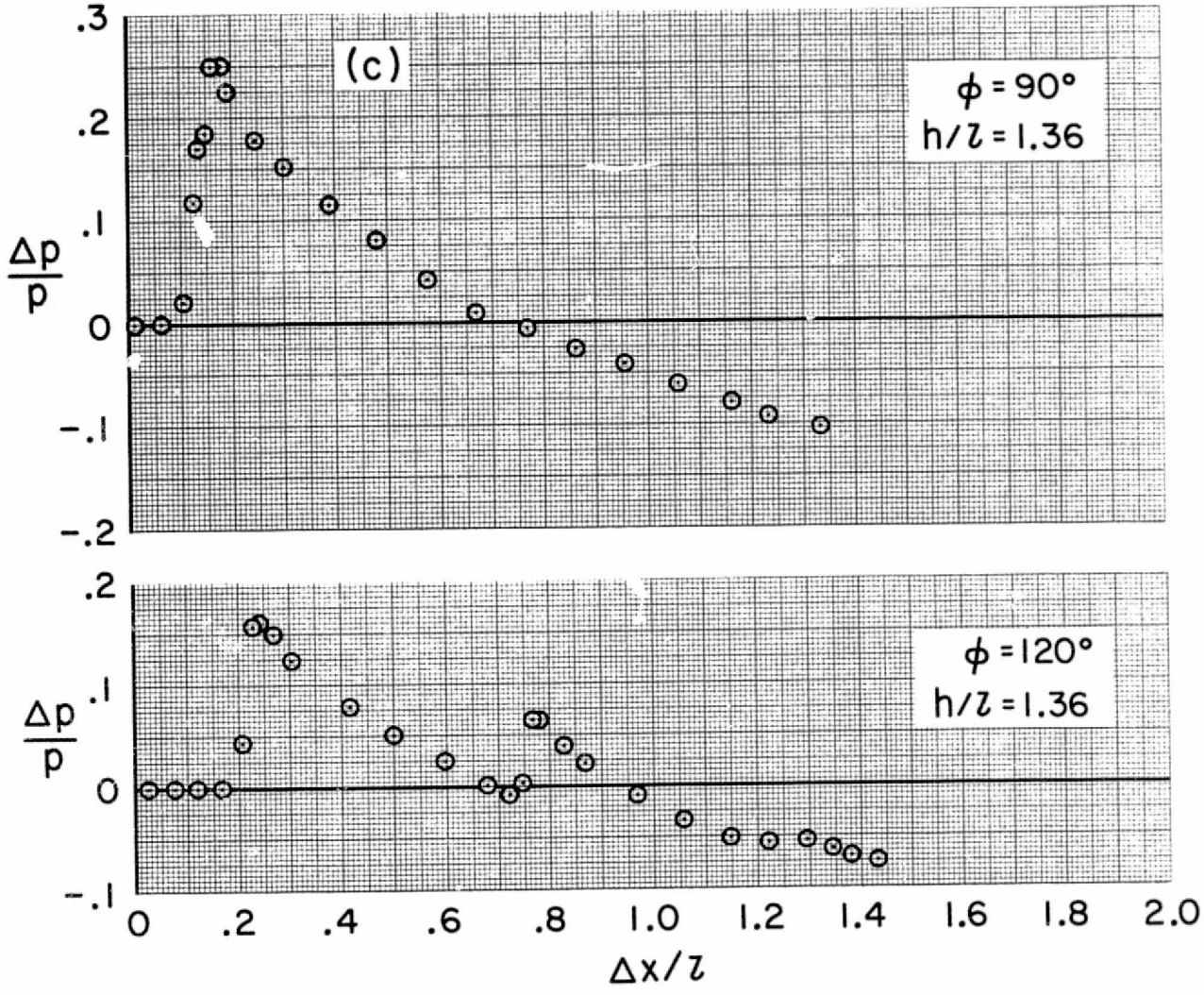

(c) $\phi = 90°$, $120°$.

Figure 15.- Continued.

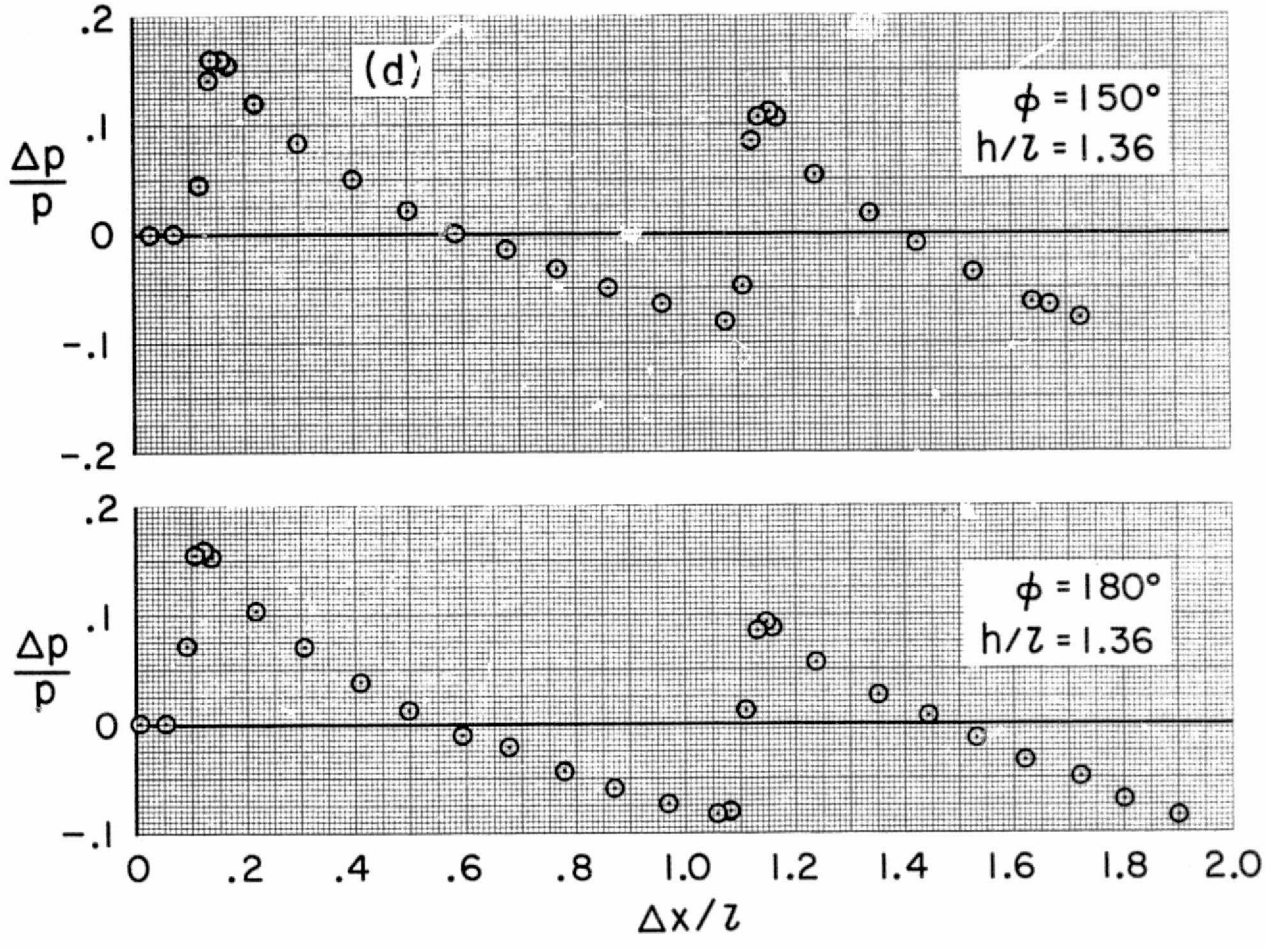

(d) ϕ = 150°, 180°.

Figure 15.- Concluded.

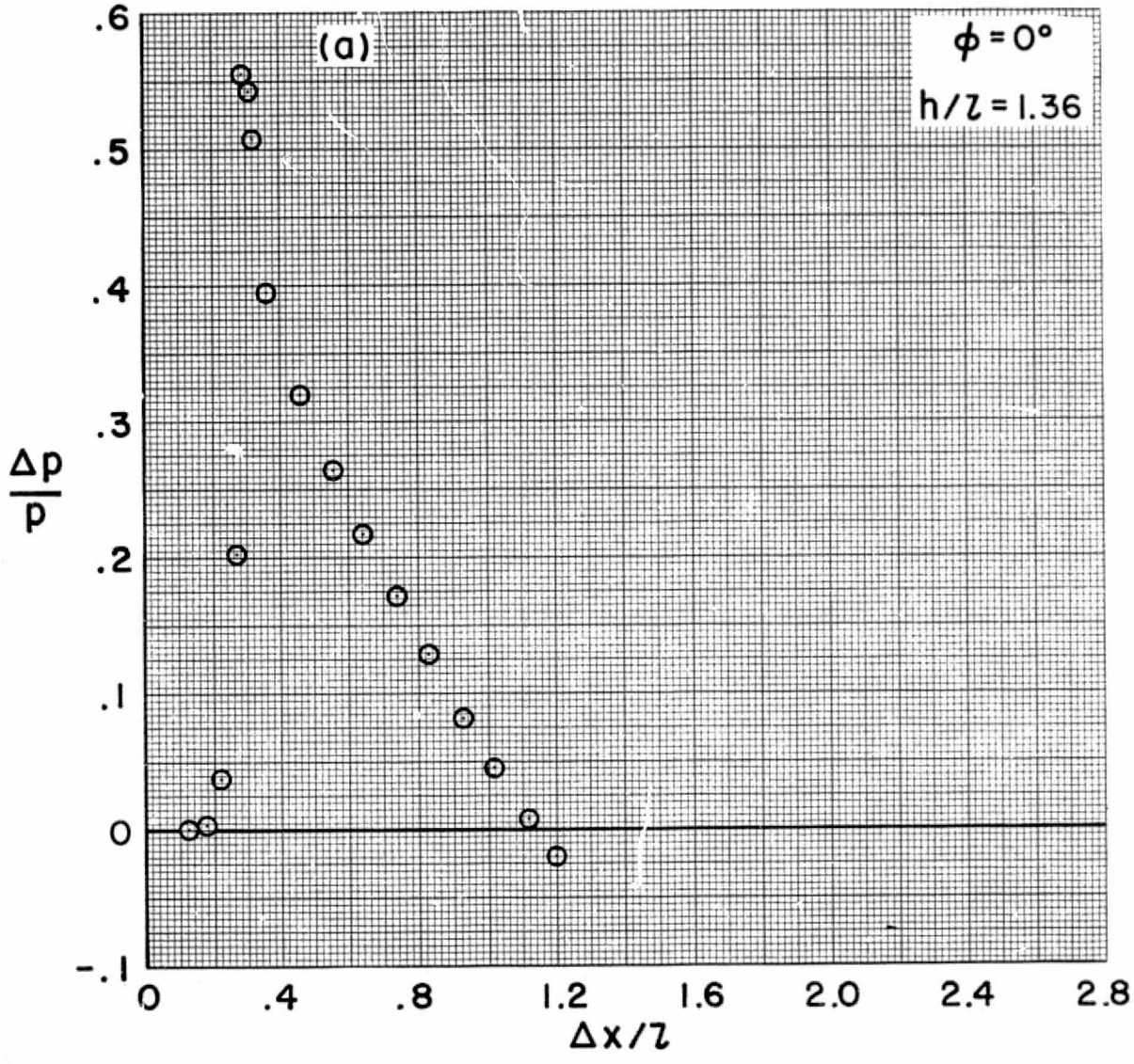

(a) $\phi = 0°$.

Figure 16.- Pressure signatures for the 0.0041-scale orbiter model, M = 2.61, $\alpha = 10°$.

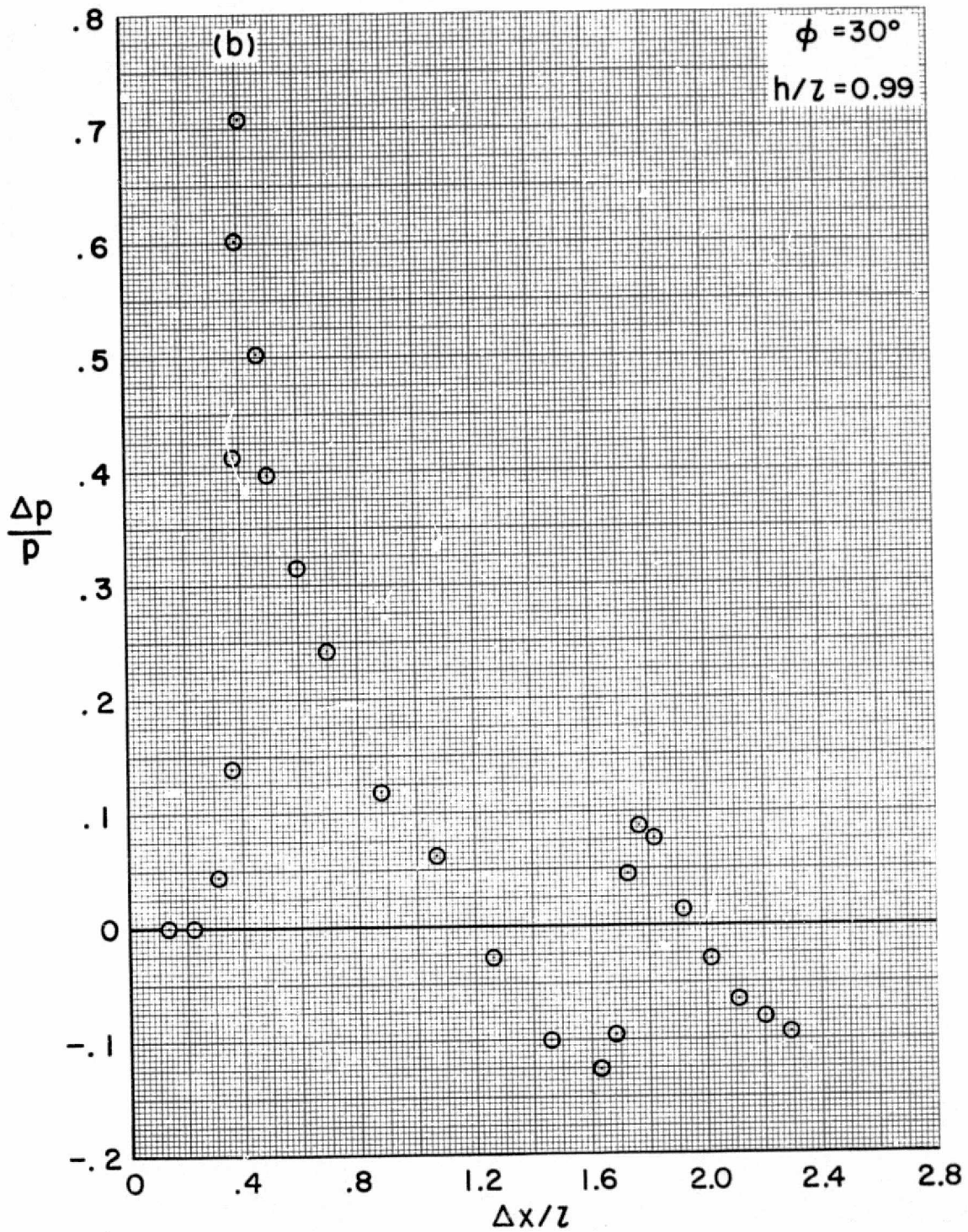

(b) $\phi = 30°$.

Figure 16.- Continued.

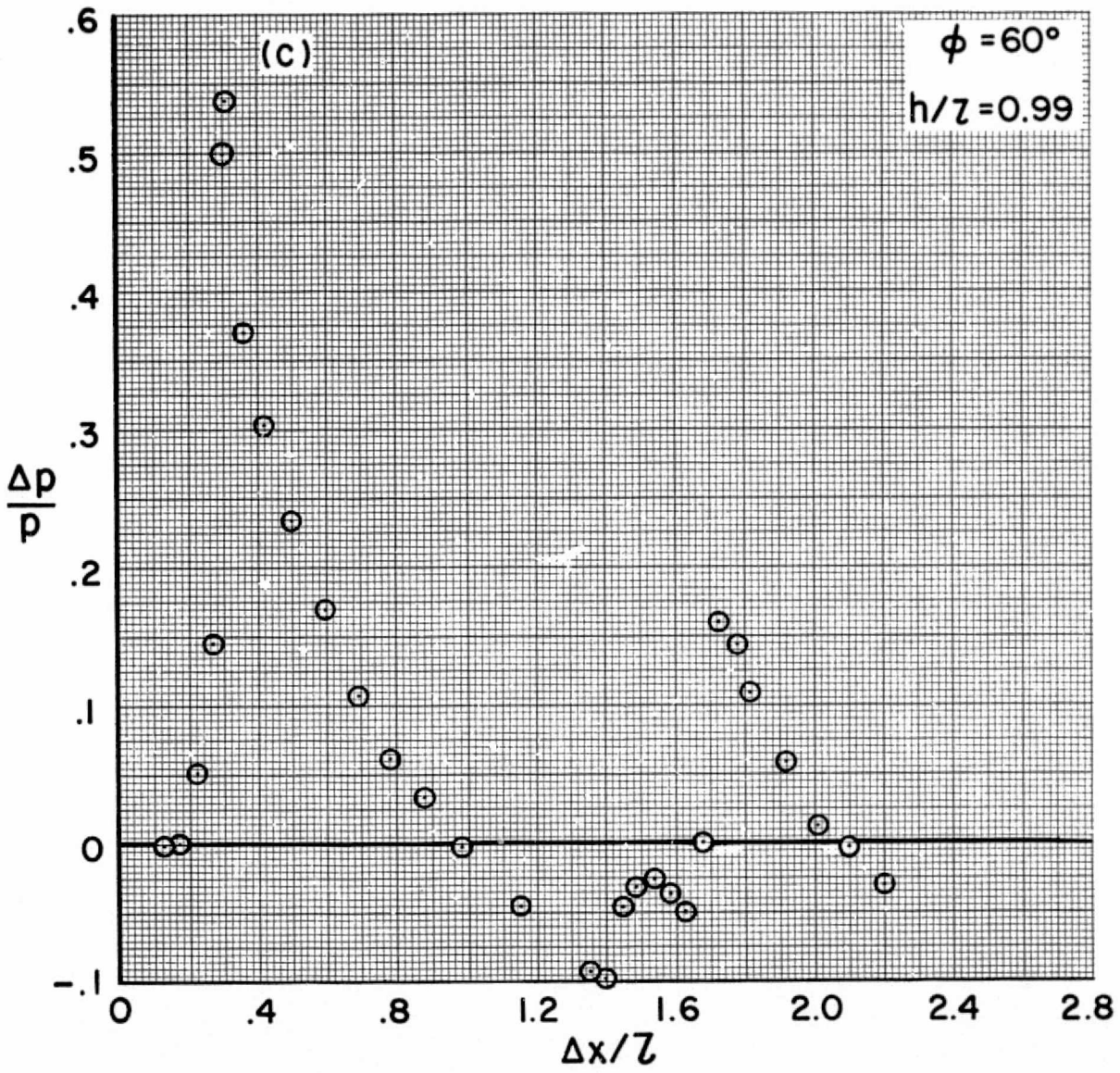

(c) $\phi = 60°$.

Figure 16.- Continued.

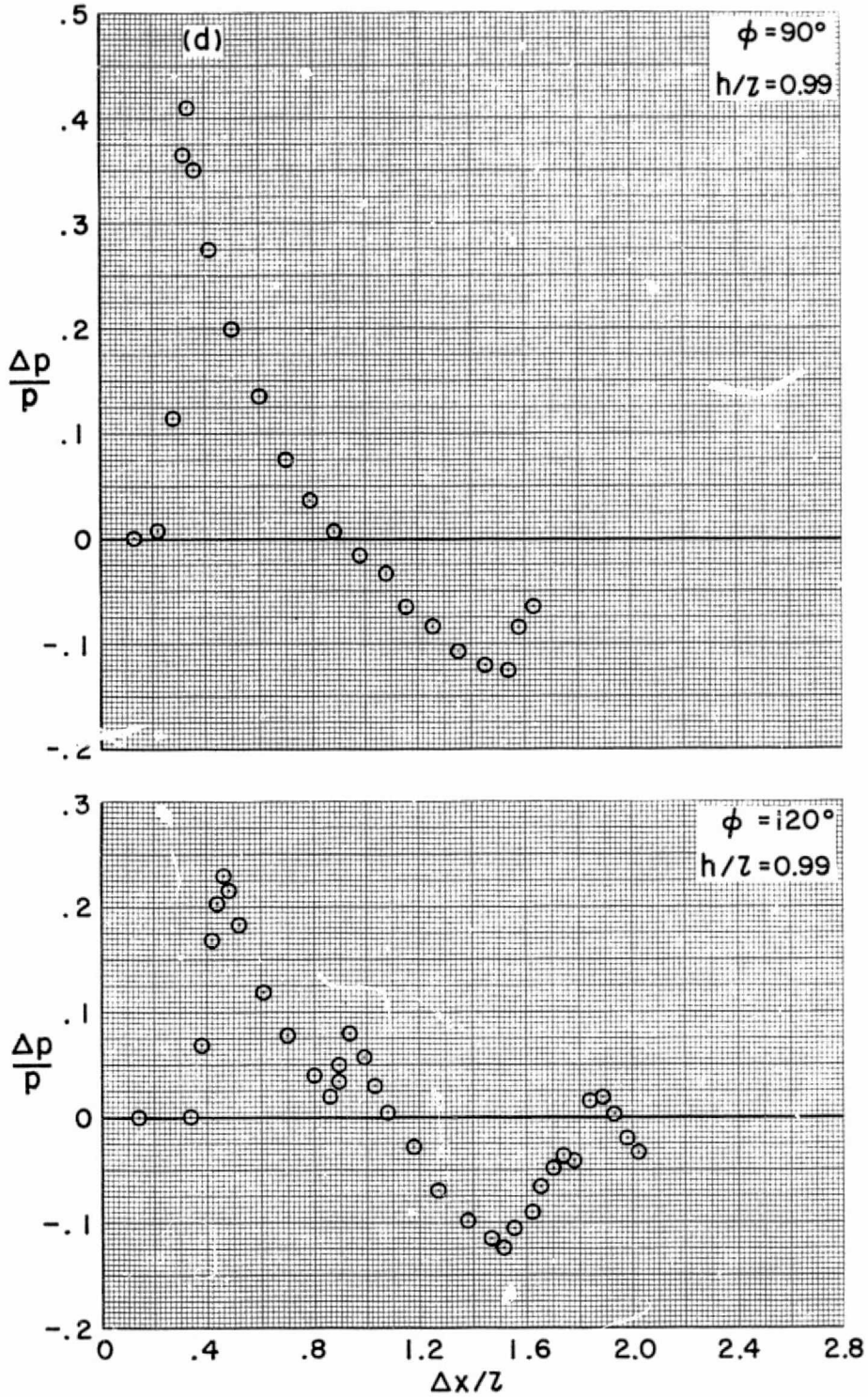

(d) ϕ = 90°, 120°.

Figure 16.- Continued.

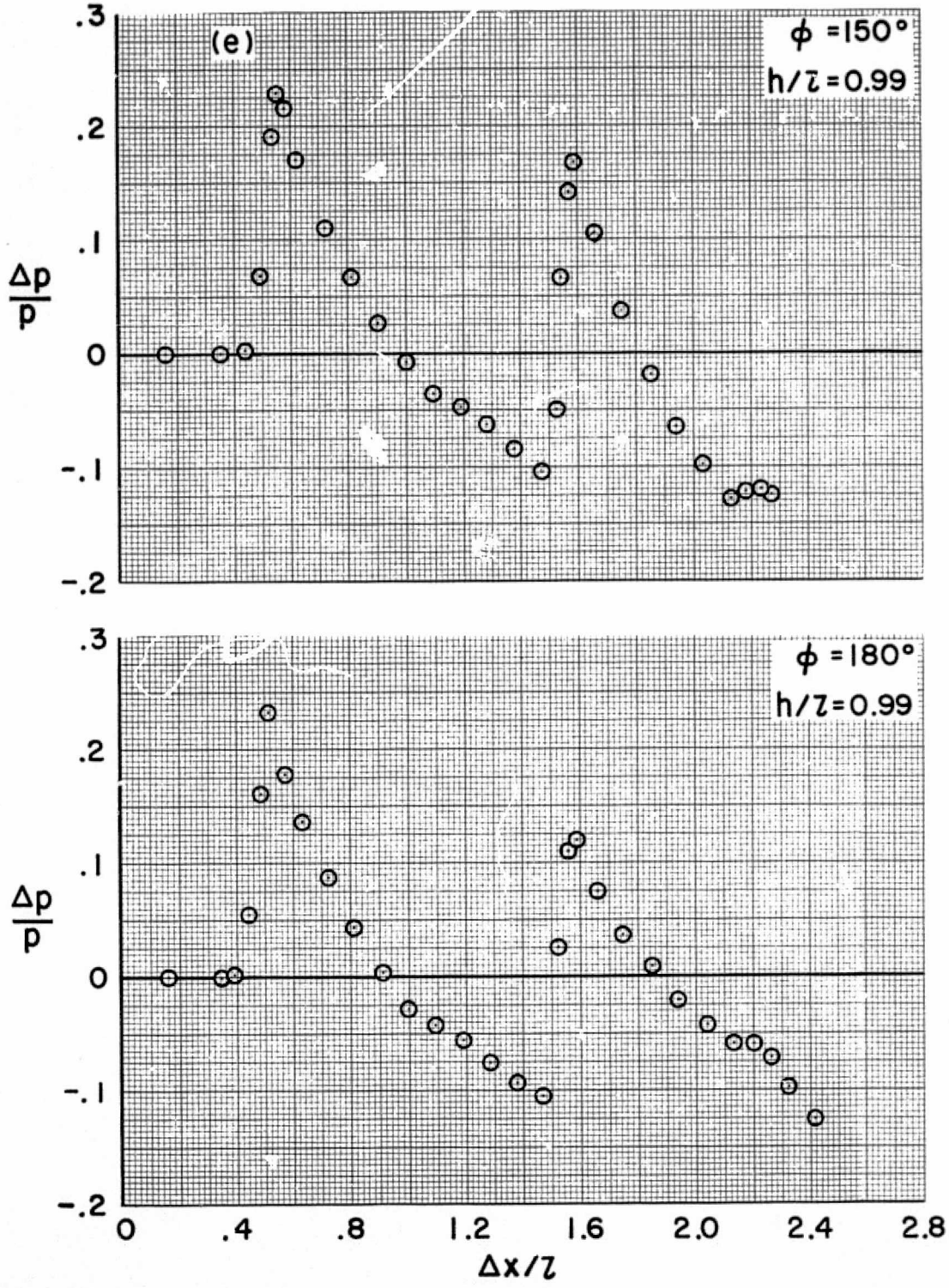

(e) ϕ = 150°, 180°.

Figure 16.- Concluded.

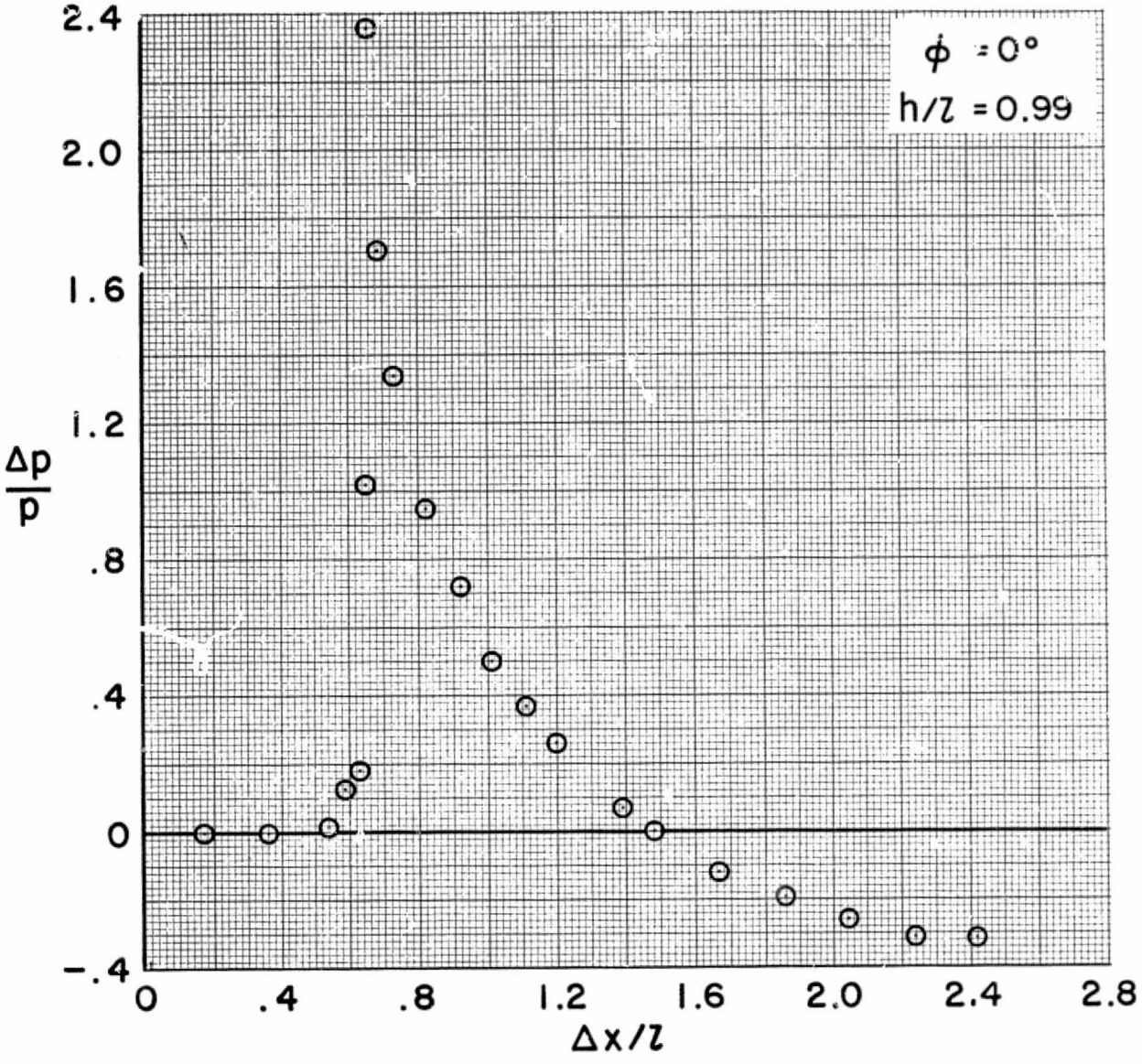

(a) $\phi = 0°$.

Figure 17.- Pressure signatures for the 0.0041-scale orbiter model, M = 2.61, $\alpha = 25°$.

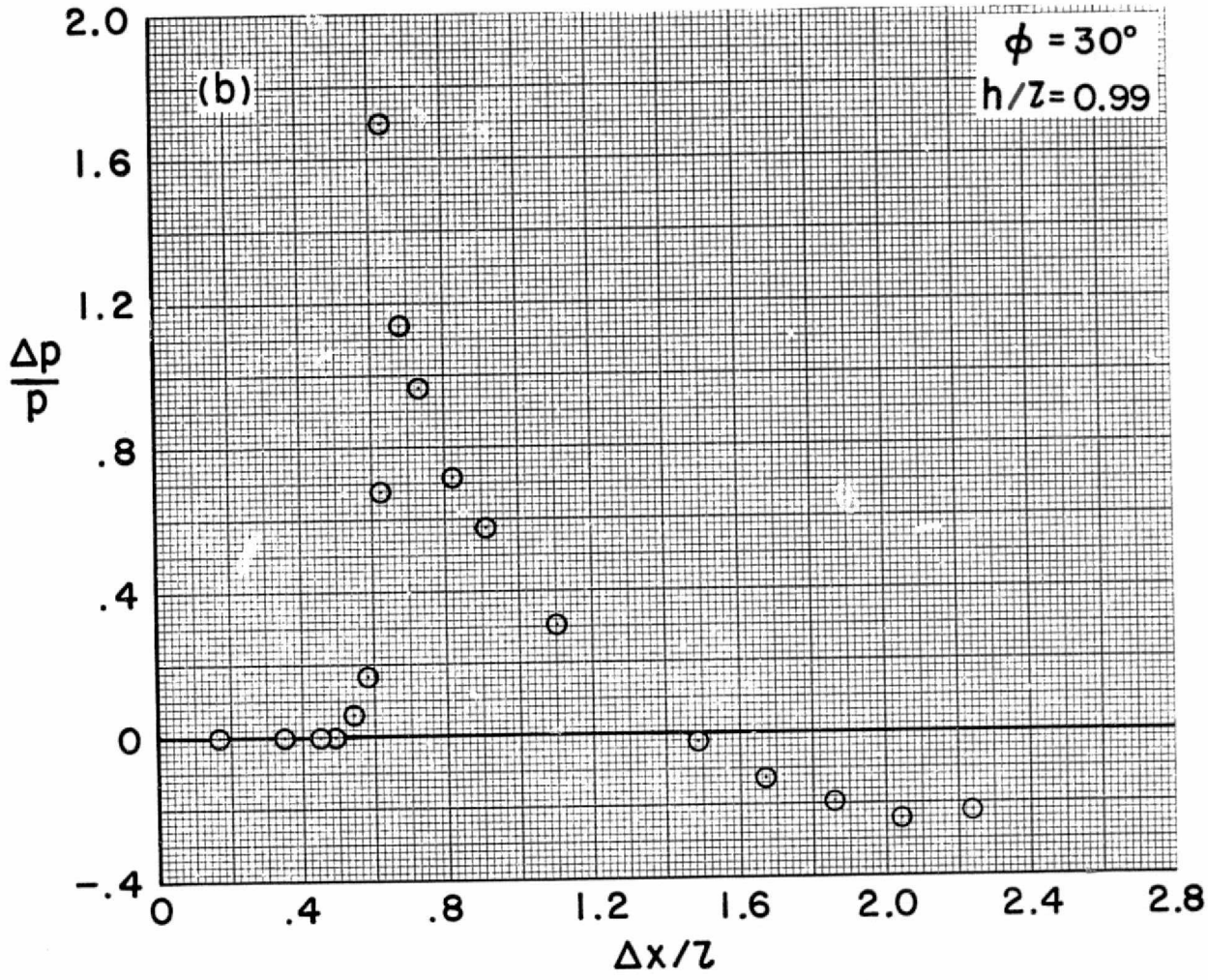

(b) ϕ = 30°.

Figure 17.- Continued.

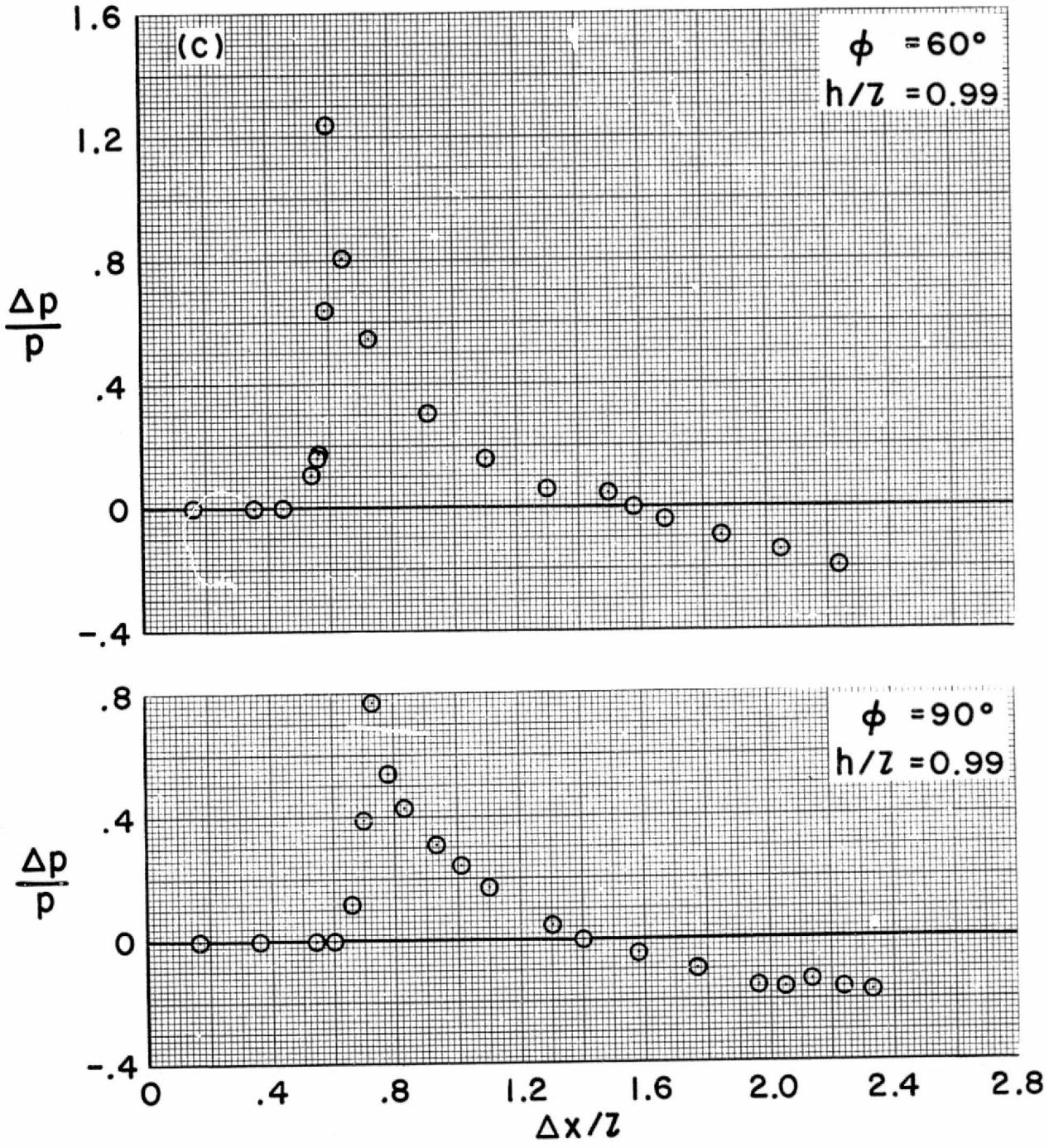

(c) ϕ = 60°, 90°.

Figure 17.- Continued.

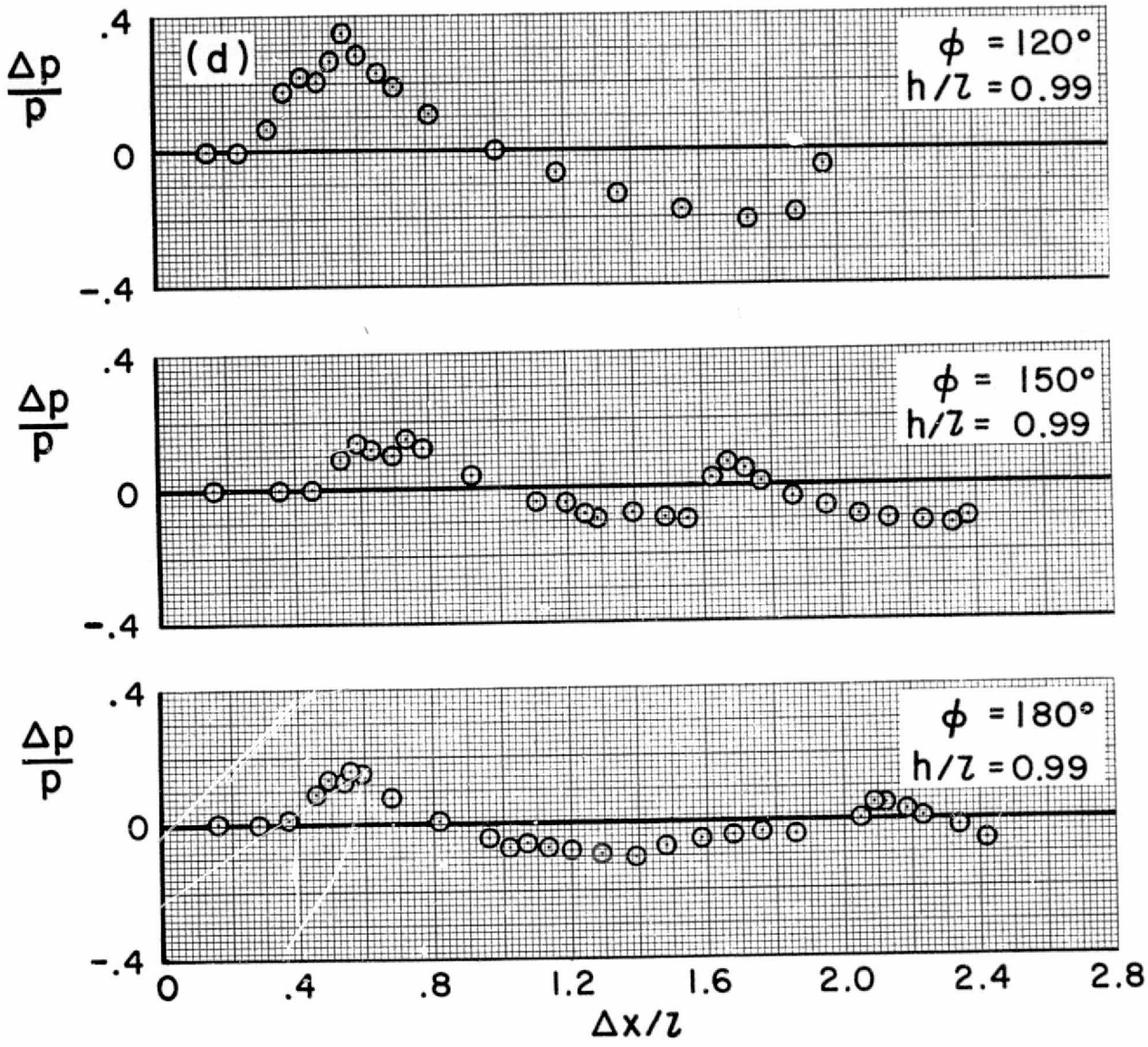

(d) ϕ = 120°, 150°, 180°.

Figure 17.- Concluded.

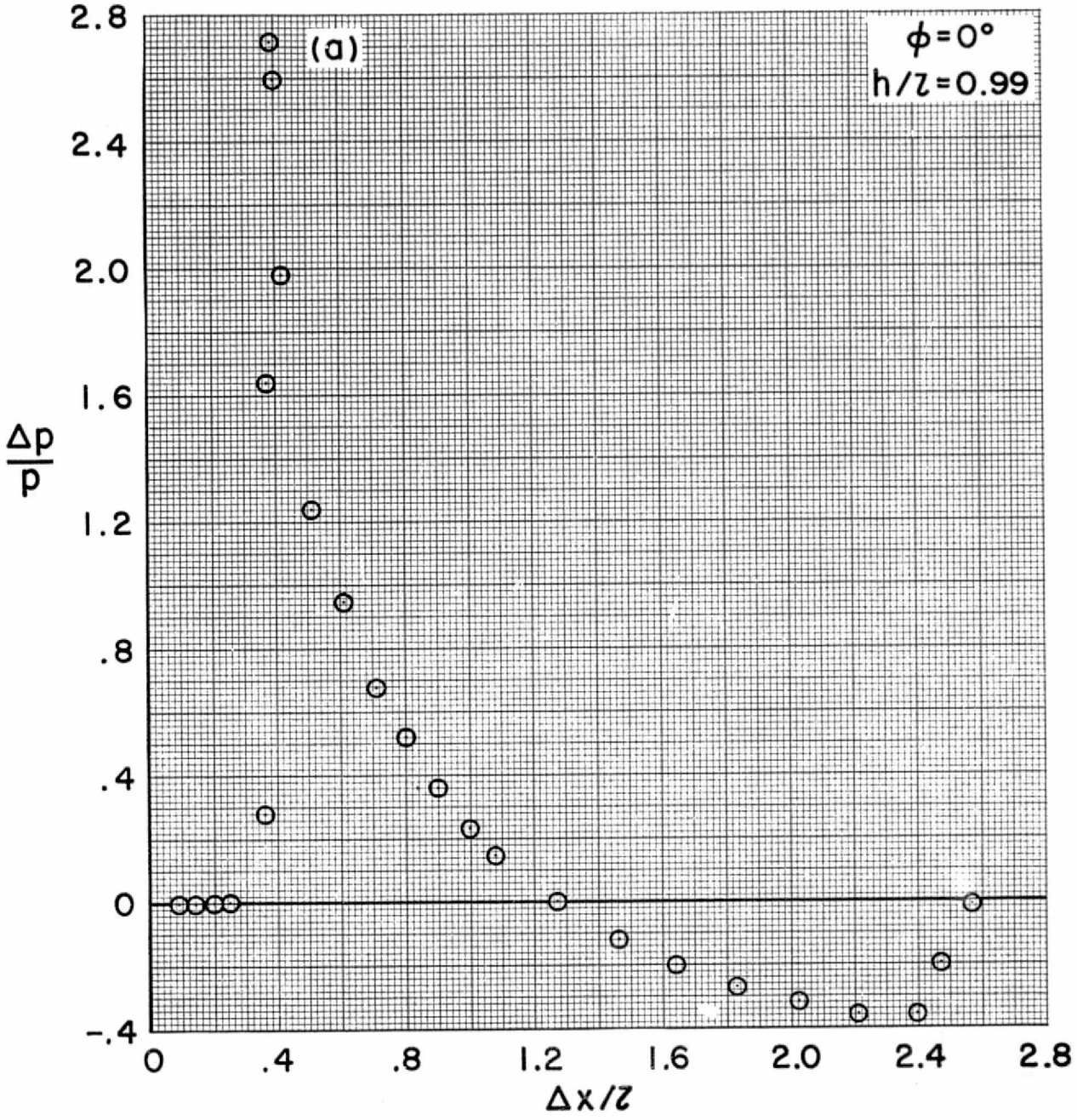

(a) $\phi = 0°$.

Figure 18.- Pressure signatures for the 0.0041-scale orbiter model, M = 3.02, $\alpha = 25°$.

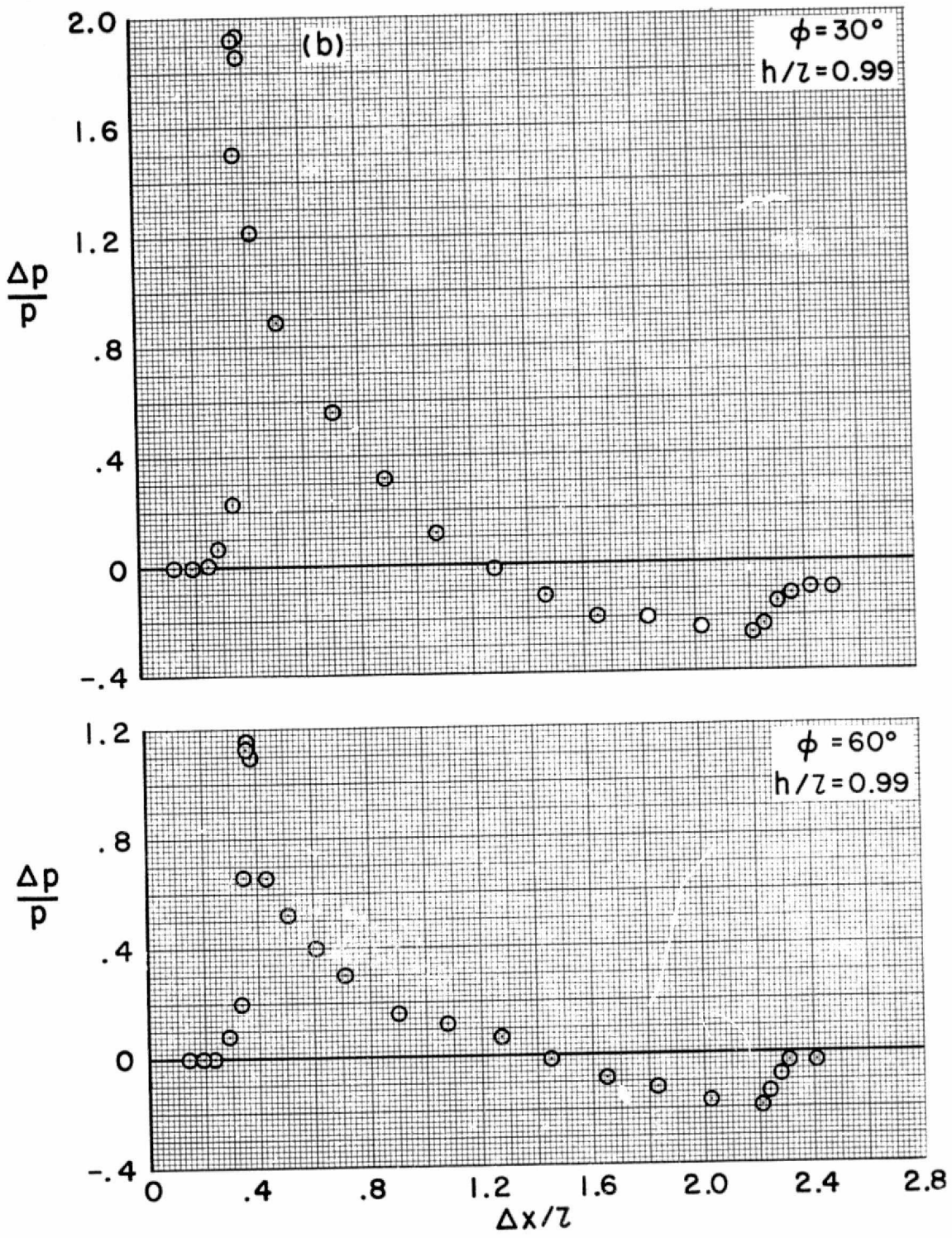

(b) ϕ = 30°, 60°.

Figure 18.- Continued.

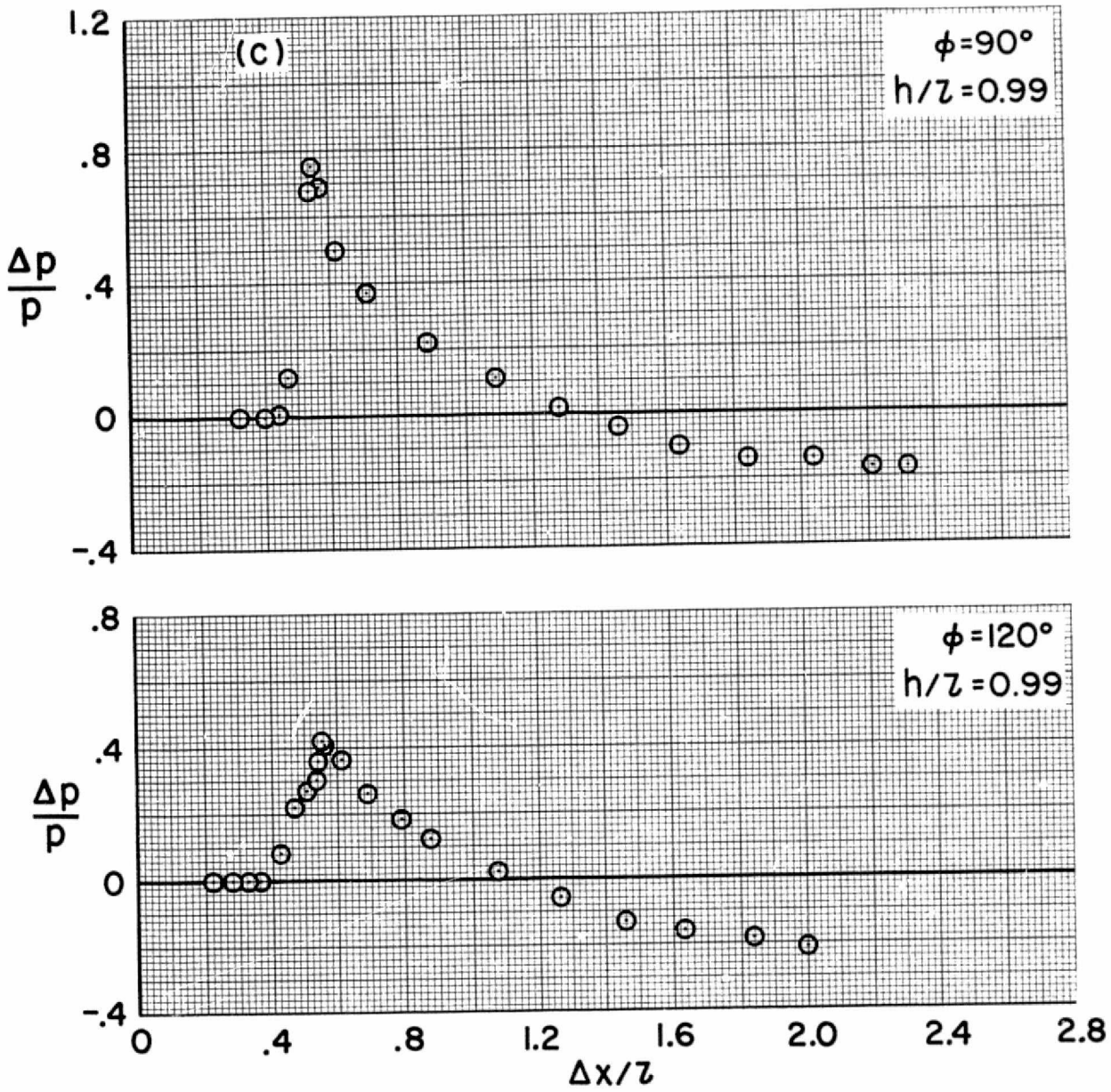

(c) ϕ = 90°, 120°.

Figure 18.- Continued.

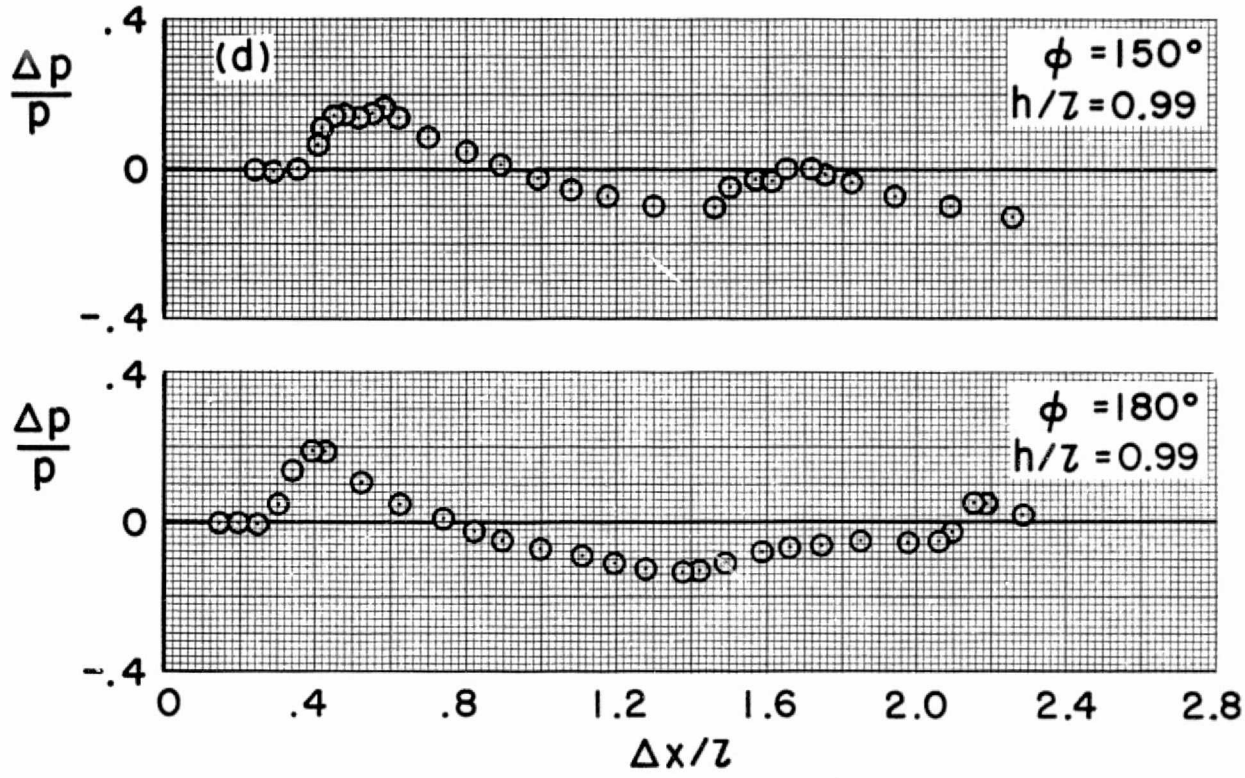

(d) ϕ = 150°, 180°.

Figure 18.- Concluded.

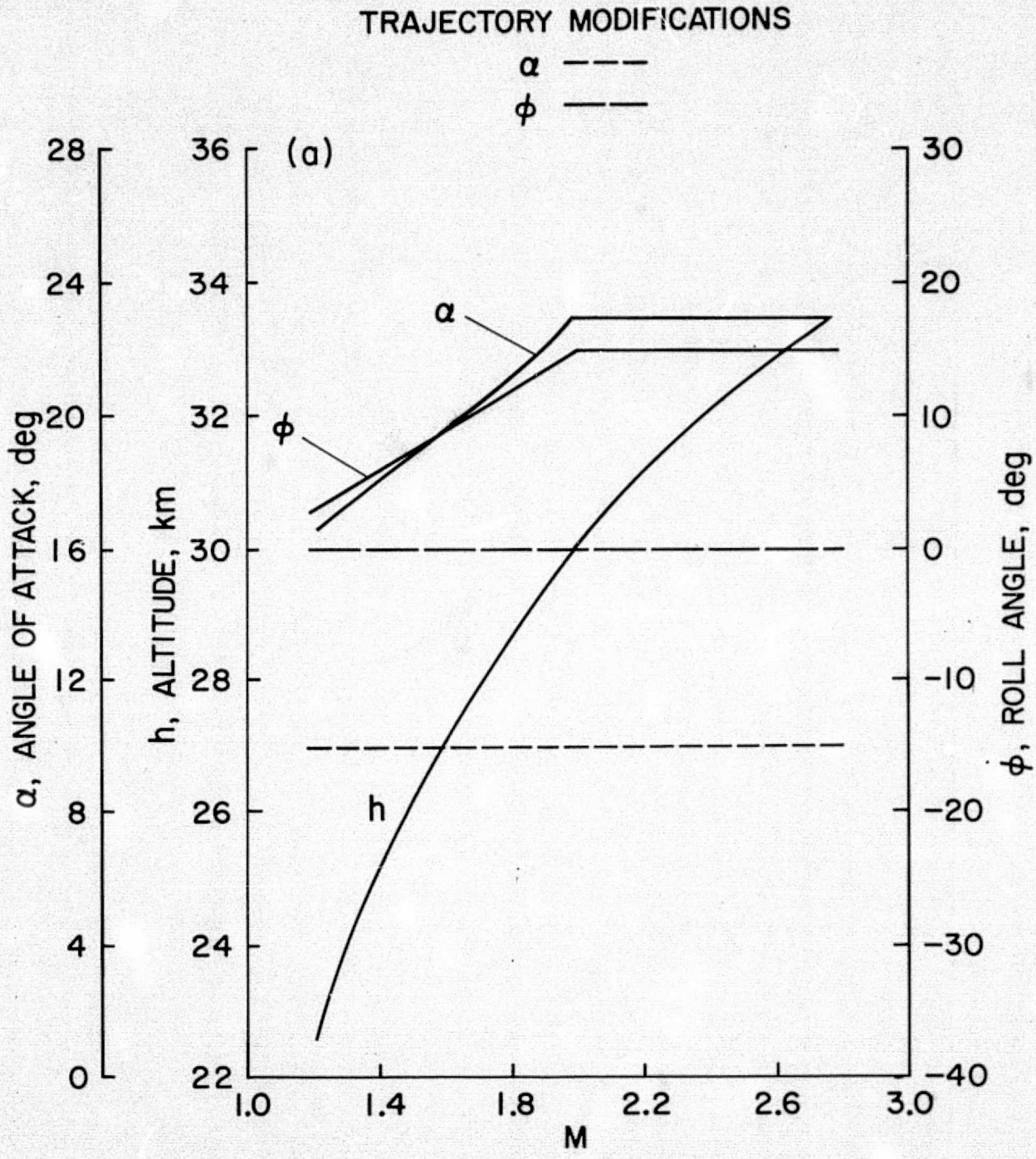

(a) Trajectory A.

Figure 19.- Space shuttle entry trajectory parameters.

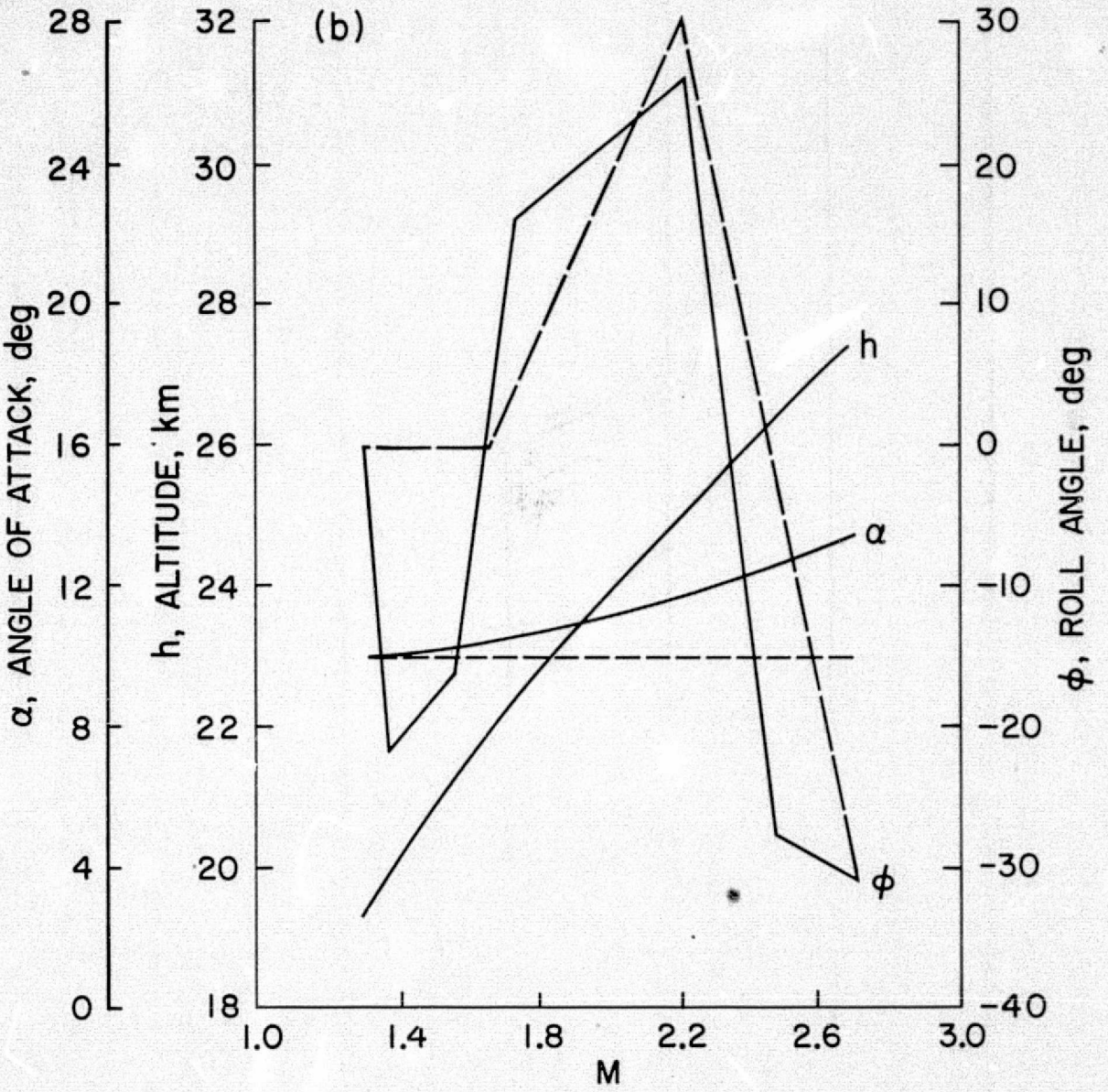

(b) Trajectory B.

Figure 19.- Concluded.

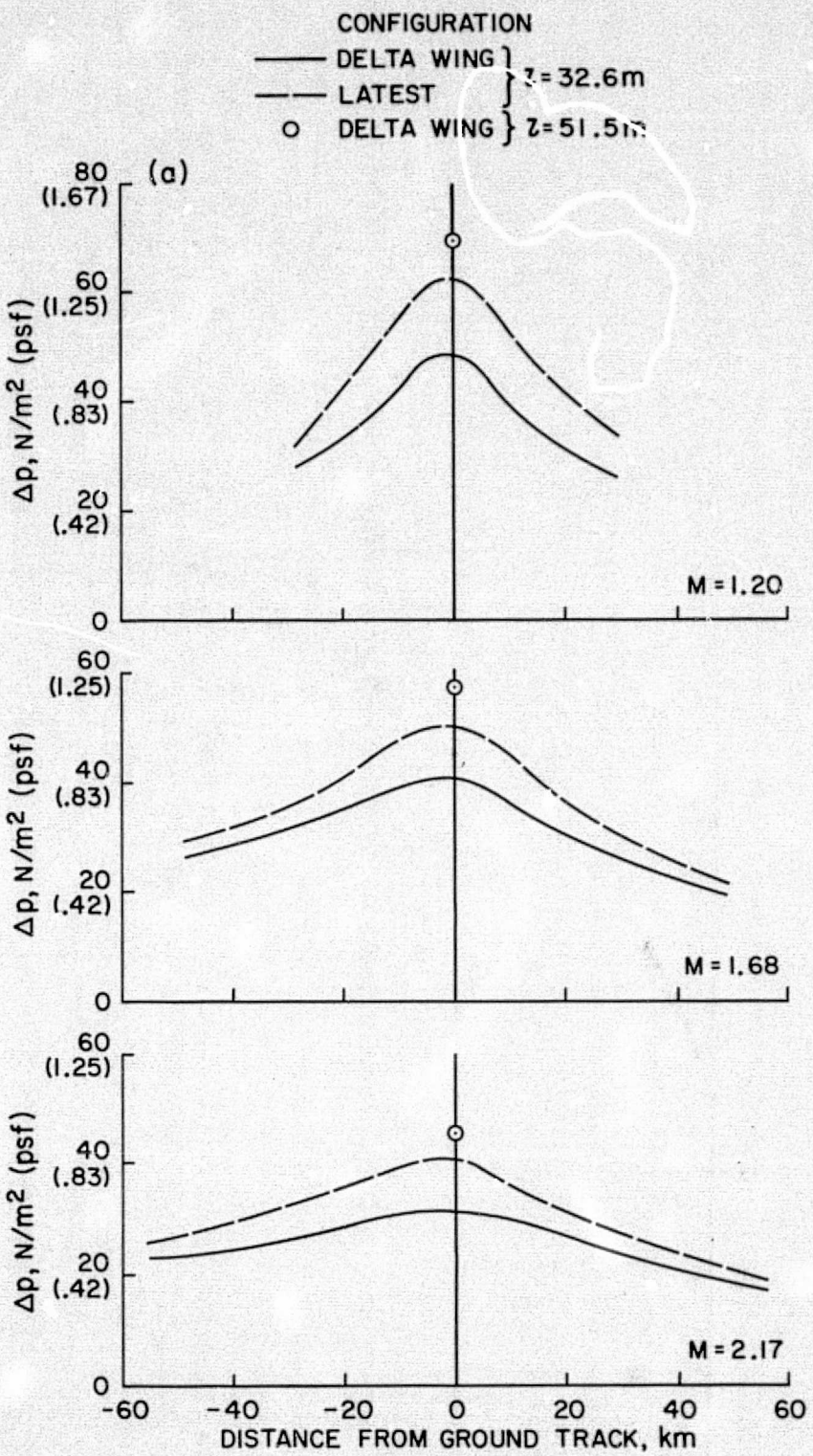

(a) Trajectory A.

Figure 20.- Comparisons of the sonic boom footprints for the various space shuttle vehicles, K_r = 1.9.

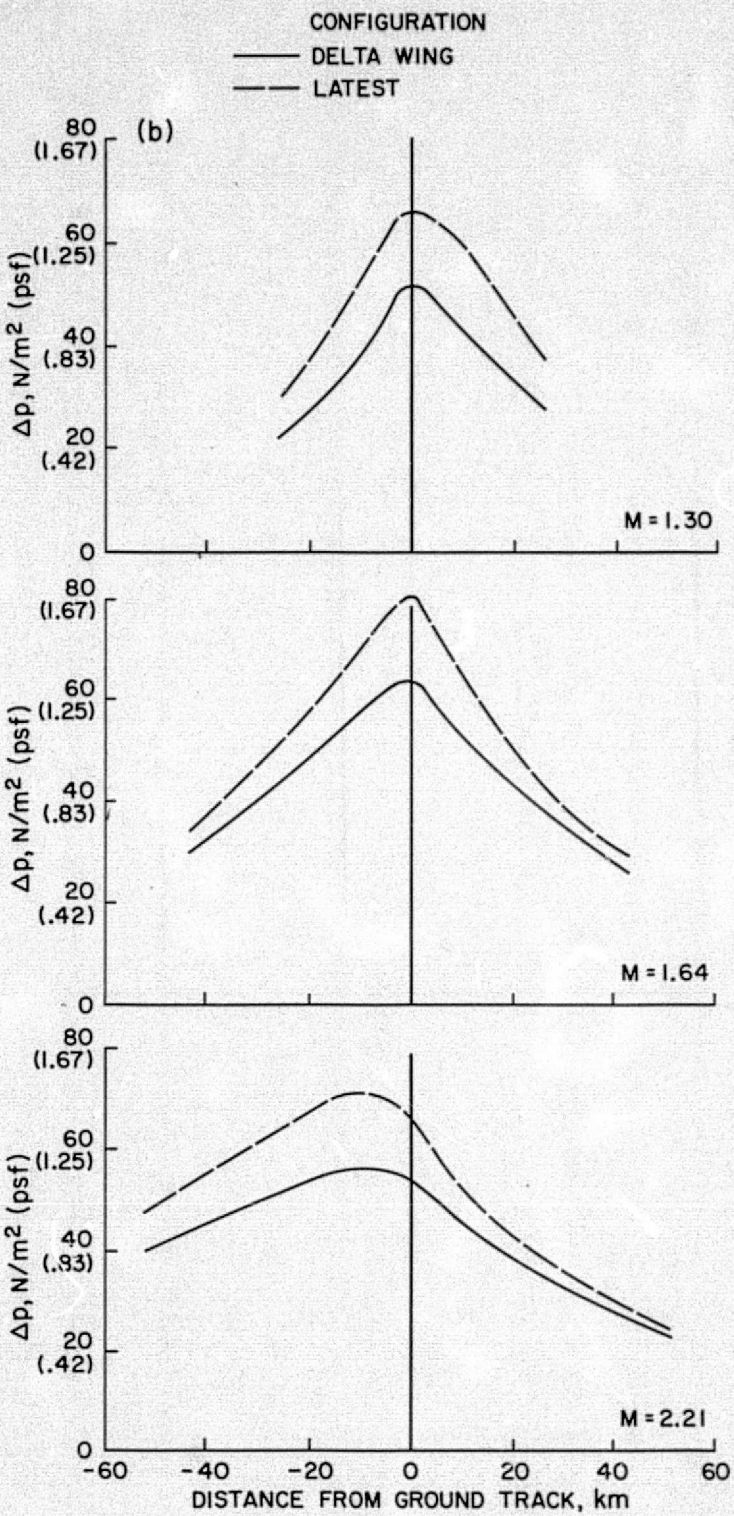

(b) Trajectory B.

Figure 20.- Concluded.

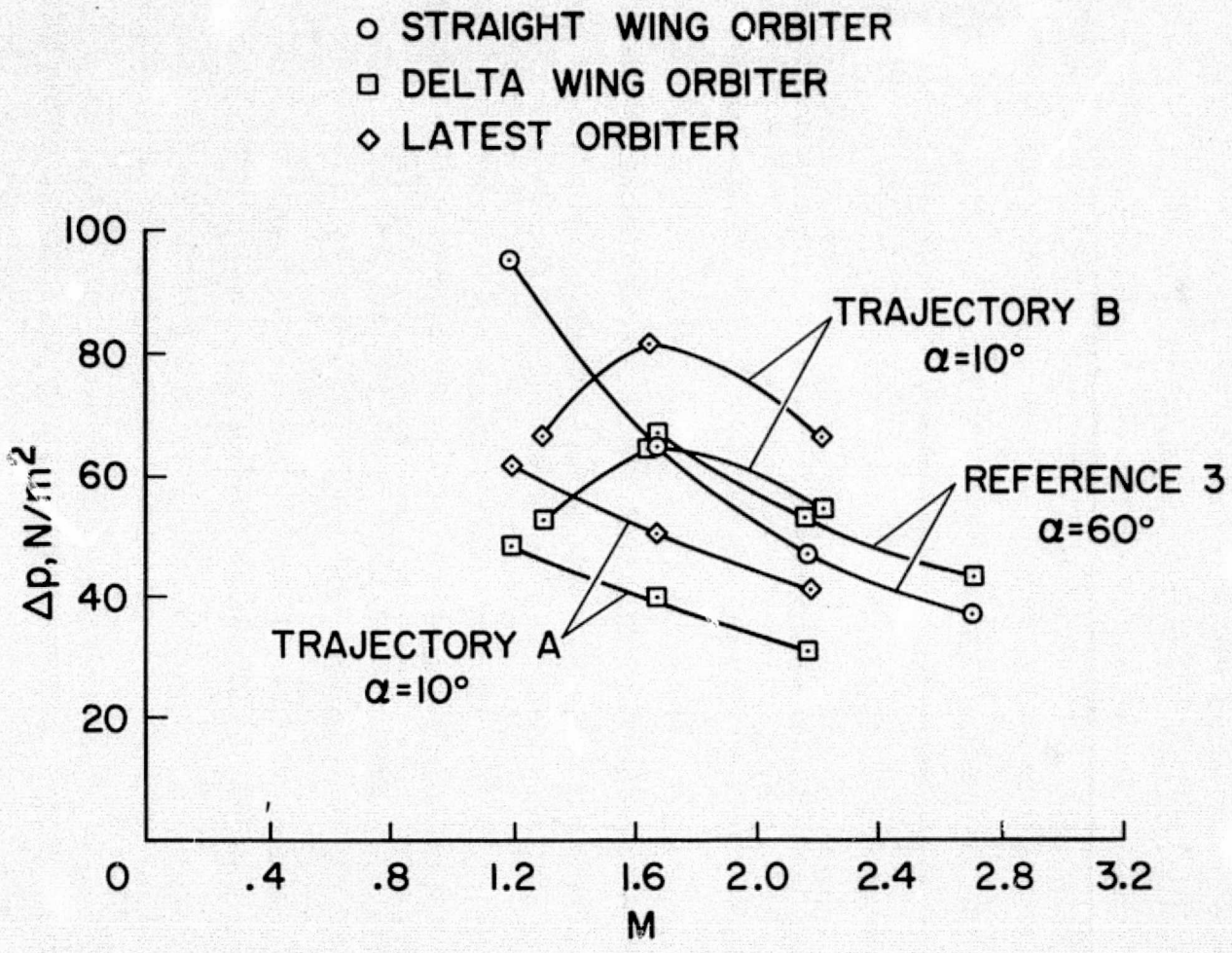

Figure 21.- Ground track sonic boom levels for three orbiter configurations.

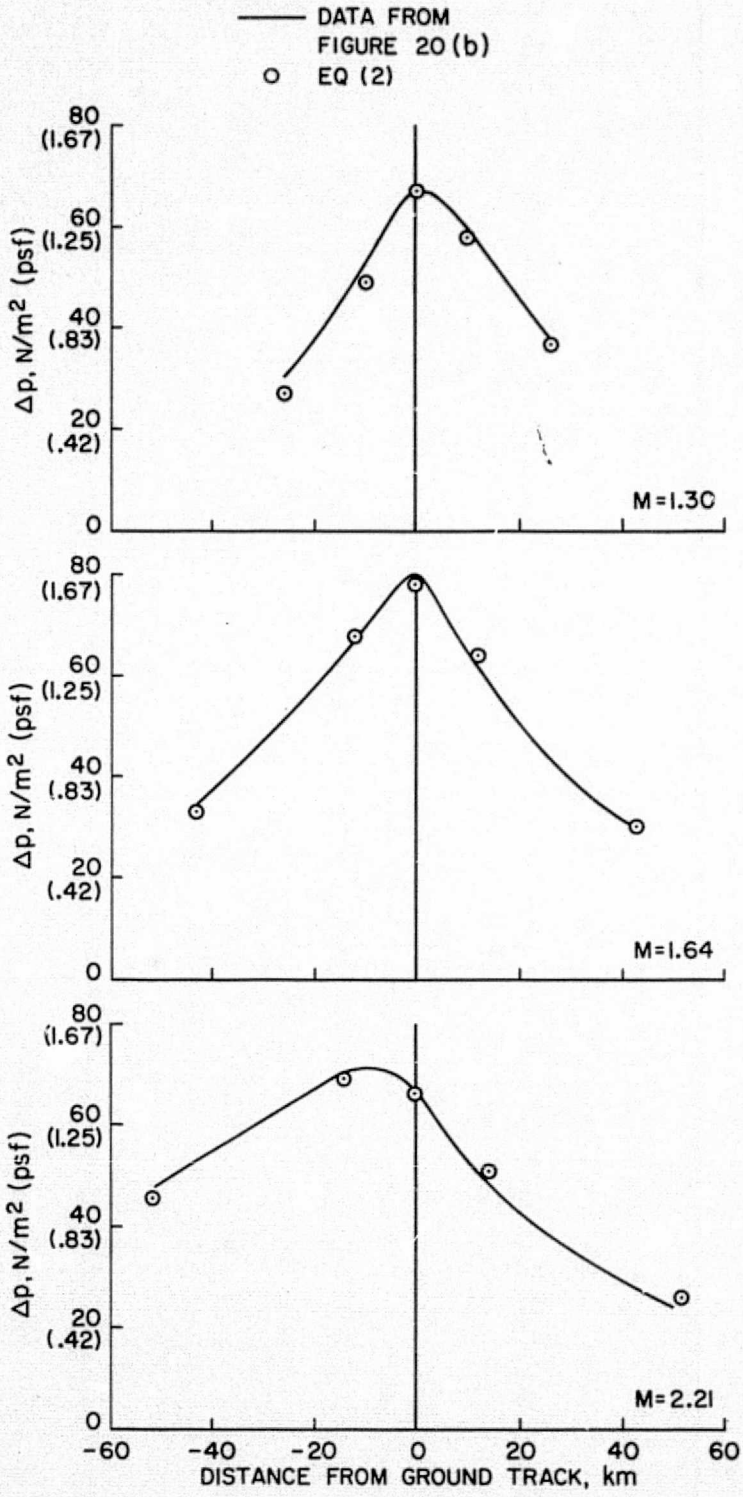

Figure 22.- Comparisons of the sonic boom footprint for the latest space shuttle vehicle calculated by two different methods, trajectory B.